First Principles Simulations of Vibrationally Resolved Photodetachment Spectra of Select Biradicals

by

Prateek Goel

A thesis
presented to the University of Waterloo
in fulfillment of the
thesis requirement for the degree of
Master of Science
in
Chemistry

Waterloo, Ontario, Canada, 2012

Author's Declaration

I hereby declare that I am the sole author of this thesis. This is a true copy of the thesis, including any required final revisions, as accepted by my examiners.

I understand that my thesis may be made electronically available to the public.

Abstract

Nonadiabatic dynamical processes are ubiquitous in chemistry and biology. Such events are directly connected to the treatment of energetically close lying states which gives rise to strong vibronic interactions in which case the Born-Oppenheimer approximation tends to break down. In case of biradicals, nonadiabatic events are facilitated by conical intersections, as a result of symmetry lowering of degenerate electronic states due to Jahn-Teller distortion.

A central problem in the treatment of the nonadiabatic molecular dynamics is posed by the representation of potential energy surfaces. A point by point calculation of a potential energy surface on a multi-dimensional grid is very cumbersome and in general does not provide with an analytical functional form of the potential. This becomes even more complicated when the adiabatic surfaces have cusps, where the function becomes non-differentiable.

Vibronic model Hamiltonians, which represent the potential in the form of a potential matrix which contains the electronic energies as well as the couplings in a diabatic basis. A Taylor series expansion of the potential matrix can be done to get a smooth analytical functional form of the potential matrix elements. These models can then be used to perform nuclear dynamics using either exact diagonalization time-independent method or

the wavepacket propagation based time-dependent methods. Thus, vibronic models provide a compact representation of complicated coupled potential energy surfaces, which can be used in conjunction with non-adiabatic nuclear dynamics

Vibronic models have been constructed for selected biradicals, for which photodetachment spectra have been simulated using the time-independent (VIBRON) as well as time-dependent (MCTDH) methods. Consistent results have been obtained with both the approaches for small systems. This also assures the use of MCTDH program for larger systems, where the time-independent methods are not applicable. Moreover, for biradicals, the parent anionic state also undergoes a Jahn-Teller distortion, or often the ground state potential energy surface is highly anharmonic in nature. This requires the description of anionic ground state by a vibronic model.

Therefore, in order to simulate the photodetachment spectra of biradicals, three vibronic models are constructed for each simulation. The first model describes the ground and excited states of the parent anionic (neutral) species. Two other vibronic models describe singlet and triplet states of the target neutral (cation) species, and the spectrum is simulated using the vibronic ground state(s) of the anion (neutral) as the absorbing state in VIBRON/MCTDH. The electronic states and vibronic model parameters are obtained using the IP-EOM-CCSD and DIP-STEOM-CCSD methodology as coded in the ACESII quantum chemistry program package. The photodetachment spectra of NO_3, $C_4H_4^-$ and

$C(CH_2)_3^-$ have been studied using this methodology.

Acknowledgements

Every achievement and success in life of an individual is usually contigent on the support of numerous people, be it in any form. We as human beings are largely interdependent in our endeavours on those around us, in a direct or indirect manner. I certainly am grateful to many people in the course of completing this journey.

Firstly, I am deeply indebted to my supervisor, Prof. Marcel Nooijen, for his consistent guidance and support all along my Masters. Marcel is a vast ocean of knowledge, and is excellent in bringing out the interest and capability of a student. His enthusiasm for doing Science, and doing so in the right spirits is infectious, to say the least. There is literally so much one can learn from him. He pushed my limits (and continues to do so). Often I would go to his office to ask something, and sentences like "Frame your question properly" or "This is not true, Prateek" will make me question my own sanity (or lack thereof!). And the epic, "If you get a funny result, check your input file first". I believe my input file errors have reduced significantly over time. As a supervisor, Marcel is very patient and supportive too. I remember going through a tough personal time for a while and he allowed me to handle things in a certain way and provided a lot of emotional support as well. I feel fortunate that my journey with Marcel does not end here, and I have a long way to go with him. Thank you for everything, Marcel!

I would like to thank my collaborators Yao Li and Julia Endicott. I thoroughly enjoyed the discussions on Science as well as on life with both of you! I would also like to thank Dipayan Datta, the former postdoc in our group, for his valuable guidance on graduate studies, for good discussions on research, and most of all for the delicious Bengali food! Your cooking skills are as excellent as your research skills, Dipayan Da!

I would like to thank Prof. Michael Palmer for teaching me many useful scientific tools, most importantly for making me a fan of Python programming language! Thank you so much for being available at any time and listening to me. Your sense of humor blows me away, so does your skills with computers and programming. I will keep bugging you for a few more years to come.

I would like to thank my friends Yalina Tritzant, Rahul Katyayan, Abhishek Kumar, Apurva Narayan, Debolina Banerjee, Saurabh Srivastava and many others whom names I am forgetting here for always being there with me, for wonderful times together, for making my stay at Waterloo memorable and last but not the least for tolerating me consistently for a period of two years! Friendship knows no boundaries and I am grateful to my old friends Nilesh Mishra (LA, California), Ketan Sharma (Berlin, Germany), Ankur Jalan (Mumbai, India), and Amit Vikram Singh (Kanpur, India) for always believing in me, giving me perspective, and keeping my spirits high. Some bonds are not broken even if you make the distance large enough!

Dedication

To **Kailash Kasala**, my role-model, not just for Grad School, but for life as well!

Table of Contents

List of Tables

List of Figures

List of Abbreviations

MO	Molecular Orbital
HF	Hartree-Fock
RHF	Restricted Hartree-Fock
ROHF	Restrcited open-shell Hartree-Fock
UHF	Unrestricted Hartree-Fock
SCF	Self-consistent field
CI	Configuration Interaction
CISD	Configuration Interaction Singles and Doubles
MBPT	Many-body Perturbation Theory
CC	Coupled-Cluster
CCSD	Coupled-Cluster Singles and Doubles
DFT	Density Functional Theory
MRCI	Multireference Configuration Interaction
MCSCF	Multiconfiguration Self-consistent field
CASSCF	Complete active space Self-consistent field
EOM-CC	Equation-of-Motion Coupled-Cluster

IP-EOM-CC	Ionization-potential Equation-of-Motion Coupled-Cluster
EA-EOM-CC	Electron-attachement Equation-of-Motion Coupled-Cluster
SF-EOM-CC	Spin-Flip Equation-of-Motion Coupled-Cluster
STEOM-CC	Similarity-transformed Equation-of-Motion Coupled-Cluster
DIP-STEOM	Double Ionization-potential Similarity-transformed Equation-of-Motion
DEA-STEOM	Double Electron-attachement Similarity-transformed Equation-of-Motion
MR-EOM-CC	Multireference Equation-of-Motion Coupled-Cluster
PES	Potential Energy Surface
JT	Jahn-Teller
PJT	Pseudo Jahn-Teller
MCTDH	Multiconfiguration Time Dependent Hartree
SPF	Single Particle Function

Chapter 1

Introduction

The advent of quantum mechanics in early twentieth century made it possible to study the science of Chemistry at the atomic scale. To come up with answers for puzzling questions of Chemistry became possible in principle, such as − what happens when two substances are mixed, why a certain product is formed, will a product be formed at all, if yes in what time, it may be a matter of seconds or even a matter of years! What more, to explore properties of matter became possible and so did our ability to design new materials. If we look at our kitchen today, and a picture of our kitchen in our grandparents days, we would notice how much *progress* Chemistry has made over the years. It has completely changed the way of living life (whether for the good or the bad, is a very subjective question, and let us not get into that here!).

All this became possible due to the study of molecular processes at atomic level. Theory along with the experiments has played a major role in the progress of Science, and often has motivated experimentalists to carry out new and challenging experiments. Talking about molecules, one can readily identify the two components which make the *chemistry* happen - Electrons and Nuclei. It turns out that in general the time scale of motion of electrons and nuclei differ greatly (attosecond for electrons, femtosecond for nuclei) and one can independently solve for the Schroedinger equation for the two cases and come up with many possible answers of the interesting questions posed above. This formulation has been the central backbone of *doing* chemistry – be it energetics, kinetics or spectroscopy, and is famously known as the Born-Oppenheimer or the *adiabatic* approximation. The first part of dealing with the motion of electrons is known as *Electronic Structure Theory* while the theory dealing with motion of nuclei is termed *Nuclear Dynamics*.

Simplicity lies on the other side of the complexity. Nature is complex, and one tries to understand nature with the use of simple yet beautiful physical models. One such complexity arises when the aforementioned Born-Oppenheimer approximation starts to break down in certain cases. This happens more often than one would like to think. Such processes where the motion of electrons and nuclei can no longer be treated independently are called *nonadiabatic* processes. Even though such processes were known for a long time in history, the theoretical developments for treating such processes started in 1980s with

the advent of *vibronic models* by Koppel, Domcke and Cederbaum. [1]

Vibronic models provide a great tool to study the nonadiabatic processes by providing a compact representation of potential energy surfaces in close energetic proximity. The parameters of the model responsible for the *coupled* motion of electrons and nuclei can be obtained by high-level *ab initio* electronic structure methods. One such method, the Similarity Transformed Equation of Motion (STEOM) will be used to obtain the electronic excitation energies and the vibronic model parameters in the work presented here. This is where the first part of simulating the spectra ends: it lays the foundation for performing nuclear dynamics by formulating the electronic structure problem of the molecular systems.

It goes without saying that the electronic structure aspects of any nonadiabatic process represent only half of the picture. In order to determine the observables associated with the experiment, one must solve the nuclear motion problem. This will be accomplished through the use of time-independent exact diagonalization as well as the time-dependent wavepacket propagation methods. The systems of interest are biradicals, a very interesting and challenging type of species holding much importance in different areas of chemistry, and the observable quantity we will be looking at is the electron binding energy through Photodetachment spectroscopy.

In recent years, a large number of spectroscopic data has been obtained for radicals and biradicals, for which there is no characterization available. By using the theoretical

methods and computational tools used in this work, one can readily simulate and interpret the experimental spectra, and a lot of physical insight can be gained into the molecular properties. Explanation is one thing, and prediction is other. Besides the ability to interpret and explain the features of experimental spectra, new spectra can be predicted by using these methods for which there is no experimental data available. This also motivates experimentalists to carry out new and challenging experiments opening up a whole new world of possibilities.

In this thesis, an attempt on both fronts has been made on a preliminary level, to *explain* and to *predict* the photodetachment spectra of selected biradicals. The theoretical formulation behind our approach to simulate the spectra will be laid out in Chapter 2, while Chapter 3 will try to provide a detailed account of the actual computational process involved in performing such calculations, and essentially lays out much of the machinery of the entire process. The steps involved have been illustrated using NO_2 as an example and the input files also have been provided which should give the reader some idea of what goes in and what comes out in doing these calculations. Chapter 4 deals with interesting application of these methods to the small but rather complicated system, NO_3 while Chapter 5 deals with complicated systems of larger size, namely cyclobutadiene (C_4H_4) and trimethylenemethane ($C(CH_2)_3$) where the simulated spectrum for C_4H_4 will be predictive in nature. The thesis finishes with few concluding remarks and developments in

sight in Chapter 6. Get ready for a bumpy ride and enjoy the journey!

Chapter 2

Theoretical Background

2.1 Electronic Structure of Biradicals

According to Salem,[2] biradicals can be defined as molecules in which two electrons occupy two degenerate, or nearly degenerate, spatial orbitals. A few examples of biradical molecules are carbenes, conjugated hydrocarbons which can not be represented by classical Kekule structures, antiaromatic annulenes, and others. Also, biradicals often act as reactive intermediates, or transition states in the course of a chemical reaction.

There are six different possible ways in which two electrons can be placed in two orbitals, or equivalently in four spin orbitals. This is shown in figure 2.1 . Among these six possible

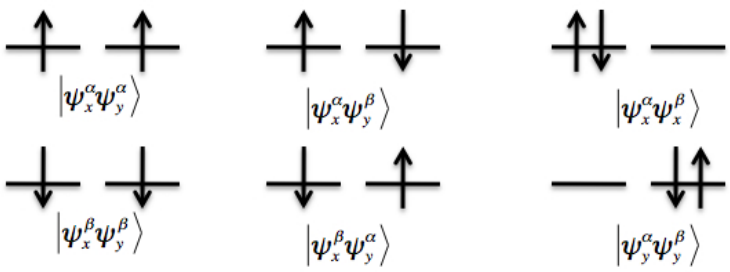

Figure 2.1: *Possible configurations for the occupancy of two electrons in two orbitals*

configurations, $|\psi_x^\alpha \psi_y^\alpha\rangle$ and $|\psi_x^\beta \psi_y^\beta\rangle$ are clearly triplet states, while $|\psi_x^\alpha \psi_x^\beta\rangle$ and $|\psi_y^\alpha \psi_y^\beta\rangle$ are singlet states. Also, the sum of configurations $|\psi_x^\alpha \psi_y^\beta\rangle$ and $|\psi_x^\beta \psi_y^\alpha\rangle$ represents the third component ($M_s = 0$) of the three-fold degenerate triplet, while their difference represents the third singlet state. The important point to note here is that the individual determinants are not spin eigenstates.

In total, four closely lying multiplets are present overall, one three-fold degenerate triplet and the three singlets. The question that arises here is: what are the relative energies of these states, and which one is the ground state? Furthermore, the (near)degeneracy of the singlet states and the mixing of configurations can lead to distortion in molecular geometry resulting in the lowering of energy. This makes the prediction of the ground state more complicated.

Let us look at the relative energies of these four states in quantum-mechanical terms. Assuming that $|\psi_x\rangle$ and $|\psi_y\rangle$ are degenerate, the energy terms for one- and two-electron

operators are:

h = one electron energy of ψ_i or ψ_j

K_{ij} = exchange energy between ψ_i and ψ_j

$\bar{J}$ = average coulombic repulsion between two electrons in ψ_i or ψ_j

J_{ij} = coulombic repulsion between two electrons; one in ψ_i, one in ψ_j

The relative energies of these states can be written as follows:

Triplet

$$|\psi_i\psi_j\,(\alpha\beta\,+\,\beta\alpha)/2\rangle \qquad E\,=\,2h\,+\,J_{ij}\,-\,K_{ij} \tag{2.1}$$

Singlet

$$|\psi_i\psi_j\,(\alpha\beta\,-\,\beta\alpha)/2\rangle \qquad E\,=\,2h\,+\,J_{ij}\,+\,K_{ij} \tag{2.2}$$

Singlet

$$\frac{1}{\sqrt{2}}(|\psi_i^\alpha\psi_i^\beta\rangle\,-\,|\psi_j^\alpha\psi_j^\beta\rangle) \qquad E\,=\,2h\,+\,\bar{J}\,-\,J_{ij} \tag{2.3}$$

Singlet

$$\frac{1}{\sqrt{2}}(|\psi_i^\alpha\psi_i^\beta\rangle\,+\,|\psi_j^\alpha\psi_j^\beta\rangle) \qquad E\,=\,2h\,+\,\bar{J}\,+\,J_{ij} \tag{2.4}$$

In consideration of different terms contributing to E, a few conclusions can be made. First, $\bar{J} >> J_{ij} > K_{ij} > 0$, which means that the triplet should be the ground state as

there is a reduction in energy due to the exchange correlation. However, a difficulty lies in the comparison of $J_{ij} - K_{ij}$ and $\bar{J} - J_{ij}$. No certain rule is followed in general. An important point to note in the above analysis is that we are not considering energetic terms which involve the other orbitals of the system. Even if the two orbitals are closely degenerate, those terms may not be equal for different configurations, and may eventually lead a singlet to fall below the triplet in energy. [3]

To obtain the energies from equation $2.1 - 2.4$, a knowledge of MOs ψ_i and ψ_j is required. In a closed-shell molecule, where the N MOs of lowest energy contain the total number of $2N$ electrons, optimal MOs are obtained by solving the SCF equations. The form of the equations remain the same for all MOs. This approach is also known as the Restricted Hartree-Fock (RHF) method, since the MOs occupied by α and β electrons are restricted to be the same.

SCF methods have also been developed for the open-shell systems, Restricted open-shell Hartree-Fock (ROHF) in which the MOs occupied by α and β electrons are restricted to be the same, and Unrestricted Hartree-Fock (UHF) where this restriction is lifted. Though the UHF energy is always equal to or lower than the ROHF energy, qualitatively it can only describe wavefunctions which are of a single Slater determinantal form. Therefore, while UHF can treat the high spin triplets ($|\psi_i^\alpha \psi_j^\alpha\rangle$ and $|\psi_i^\beta \psi_j^\beta\rangle$) correctly, it fails to provide a qualitatively correct description for the corresponding singlets where the wavefunction

requires two Slater determinants. In addition, singlet states in 2.3 and 2.4 are linear combinations. Also, UHF leads to a mixture of singlet and triplet states when applied to the low spin ($M_s = 0$) component of triplet and the corresponding open-shell singlet. In addition, correlation between the two partially occupied MOs, and the rest of the "core" electrons can play an important role in determination of the relative energies. This correlation is missing in the above discussed treatments. Electron correlation techniques, and multiconfigurational wavefunction approach is briefly discussed later.

2.2 Overview of quantum chemical approaches

Among the single determinant based techniques of electron correlation, configuration interaction (CI) is the oldest method. In CI, contributions to the ground electronic state are made by mixing in excited configurations. From the reference ground state, the electrons are promoted to the virtual orbitals to build all possible configurations and the electronic Hamiltonian thus obtained is diagonalized. This leads to what is known as Full CI (FCI), and gives the exact energy for the electronic Hamiltonian in a given basis set. However, FCI becomes highly impractical for medium sized molecules, or even for very small molecules in a larger basis set. However, if the diagonalization is performed in the basis consisting of the reference determinant (obtained by HF-SCF) and the single and double excitations only,

the resulting truncation is known as Configuration interaction singles and doubles (CISD). Although CISD is computationally tractable as compared to FCI, it suffers from the size-inconsistency problem. CISD has lost popularity in past few decades, and is no longer used very widely compared to its descendant many-body perturbation theory (MBPT), and coupled-cluster (CC) techniques.

MBPT is the simplest size-consistent electron correlation technique, particularly when the perturbation is carried out to second order, referred to as MBPT(2). This method has been extensively used to treat electron correlation, and has provided quite good results in terms of accuracy. While the third order MBPT does not yield an improved accuracy, MBPT(4) results in a significant improvement over MBPT(2). Going beyond MBPT(4) makes it computationally very expensive. MBPT is losing favor due to a number of reasons, which are discussed in a review article. [4]

The CC theory is based upon an exponential *ansatz*, and the wavefunction is written as

$$|\psi\rangle \;=\; e^{\hat{T}}|\phi_0\rangle \tag{2.5}$$

where $|\phi_0\rangle$ is the single Slater determinant reference state, and $\hat{T}$ is the cluster operator which produces excited determinants. It can be written as

$$\hat{T} \;=\; \hat{T}_1 \;+\; \hat{T}_2 \;+\; \ldots \hat{T}_n \tag{2.6}$$

$$\hat{T}_1 = \sum_{ai} t_i^a \hat{a^\dagger} \hat{i} \tag{2.7}$$

$$\hat{T}_2 = \frac{1}{4} \sum_{abij} t_{ij}^{ab} \hat{a^\dagger} \hat{a^\dagger} \hat{i} \hat{j} \tag{2.8}$$

$$\vdots$$

where $t_{ij\cdots}^{ab\cdots}$ are the t-amplitudes which represent the corresponding weights of the excitation operators. The operators following the t-amplitudes are creation and annihilation operators, which when acting on the reference state promotes an electron from the occupied orbital i to virtual orbital a (in $\hat{T}_1$) as well as from from the occupied orbital j to virtual orbital b (in $\hat{T}_2$). The coupled-cluster equations which are solved for ground state energy E, and the t-amplitudes can be written as:

$$\langle \phi_0 | e^{-\hat{T}} H e^{\hat{T}} | \phi_0 \rangle = E \tag{2.9}$$

$$\langle \phi_\lambda | e^{-\hat{T}} H e^{\hat{T}} | \phi_0 \rangle = 0 \tag{2.10}$$

The cluster operator $\hat{T}$ is usually truncated at $n = 2$ resulting in computationally tractable CCSD (coupled-cluster singles and doubles) model. CCSD is size-consistent, and the exponential operator makes sure the presence of determinants of all excitation levels. To reach the desired accuracy, a perturbative triples correction is included to CCSD which results in the highly accurate CCSD(T) model. CCSD(T) is often called "the gold standard of quantum chemistry". [4]

Density functional theory (DFT) is another widely used *ab-initio* method in which the ground-state energy of an N particle system is expressed as a functional of the one-electron density.

In many systems, such as biradicals, more than one configuration contributes substantially to the wavefunction. For such situations, multiconfigurational approaches are applied. The starting wavefunction is expressed as a linear combination of the important configurations with corresponding weights:

$$|\psi\rangle = \sum_i C_i |\phi_i\rangle \tag{2.11}$$

where an optimization is performed for the coefficients C_i and orbitals ϕ_i. Such an approach is known as multiconfigurational SCF (MCSCF). The selection of relevant configurations is by no means a trivial task. Usually, the orbitals are divided into two spaces, namely active and inactive, and the active space is selected in the valence region. This also requires a fair amount of chemical intuition. The most widely used version of MCSCF is often known as complete active space SCF (CASSCF) which results from doing the complete (full) CI in a set of active orbitals. A clear advantage of multiconfigurational approaches is that all the contributing determinants to the wavefunction are treated in a balanced way. Although MCSCF calculations take nondynamical correlations into account effectively, MCSCF wavefunctions often overestimate bond lengths and underestimate vibrational frequencies.[5]

Multireference CI (MRCI) calculations have proven to be highly accurate in the treatment of residual correlation effects, and have even been remarked as *the* method for generating potential energy surfaces. [4] However, like CI, MRCI is not size-consistent. Also, MRCI calculations become highly expensive as the size of the molecule increases.

In a lesser known class of methods, the reference state is calculated for a state in which the number of electrons are not the same as the actual state of interest! One such class of methods, the equation-of-motion coupled-cluster (EOM-CC) will form the basis of the work presented in this thesis. The great feature of these methods is a balanced treatment of mixed configuration, and dynamical electron correlation; while avoiding the inherent difficulties of the multireference methods. These methods will be explored in some detail now, and their potential application to biradical systems will be discussed.

2.3 Equation-of-Motion Coupled-Cluster Methods

According to Krylov, [6] "The Equation-of-motion coupled-cluster (EOM-CC) method is a versatile electronic structure tool that allows one to describe a variety of multiconfigurational wavefunctions within a single reference formalism." The Fock space formalism, in which one can talk about wavefunctions with varying number of electrons, is exploited to separate the *target* and *reference* states. As stated in an earlier section, these methods

provide a useful means to study the electronic structure of open-shell systems, in particular biradicals. A brief formalism of various EOM-CC methods is presented in this section.

The starting point of traditional EOM methods is to have a closed-shell reference state $|\phi_0\rangle$, which has a few more, or a few less electrons than the target state. This reference state is a single Slater determinant, and a well behaved state for the closed-shell methods. In EOM-CC, the HF-SCF orbitals are optimized and the CCSD equations are solved to obtain $\hat{T}$ for the reference state. However, to obtain the target states, the transformed Hamiltonian $\bar{H} = e^{-\hat{T}}\hat{H}e^{\hat{T}}$ is diagonalized in a selected basis of determinants, which correspond to the configuration of target states. What this means is that, if the target state has $N-1$ electrons , where N is the number of electrons in the reference state $|\phi_0\rangle$, the diagonalization will be performed in a basis consisting of determinants obtained by the removal of one electron from $|\phi_0\rangle$. The target states are accessed with the help of an excitation operator $\hat{R}$, which acts on $|\phi_0\rangle$. Depending on the number of electrons in the target state, the form of $\hat{R}$ will change so as to obtain the relevant target states.

Let us analyze this situation for Ionization-Potential EOM (IP-EOM) approach, where the target state has one less electron than the reference state. This approach is suitable for doublet radicals. The target state is defined as

$$|\psi_k\rangle = \hat{R(k)}\,|\phi_0\rangle \tag{2.12}$$

where $\hat{R(k)}$ is the excitation operator. If we limit $\hat{R(k)}$ to singles and doubles excitation, we can write

$$\hat{R(k)} \;=\; \hat{R_1(k)} \;+\; \hat{R_2(k)} \tag{2.13}$$

where

$$\hat{R_1(k)} = \sum_i r_i(k)\hat{i} \tag{2.14}$$

which is a 1-hole operator. And,

$$\hat{R_2(k)} = \frac{1}{2}\sum_a \sum_{i,j} r_{ij}^a(k)\hat{a^\dagger}\hat{j}\hat{i} \tag{2.15}$$

which is a 2-hole 1-particle operator. The indices $i, j \ldots$ represent the occupied orbitals, and $a, b \ldots$ represent the virtual orbitals.

Since the transformed Hamiltonian $\bar{H}$ is not hermitian, the final states have to be represented by a biorthogonal set of bra and ket functions.[7] These functions can be written as follows:

$$|\psi_k\rangle \;=\; e^{\hat{T}}\hat{R(k)}\,|\phi_0\rangle \tag{2.16}$$

$$\langle\psi_k| \;=\; \langle\phi_0|\hat{L(k)}e^{-\hat{T}} \tag{2.17}$$

L can be defined in a similar manner to that of R,

$$L\hat{(k)} \;=\; \sum_{i} l^{i}(k)\hat{i^{\dagger}} \;+\; \frac{1}{2}\sum_{a}\sum_{i,j} l_{a}^{ij}(k)\hat{i^{\dagger}}\hat{a}\hat{j^{\dagger}} \tag{2.18}$$

Now, the IP-EOM-CCSD energy is obtained by the diagonalization of $\bar{H}$, so that

$$E \;=\; \langle\phi_0|L\hat{(k)}\bar{H}R\hat{(k)}|\phi_0\rangle \tag{2.19}$$

or

$$E \;=\; \langle\phi_0|L\hat{(k)}\hat{e^{-T}}He^{\hat{T}}R\hat{(k)}|\phi_0\rangle \tag{2.20}$$

The geometry of different target states can be optimized, and subsequently vibrational frequencies can be calculated. Importantly, a number of different states can be obtained from diagonalization of $\bar{H}$.

Similarity-Transformed Equation-of-Motion Coupled-Cluster

The purpose of STEOM is a further simplification of the transformed eigenvalue problem. To accomplish this, a series of similarity transformations is performed on the Hamiltonian. [8, 9] In essence, the EOM methodology is carried one additional step forward, where a second transformation is performed resulting in the removal of the first order coupling between the singly and the doubly excited determinants.[10]

The transformations are executed at the level of second quantization in STEOM. Let us write our Hamiltonian, and the transformed Hamiltonian (EOM level) in the second

quantization form:

$$\hat{H} \;=\; h_0 \;+\; \sum_{p,q} h_{p;q}\{\hat{p}^\dagger \hat{q}\} \;+\; \frac{1}{4}\sum_{p,q,r,s} h_{pq;rs}\{\hat{p}^\dagger \hat{r}\hat{q}^\dagger \hat{s}\} \tag{2.21}$$

where h_0 is the energy of reference determinant, and $h_{p;q}$ is the corresponding Fock operator. Also,

$$\hat{\bar{H}} \;=\; e^{-\hat{T}}\hat{\bar{H}}e^{\hat{T}} \;=\; \bar{h_0} \;+\; \sum_{p,q} \bar{h}_{p;q}\{\hat{p}^\dagger \hat{q}\} \;+\; \frac{1}{4}\sum_{p,q,r,s} \bar{h}_{pq;rs}\{\hat{p}^\dagger \hat{r}\hat{q}^\dagger \hat{s}\} \;+\; ... \tag{2.22}$$

In the EOM picture, the coupling between the singly excited and the doubly excited determinants is given by operators $\bar{h}_{ab;ej}\{\hat{a}^\dagger \hat{e}\hat{b}^\dagger \hat{j}\}$ and $\bar{h}_{mb;ij}\{\hat{m}^\dagger \hat{i}\hat{b}^\dagger \hat{j}\}$, where e represents an active virtual orbital and m is an active occupied orbital. Now, the second transformation is defined as a $e^{\hat{S}}$, with $\hat{S} \;=\; \hat{S^+} \;+\; \hat{S^-}$

$$\hat{S^+} \;=\; \sum_{a',e} s_{a';e}\{\hat{a}'^\dagger \hat{e}\} \;+\; \frac{1}{2}\sum_{a,b,j,e} s_{ab;ej}\{\hat{a^\dagger}\hat{e}\hat{b^\dagger}\hat{j}\} \tag{2.23}$$

$$\hat{S^-} \;=\; \sum_{i',m} s_{m;i'}\{\hat{m}^\dagger \hat{i'}\} \;-\; \frac{1}{2}\sum_{i,j,b,m} s_{mb;ij}\{\hat{m^\dagger}\hat{i}\hat{b^\dagger}\hat{j}\} \tag{2.24}$$

where the prime indices represent explicitly inactive orbitals. The doubly transformed Hamiltonian is given by

$$\hat{G} \;=\; \{e^{\hat{S}}\}^{-1}\hat{\bar{H}}\{e^{\hat{S}}\} = \; g_0 \;+\; \sum_{p,q} g_{p;q}\{\hat{p^\dagger}\hat{q}\} \;+\; \frac{1}{4}\sum_{p,q,r,s} g_{pq;rs}\{\hat{p^\dagger} r\hat{q^\dagger}\hat{s}\} \;+\; ... \tag{2.25}$$

The parameters which enters $\hat{S}$ are calculated by solving the equations:

$$g_{a';e} = g_{ab;ej} = 0 \longrightarrow \hat{S}_+ \tag{2.26}$$

$$g_{m;i'} = g_{mb;ij} = 0 \longrightarrow \hat{S}_- \tag{2.27}$$

To obtain the s-amplitudes, a normalization condition is used on a proper subset of IP-EOM-CC (EA-EOM-CC) eigenvectors which correspond to principal IPs(EAs). This makes STEOM very robust numerically, as only eigenvalue problems are solved beyond the CCSD ground state problem.

The DIP scheme

On a similar line of the EOM approach, STEOM can be used in diagonalization problems which involve a different number of electrons with respect to the reference state. More specifically, systems which have two more electrons than a closed-shell parent state can be described by Double Electron-attachment STEOM (DEA-STEOM). On the other hand, systems which have two less electrons than a closed-shell parent state can be described by Double Ionization-potential STEOM (DIP-STEOM). The DIP approach can be used to study systems in which apart from the closed-shell "core", two electrons in two orbitals, or four electrons in three orbitals are present. Biradicals fall in the former category. In application of the DIP scheme, a di-anion is created as the reference state by filling the partial occupied orbitals at first. Optimal MOs are obtained for this state. In the final

step, the effective Hamiltonian is diagonalized in the basis of determinants which have two less electrons than the dianion, the two-hole configurations, to obtain the target states of the biradical. [9] If truly di-anion states are used, which are unbound, the DIP-STEOM description is physically unsound. In practice even then the method can give reasonable results, as long as the one-particle basis set is not too large.

The DIP-STEOM approach will be used to analyze the energetics of ground and excited states, as well as to generate vibronic model Hamiltonians for biradicals. A summary of important steps involved in a general STEOM calculation is as follows:[10]

1. Solve the CCSD equations. $\langle\phi_\lambda|e^{-\hat{T}}\hat{H}e^{\hat{T}}|\phi_0\rangle == 0$
2. Transform the Hamiltonian. $\bar{H} = e^{-\hat{T}}\hat{H}e^{\hat{T}}$
3. Select active occupied orbitals. Solve IP-EOM-CC equations $\rightarrow \hat{S^-}$
4. Select active virtual orbitals. Solve EA-EOM-CC equations $\rightarrow \hat{S^+}$. (This step is not needed in the DIP version)
5. Get relevant matrix elements of the doubly transformed Hamiltonian.
   $\hat{G} = \{e^{\hat{S^+}+\hat{S^-}}\}^{-1}\hat{\bar{H}}\{e^{\hat{S^+}+\hat{S^-}}\}$
6. Diagonalize G over $\hat{i}\hat{j}|\phi_0\rangle$, states with two less electrons than $|\phi_0\rangle$.

7. Obtain approximate left-hand states and calculate properties as biorthogonal expectation values.

Spin-Flip Equation-of-Motion Coupled-Cluster

In Spin-flip equation-of-motion coupled-cluster method,[5] the reference is a high-spin triplet state, which can be described in a qualitatively correct manner by the single reference wavefunction (usually UHF). Then the target states are obtained via spin-flip excitations (e.g. $\alpha \rightarrow \beta$) as

$$\psi^{s,t}_{M_s=0} \;=\; \hat{R}_{M_s=-1}\tilde{\psi}^{t}_{M_s=+1} \tag{2.28}$$

where $\tilde{\psi}^{t}_{M_s=+1}$ represents the $\alpha\alpha$ component of the triplet reference state, $\psi^{s,t}_{M_s=0}$ represents the target low-spin singlet and triplet states $M_s = 0$, and $\hat{R}_{M_s=-1}$ is the excitation operator which flips the spin of an electron. SF-EOM has been applied to describe a variety of systems such as excited states, bond-breaking problems, biradicals, and triradicals, and have achieved good results. [11] Further developments of SF-EOM methods are in active development at the iOpenshell center, University of Southern California. [12]

2.4 Concepts of Vibronic Theory

2.4.1 The Born-Oppenheimer Approximation

The Born-Oppenheimer approximation is the central approximation in the study of chemical systems which lays the foundation for the most important concept in Chemistry –

Potential Energy Surface (PES), defining much of the basic chemical concepts such as molecular structure with chemical kinetics, spectroscopy, molecular dynamics, photochemistry and others. PES gives a description of the energy of a molecule in terms of its structure. The global minimum on the surface corresponds to an equilibrium structure of the molecule. In fact, all minima are some sort of stable conformations of the molecule. First order saddle point corresponds to a transition state for a reaction. A reaction path is the minimum energy path which connects a transition state to the minima. Let us try to formulate the Born-Oppenheimer approximation, first in simple theoretical terms, and then diving into more mathematical details. This will form the basis for our journey of going from the Born-Oppenheimer approximation to Vibronic Models.

As most of the chemistry textbooks like to put it, the time scale of electronic and nuclear movement differ greatly, nuclei being much heavier than electrons, therefore the two degrees of freedom can be decoupled effectively . The molecular Hamiltonian can be written as a sum of two terms, $\hat{T}_N + \hat{H}_e$, where the first term is the nuclear kinetic energy while the latter term refers to the electronic Hamiltonian including electron kinetic energy as well as all the potential terms.

According to the Born-Oppenheimer approximation, the electronic problem involving $\hat{H}_e$ is solved first at a fixed geometry Q (clamped nuclei), which gives the electronic wavefunction $\phi_n(r, Q)$ as well as a single *adiabatic* energy $V_n(Q)$ for each electronic state. By

varying Q one can obtain the full PES which is a function of nuclear coordinates.

To solve for nuclear wavefunction in the Born-Oppenheimer framework, the molecular wavefunction is written as a product of the electronic wavefunction $\phi_n(r, Q)$ and a function $\chi_n(Q)$ which depends on the nuclear configuration

$$\Psi^{BO} = \chi_n(Q)\phi_n(r, Q) \tag{2.29}$$

The molecular Hamiltonian is a sum of two terms, as described above

$$\hat{H} = \hat{T}_N + \hat{H}_e \tag{2.30}$$

Where

$$T_N = -\frac{\hbar}{2\mu}\frac{\partial^2}{\partial Q^2} \tag{2.31}$$

Applying equation 2.30 on 2.29, it can be shown that

$$\hat{H}\Psi^{BO} = \chi_n\hat{H}_e\phi_n - \frac{1}{2}(\phi_n{\nabla_R}^2\chi_n + \chi_n{\nabla_R}^2\phi_n + 2\nabla_R\chi_n\nabla_R\phi_n) \tag{2.32}$$

The last two terms in the equation 2.32 are neglected which leads to the Born-Oppenheimer approximation. This essentially justifies the assumption that the electronic and nuclear motion are decoupled (i.e., they are governed by two different equations). As stated earlier, the interpretation here is that the motion of electrons do not depend on the motion of the nuclei, though it clearly depends on the *position* of the nuclei!

Before getting into the mathematical formulation of the Born-Oppenheimer approximation and the issue of non-adiabatic couplings, let us briefly look at one of the most widely used methods in molecular spectroscopy – the harmonic Franck-Condon approach. The Franck-Condon approach uses harmonic potentials along with the Born-Oppenheimer approximation. What follows in the actual calculation is the geometry optimization of the ground state and the calculation of a quadratic force field which gives the vibrational frequencies. A similar procedure is repeated for the excited states of interest. The intensity of individual transitions can be calculated from the overlap factors of the harmonic oscillator states between ground and excited states. A combination of the Born-Oppenheimer approximation with the Franck-Condon approach provides us with the familiar picture of spectroscopy, as shown in the figure 2.2 .

Although the aforementioned scheme of calculating the spectra is computationally efficient and has been successful in studying a wide range of molecular systems, there are limitations of the approximation and in certain situations the Franck-Condon methodology faces a number of disadvantages. This can largely be categorized into two cases:

- **Anharmonicities**: It is possible that the equilibrium geometry of an excited state of interest is considerably far from the geometry of the absorbing state. If such a situation arise, the harmonic approximation to the PES of the excited state might result in an inadequate approximation to the true PES in the Franck-Condon region

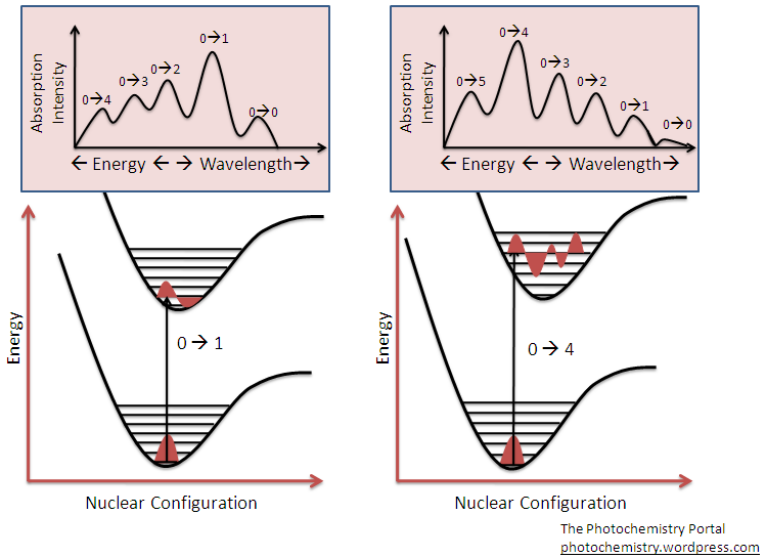

Figure 2.2: The textbook picture of Spectroscopy: The Franck-Condon Approach

of the molecule, which is vital from the spectroscopic point of view. Moreover, often excited electronic states are very close to each other resulting in complicated surface topologies which again leads to a breakdown of the harmonic approximation.

- **Conical Intersections**: Excited state PESs often cross each other giving rise to conical intersections. Due to surface crossings, it could well be that an excited state minimum may not even exist! As an example, it is possible that the lowest point on a PES is a conical intersection, or, if the PES is followed through the crossing the final minimum coincides with the minimum located for another excited state!

In a nutshell, nuclear motion takes place on complicated potential energy surfaces which

may not be described adequately by a single excited state surface. This necessitates to move beyond the Born-Oppenheimer approximation in order to perform accurate studies of spectroscopy.

Let us discuss the issue of nonadiabatic couplings now, which will eventually lead us to a discussion on vibronic models, the heart of the studies performed in this work.

2.4.2 Nonadiabatic Couplings: From Adiabatic to Diabatic States

We have seen in the last section that the Born-Oppenheimer approximation is not suitable to describe certain systems, which requires a form of analysis where the *coupling* between electronic and nuclear motion is taken into account. Let us first try to formulate the complete electronic and nuclear problem to understand the origin of this *coupling*, and then provide a motivation towards why vibronic models are a good tool to study such systems.

Let us write the full molecular Hamiltonian in a slightly different form now as compared to the last section,

$$\hat{H} = \hat{T}_e + \hat{T}_N + \hat{U}(r, Q) \tag{2.33}$$

where $\hat{T}_e$ and $\hat{T}_N$ are the electronic and nuclear kinetic energy operator, and $\hat{U}(r, Q)$ is the potential energy operator for the complete system. As before, r and Q stand for the

electronic and nuclear coordinates.

In order to solve for the full Schroedinger equation, the electronic part of the problem is solved first by setting the nuclear kinetic energy term to zero i.e., $\hat{T}_N = 0$

$$\hat{H}_e = \hat{T}_e + \hat{U}(r,Q); (\hat{H}_e - V_n)\phi_n(r,Q) = 0 \tag{2.34}$$

which gives us the Born-Oppenheimer adiabatic electronic states $\phi_n(r,Q)$ and the corresponding adiabatic PES $V_n(Q)$ for each electronic state as a function of nuclear geometry. The full molecular wavefunction is then expressed as what is called the Born-Huang expansion employing $\phi_n(r,Q)$ as basis functions and the coefficients $\chi_n(Q)$ which depend on the nuclear coordinates

$$\Psi = \Sigma_n \chi_n(Q)\phi_n(r,Q) \tag{2.35}$$

This raises a doubt about the form of molecular wavefunction described in the previous section. There, a single adiabatic states was multiplied by a coefficient depending on the nuclear geometry. When electronic states start to come into close energetic proximity of each other, it becomes important to include more than one of them in the expansion. In fact, it should be noted that the equation 2.35 is formally exact if the set of adiabatic states $\{\phi_n(r,Q)\}$ is complete. In practice, however, the expansion is truncated to a small number of states.

Now, the coefficients $\chi_n(Q)$ can be obtained by solving the full Schroedinger equation

$$(\hat{H} - E)\Psi_n = 0 \tag{2.36}$$

Inserting equation 2.35 into 2.36 and multiplying both sides from the left by $\int dr\phi_m{}^*$ leads to a set of coupled equations

$$(\hat{T_N} + V_m(Q) - E)\chi_m(Q) = \sum_n \hat{\Lambda}_{mn}\chi_n(Q) \tag{2.37}$$

where

$$\hat{\Lambda}_{mn} = -\int dr\phi_m{}^*[\hat{T_N}, \phi_n] \tag{2.38}$$

The operator $\hat{\Lambda}_{mn}$ is known as the nonadiabatic operator, which is also the *coupling* between the nuclear and the electronic motions as $\hat{T_N}$ contains the nuclear coordinates while ϕ_n contains the electronic coordinates. Let's look at this more closely. The nonadiabatic operator can be decomposed into first- and second-order derivative coupling by using the definition of the $\hat{T_N}$ reading as

$$\hat{\Lambda}_{mn} = \sum_k \frac{\hbar^2}{M_k} F^k_{mn} \frac{\partial}{\partial Q_k} - \sum_k \frac{\hbar^2}{M_k} G^k_{mn} \tag{2.39}$$

where M_k are nuclear masses and

$$F^k_{mn} = \langle \phi_n(r) | \nabla_k | \phi_m(r) \rangle, \tag{2.40}$$

$$G^k_{mn} = \langle \phi_n(r) | \nabla^2_k | \phi_m(r) \rangle, \tag{2.41}$$

where $\nabla_k \equiv \frac{\partial}{\partial Q_k}$.

The full Hamiltonian and the set of coupled equations can now be written as

$$\hat{H} = \hat{T_N} + V_m(Q) - \hat{\Lambda} \tag{2.42}$$

$$(\hat{H} - E \cdot I)\chi = 0 \tag{2.43}$$

The Hamiltonian matrix H describes the motion of nuclei in a selected manifold of electronic states. χ is a column vector with elements χ_n, and $V_m(Q)$ is the diagonal matrix of electronic energies. The quantity $\hat{\Lambda}$ represents the nonadiabatic coupling effects in the adiabatic electronic representation.

Let us now consider a simple example of two excited electronic states which are very close in energy and the nuclear motion takes place on both the surfaces. So the set of coupled equations for this moon can be written as

$$[\hat{T_N} + V_1(Q) - E]\chi_1 + \Lambda_{11}\chi_1 = \Lambda_{12}\chi_2 \tag{2.44}$$

and

$$[\hat{T_N} + V_2(Q) - E]\chi_2 + \Lambda_{21}\chi_1 = \Lambda_{22}\chi_2 \tag{2.45}$$

In matrix notation this can be rewritten as

$$\begin{pmatrix} T_n + \Lambda_{11} & \Lambda_{12} \\ \Lambda_{21} & T_n + \Lambda_{11} \end{pmatrix} \begin{pmatrix} \chi_1 \\ \chi_2 \end{pmatrix} + \underline{\begin{pmatrix} V_1(Q) & 0 \\ 0 & V_2(Q) \end{pmatrix}} \begin{pmatrix} \chi_1 \\ \chi_2 \end{pmatrix} = \begin{pmatrix} E & 0 \\ 0 & E \end{pmatrix} \begin{pmatrix} \chi_1 \\ \chi_2 \end{pmatrix} \quad (2.46)$$

Therefore, the kinetic energy operator is non-diagonal, while the potential energy operator is diagonal in the adiabatic electronic representation. If one can solve these coupled equations, one can get the nuclear dynamics in a quite exact manner. The question here is – can these equations be solved?

Let us look at some important points before we arrive at an answer to this question:

- When the nonadiabatic operator $\hat{\Lambda}$ is set to zero, the Hamiltonian becomes diagonal, and one arrives at the Born-Oppenheimer or adiabatic approximation. Then the nuclear motion takes place on the two surfaces independently of each other.

- In general, the elements of nonadiabatic operator $\hat{\Lambda}$ are extremely difficult to calculate, especially in the regions of conical intersections.

- Although there are quantum chemistry programs such as COLUMBUS and MOLPRO, which can calculate the nonadiabtaic couplings by analytical gradient methods, the adiabatic representation still remains conceptually challenging in the regions where two PESs come very close to each other, and the electronic wave function does not remain a single valued function.

- Representation of PESs in adiabatic approximation can be very poor, due to the presence of cusps at conical intersections. This also makes them a non-differentiable functions of nuclear coordinates.

- Last but not the least, solving nuclear dynamics equations where the kinetic energy operator is non-diagonal is a challenging task.

Therefore, the take-home message is that the adiabatic approximation is cumbersome to use in many cases. This eventually leads us to a new representation of electronic states – the diabatic representation!

In a diabatic representation, the derivative couplings of the adiabatic representation are forced to be zero and the wavefunction become a smooth function of nuclear coordinate by a suitable unitary transformation. In this representation, the nuclear kinetic energy operator becomes diagonal while the coupling between the electronic states is introduced via the off-diagonal terms of the potential energy operator of the molecular Hamiltonians. This is precisely what is termed as *vibronic coupling* and this model of studying coupled electronic-nuclear problem is known as a *vibronic model*.

An important point to note here is that the diabatic states are not unique in nature. These states are obtained by a rotation (unitary transformation) of the adiabatic states which is dependent on the nuclear coordinates. Any rotation which is independent of the

nuclear coordinate will produce different diabatic states, conserving the eigenvalues of the Hamiltonian.

Before we move to the computational scheme of calculating the diabatic states and constructing the vibronic models, let us again look at a simple example of two excited states very close in energy, this time in the diabatic framework. Also, let us vary the energy gap between the two states to see the importance of vibronic coupling as the states become closer and closer in energy. This will bring our discussion of basic concepts of vibronic theory to an end.

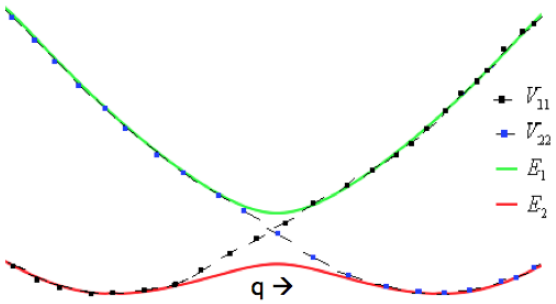

Figure 2.3: A figure showing the diabatic vs adiabatic surfaces

In the diabatic representation, the potential matrix is non-diagonal

$$V(Q) = \begin{pmatrix} V_{11}(Q) & V_{12}(Q) \\ V_{21}(Q) & V_{22}(Q) \end{pmatrix} \tag{2.47}$$

Now the nuclear motion equation can be written as

$$\begin{pmatrix} \hat{T} + V_{11}(Q) & V_{12}(Q) \\ V_{21}(Q) & \hat{T} + V_{22}(Q) \end{pmatrix} \begin{pmatrix} \chi_1 \\ \chi_2 \end{pmatrix} = E_\lambda \begin{pmatrix} \chi_1 \\ \chi_2 \end{pmatrix} \tag{2.48}$$

The form of Hamiltonian can be written as a sum of kinetic and potential energy matrix where the potential energy matrix is written in terms of excitation energies, harmonic oscillator potential, and some constants which are responsible for the coupling between the two states. A simple linear coupling model would be

$$\hat{H} = \begin{pmatrix} \hat{T} & 0 \\ 0 & \hat{T} \end{pmatrix} + \begin{pmatrix} E + \hat{h}_{ho} + \lambda_1 q_1 & \mu q_2 \\ \mu q_2 & E + \Delta\hat{h}_{ho} + \lambda_2 q_1 \end{pmatrix} \tag{2.49}$$

This is the *Vibronic Model Hamiltonians*. q are the dimensionless normal mode coordinates, while λs and μ are the *coupling constants*. Before moving further, let us look at some important points regarding "normal coordinates":

- Normal coordinates represent a set of one-dimensional nuclear displacement coordinate along which the nuclear vibrational motions are all simple harmonic motion.
- In general, potential energy surfaces are anharmonic for real systems. Nonetheless, close to the minimum, the potential can still be approximated by a harmonic potential. Small amplitude motions can be described in terms of normal mode coordinates.

For large amplitude motions, such as torsional rotation, an internal coordinate system might be needed.

Normal modes can be derived from cartesian coordinates, and the detail methodology is well-documented in the literature. [13]

Now, let us try to vary the values for the coupling constants to see their effect on potentials and in turn the spectrum

$\lambda_1 = 0.15eV$, $\lambda_2 = -0.1eV$, $\mu = 0.2eV$

$E = 0.2eV$, $\omega_1 = 0.10eV$, $\omega_2 = 0.10eV$

$\Delta = [0.2, 0.5, 1.0]eV$

Δ denotes the vertical energy gap between the two states. Let's look at the potential energy surfaces, and the Franck-Condon vs. vibronic spectra for the three different values of Δ.

Case 1: $\Delta = 1.0$

The energy gap between the two states is $1eV$, and the Franck-Condon approximation in this case gives a reasonable spectrum which is close to the vibronic spectrum.

Case 2: $\Delta = 0.5$

The two states some closer in energy, and the Franck-Condon approximation starts to

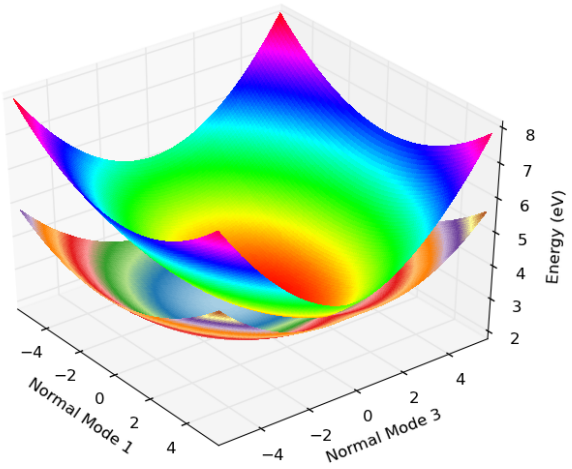

Figure 2.4: Two dimensional PESs for the two states for Case 1

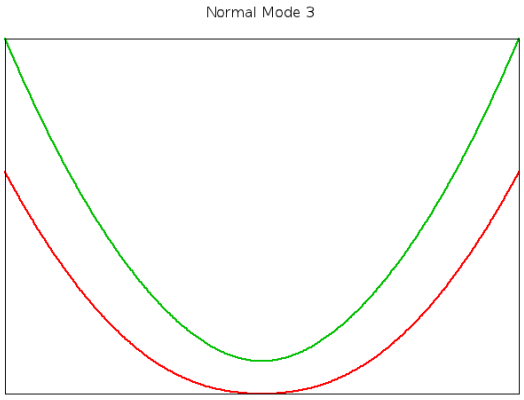

Figure 2.5: One dimensional PESs along one of the normal modes for Case 1

break down. It is also clear that a harmonic approximation to the lower PES is just not good.

Case 3: $\Delta = 0.2$

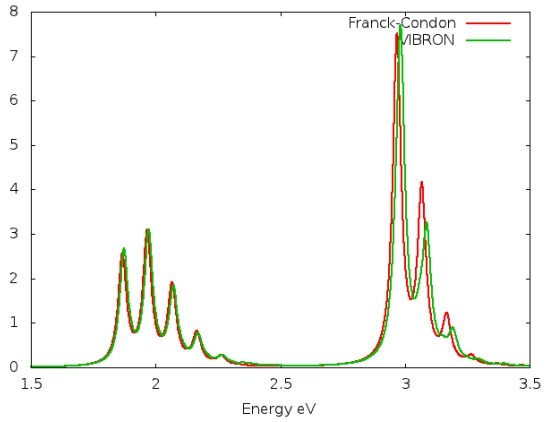

Figure 2.6: Franck-Condon vs. Vibronic Spectra for Case 1

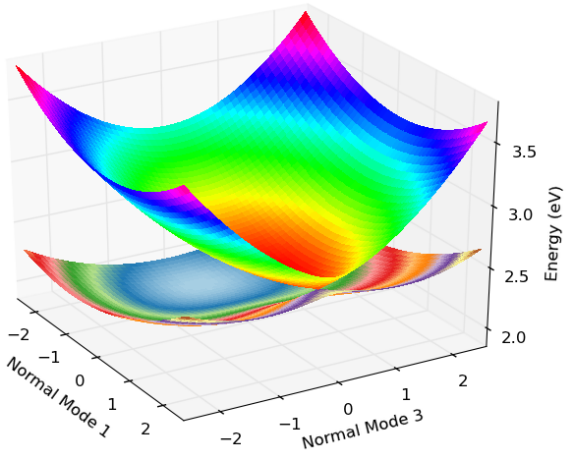

Figure 2.7: Two dimensional PESs for the two states for Case 2

The states come very close in energy now, i.e. $0.2eV$ apart, and the Franck-Condon spectrum starts to look really bad. It is important to point out that the minimum for the upper surface does not exist in this case, as discussed previously, and also the lower state PES is a double-well kind of potential and an harmonic approximation does not make any

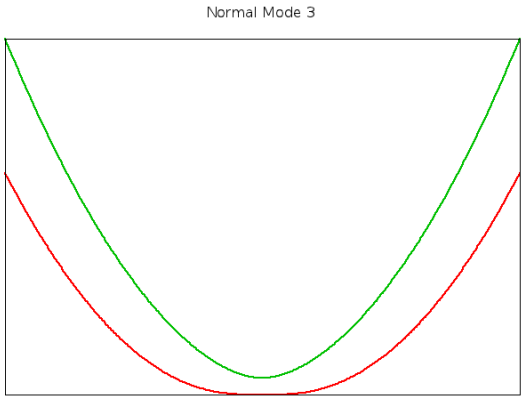

Figure 2.8: One dimensional PESs along one of the normal modes for Case 2

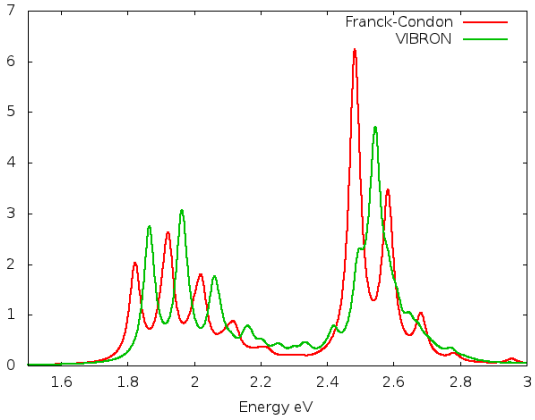

Figure 2.9: Franck-Condon vs. Vibronic Spectra for Case 2

sense at all.

The importance of vibronic coupling and the failure of the Franck-Condon approach can be seen when the states are close in energy. Let us now discuss a (routine) procedure of constructing diabatic states and calculation of coupling constants for polyatomic systems,

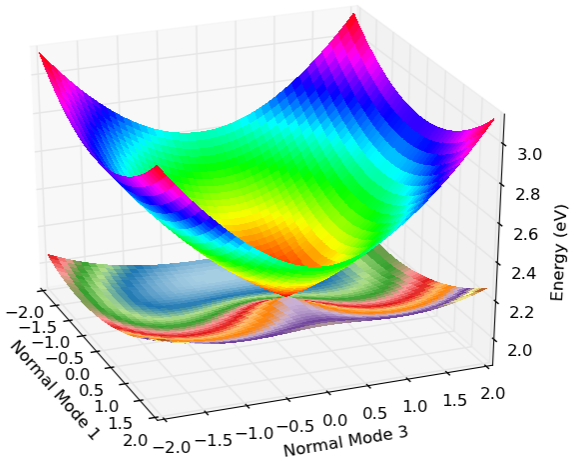

Figure 2.10: Two dimensional PESs for the two states for Case 3

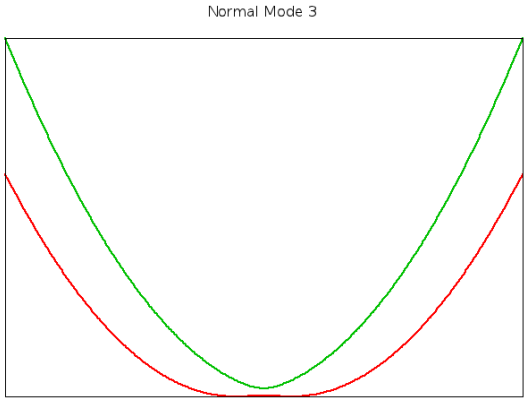

Figure 2.11: One dimensional PESs along one of the normal modes for Case 3

as implemented in the ACESII, Dalton, and ADF program suites. [14]

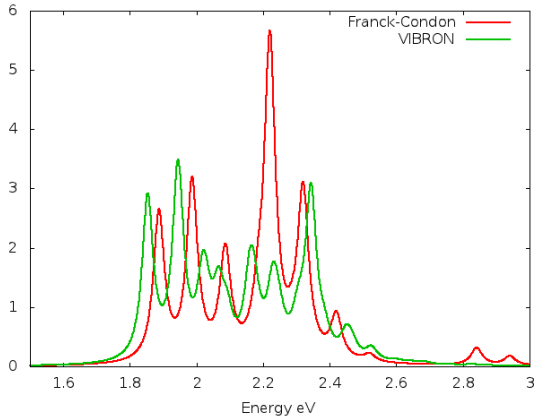

Figure 2.12: Franck-Condon vs. Vibronic Spectra for Case 3

2.4.3 Construction of Vibronic Models

We will now turn our focus towards the construction of vibronic model Hamiltonians, where the most important aspect is the diabatization scheme, which starts from the adiabatic eigenfunctions and eigenvalues and leads to a vibronic model Hamiltonian in a diabatic basis. It should be emphasized here that the adiabatic states (the BO approximate wavefunctions) are the only thing which can be calculated using the electronic structure methods.

A selected number of adiabatic states are calculated at first, a linear combination of which is used to form the diabatic states

$$\phi_d(r,Q) = \sum_{\lambda} \phi_\lambda(r,Q) U_{\lambda d}(Q) \tag{2.50}$$

where $U_{\lambda d}(Q)$ is a unitary transformation. In order to find this unitary transformation, an overlap matrix between the adiabatic states at the ground state geometry q_0 and at a slightly displaced geometry $\Delta = q_0 + dq_i$ (along the ith normal mode) is found

$$S_{\mu\lambda} \;=\; \int \phi^*_\mu(r,\Delta)\phi_\lambda(r,q_0) \tag{2.51}$$

The unitary matrix is evaluated according to the condition such that

$$S_{d\lambda} \;=\; \sum_{\mu\lambda} U_{d\mu} S_{\mu\lambda} \;\approx\; \delta_{d\lambda} \tag{2.52}$$

In general, it is not possible to find such a unitary transformation exactly [15] , but the elements of S can be made as close to zero as possible. The diabatic states thus obtained undergo as little change as possible with changes in the geometry. Now the potential matrix can be generated as

$$E_{ab} \;=\; \sum_{\lambda} U_{\lambda a} E_\lambda U_{\lambda b} \tag{2.53}$$

In order to get the vibronic coupling constants, the potential energy matrix is expanded as a Taylor series

$$V_{ab} \;=\; E_a\delta_{ab} \;+\; \sum_{i=1,N_q} E^i_{ab} q_i \;+\; \frac{1}{2}\sum_{i,j=1,N_q} E^{ij}_{ab} q_i q_j \;+\; \ldots \;\forall a,b \;=\; 1,\ldots,N_e \tag{2.54}$$

Where N_q is the number of normal modes and N_e is the number of electronic states. E_a are the vertical excitation energies, E^i_{ab} are the linear coupling constants, E^{ij}_{ab} are quadratic coupling constants and so on.

Coupling constants are obtained by the use of numerical derivatives, e.g. the linear coupling constant can be obtained as

$$E^i_{ab} = \frac{E_{ab}(q_0 + dq_i) - E_{ab}(q_0 - dq_i)}{2dq_i} \tag{2.55}$$

Coupling constants of higher order (quadratic, cubic, quartic) can also be obtained on a similar line for each normal mode. To emphasize once again, the diabatic representation is advantageous because the nonadiabatic derivative coupling elements are negligible, and equally importantly, the potential energy matrix $V_{ab}(q)$ is a smoothly varying functions of nuclear geometry, for which an accurate Taylor series expansion can be made up to low order.

Let us now move to the technique of photodetachment spectroscopy, which has used to study biradical systems and the simulation of which has been used as an application of vibronic models.

2.5 Photodetachment Spectroscopy

In photodetachment spectroscopy a molecular beam of an anionic (or neutral) species is intersected with an intense ultraviolet laser beam, resulting in photodetachment of an electron from the anion (or neutral) giving a neutral (or cationic) molecule. This process can be described as follows:

$$AB^-(E_{tot}) + h\nu \rightarrow AB(E_{tot}) + e^-(eKE) \tag{2.56}$$

As a result of the conservation of energy, measuring the electron kinetic energy (eKE) provides us with the internal energy of the neutral molecule. Photodetachment spectroscopy gives insight into the molecular structure of both the anion and the neutral species, provides information about electron affinities (EA), and also gives an idea about anharmonicities. Often if the anionic species (or any parent state) is chosen carefully, photodetachment can allow us to study a lot of unstable radical and/or cationic species, which might be difficult to study by other techniques. Let us explore briefly how some of this information can be extracted, especially in situations where the electronic states of the parent as well as the target molecule are close in energy, which will lead us to the necessity of having *multiple vibronic models*.

In the figure 2.13 the photodetachment spectra of a hypothetical system AB^- is represented schematically. Potential energy surfaces and the vibrational energy levels are shown for the ground state of the anion (A), and for the ground state (B) and first excited state (C) of the neutral AB molecule. The transition from the ground vibronic (vibrational + electronic) state of the anion to the ground vibronic state of the neutral gives the electron affinity (EA) of the neutral molecule or the ionization potential (IP) of the anion molecule. Transitions to higher vibronic levels of the neutral gives a nice vibrational progression. If a

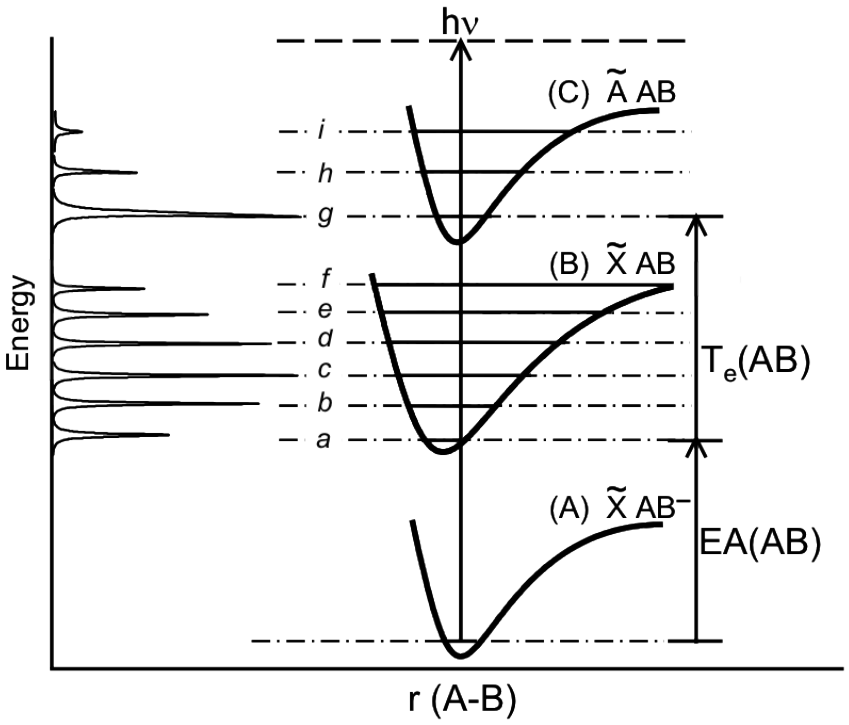

Figure 2.13: A schematic representation of the photodetachment from the ground state of the anion to the ground and first excited state of the radical

transition takes place from the excited vibronic levels of the anion to the excited vibronic levels of the neutral molecule, these peaks are termed as hot bands. One can determine the vibrational frequencies and anharmonicities by analyzing the spacings between the peaks. Moreover, the intensity pattern of the peaks can give the information about geometry changes between the anion and the neutral molecule, as is evident from the pattern of peaks for the ground and excited state of the neutral molecule.

These interpretations become difficult when the electronic states are close in energy, and the vibrational levels of different electronic state start to overlap. This is where the importance of having vibronic models comes into picture, as discussed in the previous section. What is even more important here, and is often overlooked in the literature is what happens when the electronic states of the anion are also close in energy, or even possibly the ground state is a Jahn-Teller system. This is often the case with biradical systems as we will explore further.

For such systems, a vibronic model is also constructed for the anion (or any parent state), and the ground and excited vibronic states are found in order to calculate transitions from the ground state as well as the hot bands. Let us explore the different methods of calculating the photodetachment spectra in this manner.

2.6 Calculation of Photodetachment Spectra

Till now, we have seen the theory of describing coupled nuclear-electronic problem with the vibronic model Hamiltonians. There are observables associated with these Hamiltonians which can be numerically determined. The quantities thus calculated become useful in the characterization of the dynamics of the system, and a direct comparison with the experiments can be made. As we discussed in the last section, we are interested in calcu-

lating the photodetachment spectra based on the vibronic models constructed for biradical systems. Time-independent as well as time-dependent methods of obtaining the spectra will be discussed in this section.

2.6.1 Time-independent Method

In the time-independent picture, the spectral intensity distribution is calculated for an electronic (or vibronic) transition from the parent state to the vibronically coupled manifold of target states. According to Fermi's golden rule the distribution is described by the function

$$P(E) = \sum_{\nu} |\langle \Psi_i | \hat{T} | \Psi_\nu \rangle|^2 \delta(E - E_\nu + E_i) \tag{2.57}$$

In the above equation, $\hat{T}$ represents the transition operator and E is the energy transferred to the system. Ψ_i is the set of initial states for the parent anion, while Ψ_ν is the set of final states obtained by solving for the respective vibronic Hamiltonians. A number of roots for the vibronic eigenstates of the parent state are calculated, and contribution from each root is taken in calculating the intensities depending on the temperature, and in turn the Boltzmann factor of the each state. The transition moment is obtained by the sum of vibrational projections of the electronic sub-blocks of the final state eigenvector onto the

vibronic wavefunction of the initial state.

One major step in the calculation of spectrum is solving the eigenvalue problem for the vibronic Hamiltonian of the target states. In order to do this, the state vector is expanded in a direct-product basis of suitable harmonic oscillator wavefunctions

$$|\Psi_\nu\rangle = \sum_{i,n_1,n_2,\ldots,n_k} {a_{n_1,n_2,\ldots,n_k}}^{(\nu)} |\Phi_i\rangle|n_1\rangle|n_2\rangle \ldots |n_k\rangle \tag{2.58}$$

Where the subscripts $1 \ldots k$ stand for the set of vibrational normal modes, and the expansion coefficient ${a_{n_1,n_2,\ldots,n_k}}^{(\nu)}$ are determined numerically. Numerical techniques such as Lanczos algorithm are used to solve the full eigenvalue problem, but it still remains a major computational challenge because of an exponential increase in basis function as the number of vibrational modes increases. Let's say if there 6 vibrational modes, and 20 basis functions are required to get the converged results, the total dimension of the space becomes 20^6, which means diagonalizing a Hamiltonian of this size! In order to overcome this problem, time-dependent approaches are used to solve the nuclear dynamical problem, which are computationally more efficient.

2.6.2 Time-dependent Method

Let us now look at the time-dependent method of solving the Schroedinger equation which is computationally less expensive and also provides some additional insight into the vibronic dynamics. The basic idea is the evolution of wavepacket on the coupled potential energy surfaces. Let us try to explore the time evolution of an initial wavepacket $\Psi(0)$ which is formed from an initial state Ψ_i by means of optical excitation using a short laser pulse. This can be written with the help of transition operator as

$$|\Psi(0)\rangle = \hat{T}^{\dagger}|\Psi_i\rangle \tag{2.59}$$

The Condon approximation is used during the excitation which assumes that the nuclei do not move when an electron is ejected and this amounts to vertically lifting the nuclear wavefunction of the initial state to the target state PESs. As a first step, the ground state wave function for the anion (initial state) is obtained by applying the energy relaxation (propagation in imaginary time) to a guess wavepacket using the vibronic model Hamiltonian created for the anion. Different approaches for relaxation will be discussed in the next chapter. The vertical excitation involves taking the lowest energy eigenfunction of the anion and placing it to all of the diabatic states of the target molecule.

The time evolution of the wavepacket under the influence of the vibronic Hamiltonian

changes position, shape, and electronic composition. These changes are captured by the autocorrelation function

$$C(t) \;=\; \langle \Psi(0) | \Psi(t) \rangle \;=\; \langle \Psi(0) | \exp^{-iHt/h} \Psi(0) \rangle \tag{2.60}$$

The spectrum can be calculated by taking the Fourier transform of the autocorrelation function

$$I(\omega) \;\sim\; \omega \int dt C(t) \exp i\omega t \tag{2.61}$$

We need the knowledge of the state vector $|\Psi(t)\rangle$ which is obtained by solving the time-dependent Schroedinger equation. This is done using the Multi Configuration Time Dependent Hartree (MCTDH) wavepacket propagation method. [16] In this scheme, a multiconfiguration ansatz for the wavefunction is used, where each configuration is expressed as a Hartree product of time-dependent basis functions, known as Single Particle Functions (SPFs). For a *multiset* formulation, the wavefunction can be written as

$$\Psi(Q_1, Q_2, \ldots, Q_f, t) \;=\; \Psi(q_1, q_2, \ldots, q_p, t) \;=\; \sum_{\alpha=1}^{\sigma} \sum_{j_1=1}^{n_1{}^{(\alpha)}} \cdots \sum_{j_p=1}^{n_p{}^{(\alpha)}} A^{(\alpha)}_{j_1 \ldots j_p}(t) \times \prod_{k=1}^{p} \phi^{(\alpha,k)}_{jk}(q_k, t) | \alpha \rangle \tag{2.62}$$

$$= \sum_{\alpha} \sum_{j} A_J^{(\alpha)} \Phi_J^{(\alpha)} |\alpha\rangle \tag{2.63}$$

In the above equations, f and p represent the number of vibrational degrees of freedom, and MCTDH particles respectively. $A^{(\alpha)}_{j_1 \ldots j_p}$ represents the time-dependent expansion coefficients while $\phi^{(\alpha,k)}_{jk}$ are the one-dimensional expansion functions, known as SPFs. The labels α are indices representing the manifold of electronic states. The Wavepacket , $\Psi^{(\alpha)} (= \sum_J A_J^{(\alpha)} \Phi_J^{(\alpha)}$ associated with each electronic state is described using a different set of SPFs, namely $\{\phi^{(\alpha,k)}_{jk}\}$. In a *single set* formalism, the same set of SPFs are used for every electronic state. The equations of motion can be derived for both the expansion coefficients as well as the SPFs using the variational principle.

The accuracy of a MCTDH calculation relies heavily on the chosen size of the primitive and the SPF basis functions. Convergence criteria may be different for different properties or even differing for individual systems, so it is hard to come up with a general recipe. The quality of SPF basis is reflected in the population of natural orbitals. If a calculation contains natural orbitals with a low population, these are not significant for the representation of the wavefunction, and the calculation is of a reasonable quality. As a general rule of thumb, when the population of the highest (least populated) natural orbital falls below 1 percent (i.e. a population below 0.01), the calculation will be reasonable, although strict convergence may not have been reached.

Let us briefly look at the memory requirement for the MCTDH method. The memory required by standard method is proportional to N^f , where N is the total number of grid points or primitive basis functions and f is the total number of degrees of freedom. In contrast, memory needed by the MCTDH method scales as

$$memory \sim fnN + n^f \tag{2.64}$$

where, n represent the SPFs. The memory requirements can however reduced if SPFs are used that describe a set of degrees of freedom, termed as *multimode* SPFs. By combining d degrees of freedom together to form a set of $p = f/d$ particles, the memory requirement changes to

$$memory \sim f\tilde{n}N^d + \tilde{n}^f \tag{2.65}$$

where $\tilde{n}$ is the number of multimode functions needed for the new particles. If only single-mode functions are used i.e. $d = 1$, the memory requirement is dominated by n^f . By combining degrees of freedom together this number can be reduced, but at the expense of longer product grids required to describe the multimode SPFs.

Chapter 3

Computational Framework

The theory of vibronic coupling and the methods concerning the simulation of photodetachment spectra for biradicals were discussed in the previous chapter. In this chapter, the actual computational steps involved in the calculation of the spectrum will be delineated. We will use NO_2 as an illustrative example to explain the machinery of the calculations while taking a brief look at what goes in and what comes out at each step of the calculation.

The entire process of simulating the spectrum from first principles can largely be categorized into two parts – first, the vibronic model Hamiltonians are created for the parent state as well as the target state(s). This is the *Electronic Structure* part of the calculation. Once the model Hamiltonians are created and coupling constants are obtained, the *Nuclear Dynamical* calculations are carried out in order to generate the spectrum. The ACESII

quantum chemistry program package has been used for the electronic structure part, while for the second part, VIBRON and MCTDH suites of program have been utilized.

First, let us briefly look at the general functionality of the aforementioned programs. We will then move to the detailed computational process using NO_2 as an example. To aid future users of the programs input files will be provided for each step documenting the calculations.

3.1 Brief Overview of Functionalities of ACESII, VIBRON, and MCTDH

ACESII is an electronic structure software package, [17] which is capable of performing ground and excited states calculations using the EOM and STEOM class of methods. A local version is actively maintained in our group by Prof. Marcel Nooijen. The local version provides the functionality for DIP-STEOM calculations, as well as the generation of vibronic model Hamiltonian using a suitable diabatization scheme.

VIBRON is a computer program developed in our group by Anirban Hazra and Prof. Marcel Nooijen, [18] which extracts the vibronic coupling constants which are essentially given by the ACESII program. VIBRON is also capable of simulating nonadiabatic vibronic

spectra using time-independent techniques as well as harmonic and full Born-Oppenheimer Franck-Condon spectra.

MCTDH is a suite of programs developed in the Heidelberg group of Hans-Dieter Meyer, Germany, to perform multi-dimensional quantum dynamics which uses the MCTDH algorithm to do the wavefunction propagation. The algorithm solves the time-dependent Schroedinger equation for multidimensional dynamical systems consisting of distinguishable particles. MCTDH is therefore capable of determining the quantal motion of the nuclei of a molecular system evolving on one or several coupled electronic potential energy surfaces. MCTDH by its very nature is an approximate method. However, it can be made as accurate as desired, but at an increasing computational cost, sometimes even prohibitive. [19]

3.2 The Computational Scheme

The process of simulating the photodetachment spectrum can be largely broken down into the following steps:

- Geometry optimization and vibrational frequency calculation of reference state: `ACESII`

- Calculation of Ionization energies using IP-EOM-CC/DIP-STEOM-CC methods at a single geometry to determine the number of states to be included in the vibronic model: `ACESII`
- Construction of vibronic models by calculating diabatic energy matrices at a large set of displaced geometry: `ACESII`
- Calculation of coupling constants: `VIBRON`
- Generation of potential energy surfaces: `VIBRON`
- Simulation of photodetachment spectra: `VIBRON/MCTDH`

Let us now take a closer look at the each of the steps involved in the computational process.

Geometry optimization and vibrational frequency calculation of reference state

In order to create vibronic models for the parent and target states, a suitable reference geometry is required. For biradicals, this geometry is either taken as the ground state equilibrium geometry of the closed-shell (dianionic) parent state or the ground state equilibrium geometry of the neutral triplet state of the biradical. For NO_2, the reference

geometry is taken as the equilibrium geometry of NO_2^-, the closed shell anion. The geometry optimization is performed at the CCSD level of theory using the TZ2P basis set. Following the optimization, the vibrational frequency calculation is performed in order to obtain harmonic frequencies. In addition, a force constant matrix (fcmfinal) as well as a file (normal_fdif) containing information about normal modes is generated, which will be used later on during the construction of vibronic models.

```
NO2 anion opt + freq with fcm
O
N 1 NO*
O 2 NO* 1 A*

NO=1.3
A=120.0

*ACES2(BASIS=TZ2P,CHARGE=-1,CALC=CCSD,DROPMO=1>3,VIB=FINDIF)
DAMP_TYPE=DAVIDSON)
```

Figure 3.1: Input file for the optimization and frequency calculation

Table 3.1: Optimized parameters for the closed-shell anion

$R(NO)$	$1.261A^0$
$A(ONO)$	115.911^0

Table 3.2: Vibrational normal modes for the closed-shell Anion

Normal Mode	Description	Frequency (cm^{-1})	Frequency (eV)
1 (A_1)	ONO Bending	806.55	0.099
2 (A_1)	NO Symmetric Stretch	1369.07	0.169
3 (B_1)	NO Asymmetric Stretch	1293.21	0.160

Single point IP-EOM/DIP-STEOM CC calculations

The next step is the single point STEOM calculation which provides us with the excitation energies of the target biradical, both of singlet and triplet states. By observing the energy ordering of the excited states, we can decide what states are to be included in the calculation of the vibronic model, leading to a manifold of coupled states on which nuclear dynamics will be carried out later. As discussed in the theory section, we start from the closed-shell parent state which has two extra electrons compared to the target state, and then two holes are created in order to get the different roots of the target states. First, the ionized states are calculated by creating one hole in the closed-shell species using IP-EOMCC method. These states act as an active space for the calculation of the double ionized states, which are the states of the target molecule. Usually, a large number of roots are calculated for the IP case, which can be selected by giving a cut-off value of the ionization potential using

the *ip_low* keyword in the **mrcc_gen* namelist. What value is suitable can be judged by looking at the orbital energies of the parent state. As for the roots of STEOM calculation, a large number of roots are usually asked as the calculation is very cheap computationally and the DIP_SYM keyword can be used to ask for the desired roots of a given symmetry corresponding to the point group symmetry of the molecule.

```
NO2- steom calculation
O
N 1 NO
O 2 NO 1 A

NO   =     1.2612565949
A = 115.9110634640

*ACES2(BASIS=TZ2P,CHARGE=-1,CALC=CCSD,DROPMO=1>3
IP_CALC=IP_EOMCC
DIP_CALC=STEOM,DIP_SYM=5-4-1-1/3-2-1-1)

*mrcc_gen
ip_low=-14.0
*end
```

Figure 3.2: Input file for the STEOM calculation

Construction of vibronic models

Once the excitation energies have been obtained from the STEOM calculation, we can set up the calculation for creating the vibronic models. An effective diabatic Hamiltonian yielding the energies of the excited states at displaced nuclear geometries is created using the discussed diabatization scheme for the parent as well the target state(s). One of the important keywords in this calculation is GRID_VIBRON which specifies the order of

Table 3.3: Ionization energies of the anion calculated using IP-EOM-CCSD

State	Ionization Energy (eV)
$^2A_1$	2.42
$^2B_1$	3.40
$^2A_2$	3.89
$^2B_2$	8.64
$^2A_1$	8.78
$^2B_1$	9.35

coupling constants to be calculated. Following are the specifications for associated values of GRID_VIBRON used in the calculations

Table 3.4: Double ionization energies of the anion calculated using DIP-STEOM-CCSD

State	Ionization Energy (eV)
$^1A_1$	14.59
$^1A_2$	16.06
$^1B_1$	16.84
$^1B_2$	17.70
$^1A_1$	18.01
$^3B_1$	14.45
$^3A_2$	15.66
$^3B_2$	17.06

Table 3.5: Description of GRID keywords and the couplings associated: L(Linear), DQ(Diagonal quadratic), ODQ(Off-diagonal quadratic), SS (Same Symmetry), DS (Different Symmetry), JT (Jahn-Teller), DC(Diagonal Cubic), DQR(Diagonal quartic), Degenerate OD (off-diagonal) bi-cubic/bi-quartic terms

GRID/Coupling	L	DQ	ODQ(SS)	ODQ(JT)	ODQ(DS)	DC & DQR	Degenerate OD
			Duschinsky Rotation	Nonadiabatic			
2	✓	✓	-	-	-	-	-
3	✓	✓	✓	-	-	-	-
4	✓	✓	✓	-	✓	-	-
5	✓	✓	-	-	-	✓	-
6	✓	✓	✓	-	-	✓	-
7	✓	✓	✓	-	✓	✓	-
8	✓	✓	-	✓	-	-	✓
9	✓	✓	-	✓	-	✓	✓
10	✓	✓	✓	✓	-	✓	✓
11	✓	✓	✓	✓	✓	✓	✓

Next, the manifold of states is selected using the keywords heff_low and heff_high by looking at the energy values obtained from the STEOM calculation. The lower limit is taken to be slightly below the energy of the ground state of the singlet (and similarly for triplet) while the upper limit is chosen when there is a considerable gap in the energy of excited states. Different threshold can be selected for the singlet and triplet states of the biradical.

For NO_2, three vibronic models have been constructed using $GRID = 7$:

1. NO_2 Radical: 6 lowest ionized states
2. NO_2 Cation : 5 lowest double-ionized singlet states
3. NO_2 Cation: 3 lowest double-ionized triplet states

Calculation of coupling constants

Using the output of previous calculation, coupling constants are calculated using numerical differentiation in the VIBRON program. Moreover, coupling terms that are forbidden by symmetry are set to zero during this calculation. The output file *cp.h* is copied to *cp.auto*, which is the final vibronic model, and contains all the required information in order to generate the potential energy surfaces and to simulate the photodetachment spectra.

```
NO2- prep vibron
O
N 1 NO
O 2 NO 1 A

NO   =     1.2612565949
A = 115.9110634640

*ACES2(BASIS=TZ2P,CHARGE=-1,CALC=CCSD,DROPMO=1>3
IP_CALC=IP_EOMCC,PREP_VIBRON=ON,MEM=1GB
GRID_VIBRON=7,CC_CONV=10,SCF_CONV=10,ESTATE_TOL=10
DIP_CALC=STEOM,DIP_SYM=5-4-1-1/3-2-1-1)

*ip_eom
diabatize=on
heff_low=1.0
heff_high=11.5
ee_table=on
*dip_steom
ee_table=on
diabatize=on
heff_low=10.0
heff_high=18.5
*mrcc_gen
ip_low=-14.0
*end
```

Figure 3.3: Input file for the construction of vibronic models

Let us look at the linear coupling constants for all three models of NO_2. A large coupling constant, i.e. greater than 0.1 is indicative of strong coupling between the electronic states.

Generation of potential energy surfaces

The potential energy surfaces are generated corresponding to each normal mode for all of the models using the respective *cp.auto* files. One dimensional surfaces can be generated

```
    0              ! units in eV
    6              ! Number of electronic states
    2              ! Number of symmetric normal modes
    1              ! Number of non-A1 normal modes
  500              ! Number of Lanczos iterations
  0   0
   0.099990    0.169741
  0
   0.160254
  0.100
  3.000
 auto

*vibron
 short_title=cp
 refine_coupling=on
 cubic=on
 quartic=on
*solve_coupling
 purify_couplings=on
*end
```

Figure 3.4: Input file for the calculation of coupling constants

along a particular direction for any normal mode. Two dimensional surfaces can also be generated along a pair of normal modes.

Calculation of photodetachment spectra

Once the potential energy surfaces have been generated successfully, it can be seen that the constructed vibronic model is able to give a compact representation of the complicated coupled surfaces. Now, the utility of these models lies in calculating quantities which can be observed experimentally. As it has been discussed before, the photodetachment spectra will be simulated using these vibronic models.

Table 3.6: Linear coupling constants between states of the radical for NO symmetric stretch

	$^2A_1$	$^2B_1$	$^2A_2$	$^2B_2$	$^2A_1$	$^2B_2$
$^2A_1$	-0.349426	0.000000	0.000000	0.000000	0.233663	0.000000
$^2B_1$	0.000000	0.091054	0.000000	0.000000	0.000000	0.142089
$^2A_2$	0.000000	0.000000	0.096010	0.000000	0.000000	0.000000
$^2B_2$	0.000000	0.000000	0.000000	0.344791	0.000000	0.000000
$^2A_1$	0.233663	0.000000	0.000000	0.000000	0.268042	0.000000
$^2B_2$	0.000000	0.142089	0.000000	0.000000	0.000000	0.168995

Photodetachment spectra will be simulated for NO_2 leading to a description of singlet and triplet states of $NO_2{}^+$. We will look at the time-independent as well as time-dependent method of simulating the spectra as discussed in the theory section, and a comparison will be made between the two approaches as well as to the experiment for both cases. In addition, hot bands will be calculated for the triplet states using both the approaches at a temperature of $800K$. A similar methodology will be used for all the other molecules in following chapters.

1. VIBRON: eigdirect/special-seed

In the time-independent scheme of things, the lowest vibronic eigenstates are calculated

Table 3.7: Linear coupling constants between Singlet states of the cation for NO symmetric stretch

	$^1A_1$	$^1A_2$	$^1B_1$	$^1B_2$	$^1A_1$
$^1A_1$	-0.414290	0.000000	0.000000	-0.381733	0.000000
$^1A_2$	0.000000	-0.233390	0.000000	0.000000	0.000000
$^1B_1$	0.000000	0.000000	-0.224120	0.000000	0.000000
$^1B_2$	-0.381733	0.000000	0.000000	0.232721	0.000000
$^1A_1$	0.000000	0.000000	0.000000	0.000000	0.048223

Table 3.8: Linear coupling constants between Triplet states of the cation for NO asymmetric stretch

	$^3B_1$	$^3A_2$	$^3B_2$
$^3B_1$	0.000000	0.000000	0.000000
$^3A_2$	0.000000	0.000000	0.287190
$^3B_2$	0.000000	0.287190	0.000000

```
     0              ! units in eV
     6              ! Number of electronic states
     2              ! Number of symmetric normal modes
     1              ! Number of non-A1 normal modes
   500              ! Number of Lanczos iterations
   0   0
    0.099990    0.169741
   0
    0.160254
   0.100
   3.000
 auto

*vibron
 short_title=plt
 plot_surface=on
 cubic=on
 quartic=on
*plot_surface
 stepsize=0.1
*end
```

Figure 3.5: Input file for the generation of potential energy surfaces

first using a direct diagonalization method. An output file *eig*.25 is created containing the dominant part of the lowest eigenfunctions. This file will be used to read in the absorbing states in the subsequent calculation.

Next, a Lanczos calculation is performed with the keyword *special_seed=on*, the absorbing states are read from the file *eig*.25.

In order to calculate hot bands, the two parameters in the *special_seed* calculations are changed, namely the Boltzmann threshold, and the temperature at which the simulation is taking place. Boltzmann population for each absorbing state in the *eig*.25 is calculated, and if the population is above the threshold, contribution to the spectrum from that root

is calculated. A table showing the lowest eigenstates as well as their Boltzmann population at $800K$ is shown in the table 3.9 .

Table 3.9: Vibronic eigenvalues of the radical as calculated in VIBRON and MCTDH with Boltzmann population at 800K

Root	VIBRON Energy (eV)	MCTDH Energy (eV)	Boltzmann Population
1	1.754	1.754	0.614
2	1.854	1.854	0.164
3	1.895	1.895	0.079
4	1.936	1.936	0.043
5	1.936	1.936	0.043
6	1.986	1.986	0.021
7	2.027	2.027	0.012
8	2.027	2.027	0.012
9	2.038	2.038	0.009
10	2.076	2.076	–

2. MCTDH: block-improved-relaxation/propagation

A similar set of calculations are performed in the time-dependent scheme of things. First, an operator file is created for all the three models containing all the information about vibronic Hamiltonian (similar to *cp.auto*) compatible to MCTDH program. Generating these MCTDH operator files is a feature of the VIBRON program developed in our group by Prof. Nooijen and an undergraduate student Yao Li. As the first step of calculating the vibronic eigenstates of the radical, a *block-improved-relaxation* calculation is performed which uses the block-Davidson algorithm [20]. Two such calculations are carried out for both the radical and singlet cation as well as the radical and triplet cation. For this and further calculations, we need two combined operator files for the two cases to have the same degrees of freedom for propagation as that of the relaxation. This is a technical issue in the MCTDH code. The operators files are merged using a Python script, which can be found in appendix.

In the output of *block-improved-relaxation*, a *restart* file for each eigenstate containing the information about the wavefunction is generated as *rst000*, *rst001*, *rst002* and so on. These files will be read as the absorbing state in the subsequent propagation calculation. In MCTDH, there are other methods of finding the vibronic eigenstates using different relaxation schemes, however, we have not been able to get consistent results for all the available methods, and the *block-improved-relaxation* will be used for all the subsequent calculations carried out in this work. One disadvantage of *block-improved-relaxation* is that

it only allows to perform a *single-set* kind of calculation where a same set of SPFs are used for each electronic state. However, this often is able to give reasonable results and also in the case of larger systems (chapter five - cyclobutadiene and tmm), *multi-set* calculation might be computationally very expensive! This will be discussed further in the mentioned chapter.

All the spectra are calculated as the Fourier transform of the autocorrelation functions generated by the wavepacket propagation. The `autospec84` program of MCTDH package is used to generate the spectrum. Let us say we want to calculate the spectrum for the singlet cationic states of the NO_2, the following command has to be executed

```
autospec84 -e -1.754 eV 10 16 eV 30 1
```

Since the ground state energy is not zero, -e option is used to shift the energy scale by the ground state energy amount to get the correct ionization energies. The spectrum is calculated for the energy range of 10 to 16 eV, while the linewidth is $30cm^{-1}$.

Boltzmann averaging of spectra can be performed using the `sumspec84` program which calculates the total spectrum as a weighted sum of individual spectrum where the weight is given by the Boltzmann population of the individual state. For example, the hot band spectrum for the triplet cation state can be calculated as

```
sumspec84 s0 0.614 s1 0.164 s2 0.079 s3 0.043 s4 0.043 s5 0.021 s6 0.012
```

```
s7 0.012 s8 0.009
```

This generates a file called *sumspec.pl* which is the Boltzmann sum of individual spectrum. Similarly, the total spectrum for cationic NO_2 taking individual contributions from singlet (one part) and triplet (three parts) can be calculated using the same program.

3.3 Comparison of Different Spectra

Now we are in a position to make comparison between different spectra. Comparison to the experimental spectrum is what constitutes the accuracy of a model/method to interpret the experiment in terms of theoretical concepts and to possibly resolve any existing conflicts. Theoretical models, if correct, also give the power to predict spectra for new molecules and motivation to carry out such experiments, which might be useful in various fields of chemistry and physics.

One question to ask here is, " *Why do we compare the spectrum calculated from VIBRON to that calculated from MCTDH?*" As stated earlier, MCTDH by it's very nature an approximate method, while the time-independent calculations perform *exact diagonalization* of the Hamiltonian within the basis set used to expand the wavefunctions. MCTDH can be converged to give the same results as those given by the time-independent method. Since time-independent methods can not be applied to the systems larger than $6-7$ degrees of

freedom, we have to rely on MCTDH program for the systems of bigger size, such as cyclobutadiene (18 vibrational degrees of freedom) and trimethylenemethane (24 vibrational degrees of freedom). Therefore, it is essential that an agreement is reached between the two spectra for small molecules. Specially, the calculation of spectra using the schemes outlined in this thesis is either not studied or not very well-documented in the literature to the best knowledge of the author, and thus it makes it even more important to gauge the accuracy of these programs. From a practical point of view, we need to learn how to use the MCTDH program, and also explore many different features/methods available to perform quantum dynamics.

Note:The time-independent and the time-dependent methods should give exactly the same spectrum for the same parameters as they are just different ways of looking at one thing, more like two sides of a coin. The underlying physics does not change. To think of it in simple terms, we might think of a white light passing through a prism, which splits into seven color beams on the other side of the prism. Did the information contained change? No, it has just revealed another hidden aspect of it.

For the photodetachment spectrum, $NO_2^+ \longleftarrow NO_2$, we can see an excellent agreement between the VIBRON spectrum and the MCTDH spectrum (figure 3.13) for both singlet as well as triplet states. This confirms the well-behaved nature of both the programs, and gives us confidence to apply the same methodology to other molecules.

Five bands are seen in the experimental spectrum (figure 3.14), which can be assigned to the singlet and triplet states by comparing to the simulated spectrum. The first band (labelled 1 in the experimental spectrum) in the range of $10 - 12eV$ corresponds to the lowest singlet state ($^1A_1$) of the cation. The second band in the range of $12 - 13.5eV$ corresponds to the lowest triplet state ($^3B_1$) of the cation. Band 3 and 4 are the result of overlapping bands of first excited states of singlet and triplet ($^1A_2$ and $^3A_2$ respectively) while the fifth band corresponds to the second excited state of the singlet state ($^1B_1$) of the cation.

For the hot band spectrum also, we get an excellent agreement between VIBRON and MCTDH, for the total spectrum as well as for the individual spectrum starting from different roots of neutral. We can also see in the figure 3.16 that the spectrum changes pattern significantly depending on the starting state of the neutral molecule. Also, a comparison is made for the triplet hot band spectrum (at $800K$) with the $0K$ spectrum which does not show major differences. This would seem to indicate that the vibrational levels are evenly spaced (harmonic). In that case one would only expect slight intensity changes, while the position of the bands is unchanged. This is more or less what is observed here.

3.4 Treatment of Jahn-Teller Systems: A prototype case

The reasons pertaining to the deviations from adiabatic approximation were discussed in the previous chapter. Perhaps the most striking breakdown of the Born-Oppenheimer approximation takes place due to the presence of orbitally degenerate electronic states. The Jahn-Teller theorem states that *any nonlinear polyatomic system in a symmetry induced degenerate state will undergo a geometric distortion such that the degeneracy is lifted, and the symmetry is lowered.* Longuet-Higgins in 1958 [21] calculated the vibronic energy-level structure resulting from the interaction of a doubly degenerate electronic state (E) with one doubly degenerate vibrational mode ($e^{'}$), famously known as the $E\otimes e$ JT effect. Interesting features and complications arise due to the conical intersection of two potential energy surfaces. In this section, we want to address two important aspects of JT states which arise in spectroscopy: the interference effect and the effects of the transfer of transition amplitude between the two degenerate state.

The interference effect arises due to the surface coupling (conical intersection!) between two states which shows that if we calculate the spectrum for two states individually and sum them up, the resulting spectrum is far from the spectrum of individual states. A more subtle issue arises in the definition of Jahn-Teller states. Since the states are orbitally

degenerate, how does one distinguish between the states or even label them as state 1 or 2? Are the states uniquely defined? Why is this important to consider? We know that the states are coupled, and the wavepacket dynamics takes place on both the surfaces simultaneously and the spectrum shows vibronic features from both the surfaces. Now the question arises where does one place the initial wavepacket? The simplest solution would be to place the wavepacket on one state at $t = 0$, calculate the spectrum for that state, and repeat the same procedure for the second state and then sum the spectra. But since a linear combination of the degenerate states is as good a representation of the two states as the individual state, what if we put part of the wavepacket on one surface and the remaining on the other and do the same for another orthogonal linear combination, and then sum the spectra? Will the resulting spectrum remain invariant?

We will try to find answers to these questions by looking at a simple prototype case of $E \otimes e$ JT system, the C_3 biradical at a D_{3h} geometry. The first two triplet excited states of the biradical are doubly degenerate, which couples through the normal modes 2 and 3 of $e^{'}$ symmetry. The anionic ground state is degenerate but we will lift the degeneracy manually in order to find a non-degenerate vibronic ground state which will be the absorbing state for further analysis. Let us consider a case of photodetachment spectra, where we go from the non-degenerate anionic ground state into the first excited JT pair of the neutral triplet molecule. For the sake of convenience let us the call the state $^3B_2$ as state 1 and the state

$^3A_1$ as the state 2.

Let us look at four different cases of excitation from the anionic ground state to the first excited pair of triplet JT states, the numbers corresponding to each state represent the transition moments for that state:

Case 1: State 1 = 0.1, State 2 = 0.0

Case 2: State 1 = 0.0, State 2 = 0.1

Case 3: State 1 = -0.0707, State 2 = 0.0707 (Antisymmetric)

Case 4: State 1 = 0.0707, State 2 = 0.0707 (Symmetric)

The individual spectra for these four cases are shown in figures 3.19, 3.20, 3.21 and 3.22, which all look quite different from each other. Also, the sum of spectra for case 1 and 2, and case 3 and 4 are shown in figure 3.23 which is invariant with respect to the definition of two states. It can also be seen that the individual spectra for any of the four cases are quite different from the summation of spectra of two individual cases (interference effect!).

This confirms that the sum of spectra is an invariant property, and for the other JT systems in the following chapters, only the sum of spectra will be reported for JT states, not the individual spectra for each states.

It is also worth mentioning that the sum of spectra remains the same whether calculated in VIBRON or in MCTDH, as shown in figure 3.24. This is also true for the spectrum of

individual cases. This again confirms that things are well-behaved in MCTDH and for the larger systems in Chapter five, only the MCTDH program will be used.

Table 3.10: Vibrational normal modes for C_3

Normal Mode	Frequency (cm^{-1})
1 ($A_1^{'}$)	1383.92
2 ($E^{'}$)	985.14
3 ($E^{'}$)	985.14

Table 3.11: Ionization energies of the C_3 anion calculated using IP-EOM-CCSD

State	Ionization Energy (eV)	Symmetry (D_{3h})	Symmetry (C_{2v})
1	-4.82	$^2E^{'}$	$^2B_1$
2	-4.82	$^2E^{'}$	$^2B_2$
3	-2.25	$^2A_1^{'}$	$^2A_1$

Table 3.12: Double ionization energies of the C_3 dianion calculated using DIP-STEOM-CCSD

State	Ionization Energy (eV)	Symmetry (D_{3h})	Symmetry (C_{2v})
1	-2.5	$^3A_2^{'}$	$^3B_2$
2	-0.41	$^3E^{'}$	$^3B_2$
3	-0.41	$^3E^{'}$	$^3A_1$
4	1.51	$^3E^{''}$	$^3B_1$
5	1.51	$^3E^{''}$	$^3A_2$

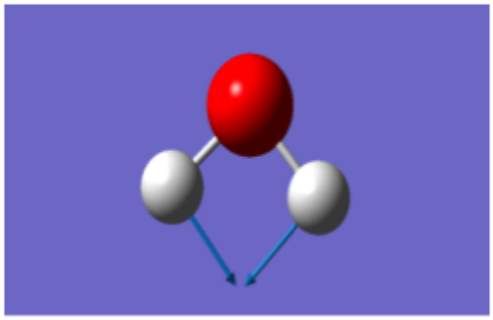

(a)

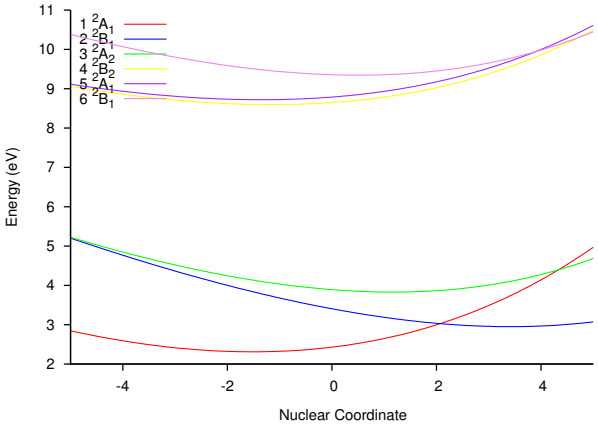

(b)

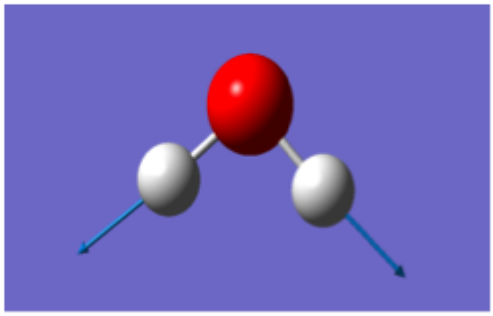

(c)

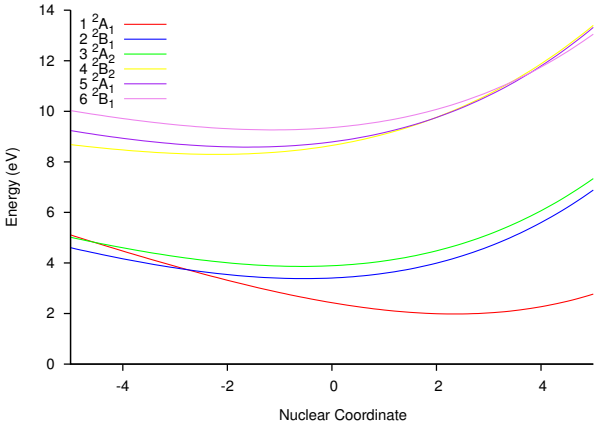

(d)

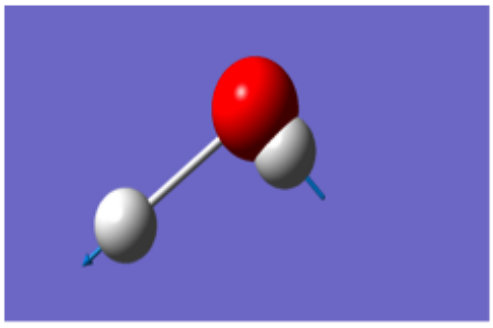

(e)

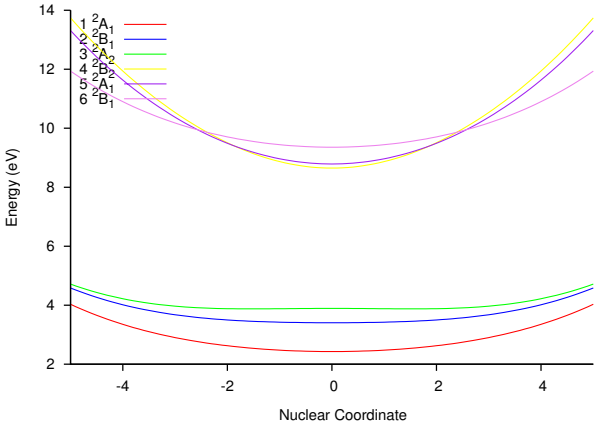

(f)

Figure 3.6: Adiabatic surfaces for the doublet states: (a,b): Bending Mode, (c,d): Symmetric Stretch, (e,f): Asymmetric Stretch

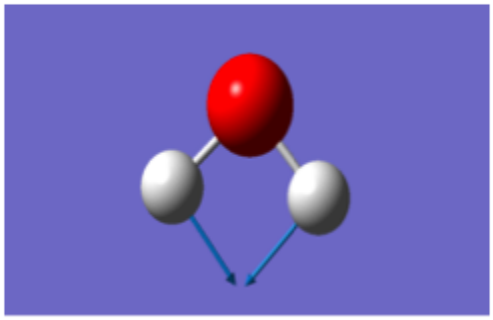

(a)

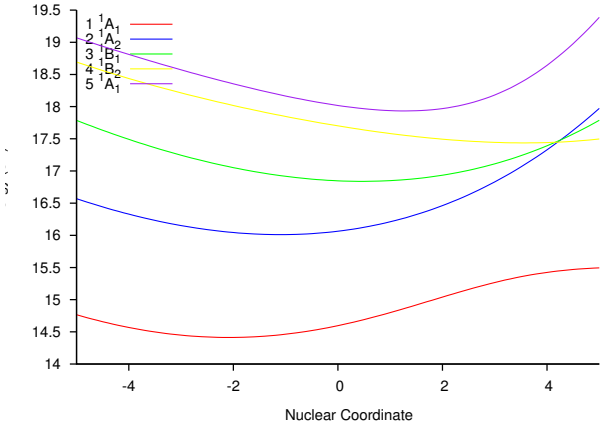

(b)

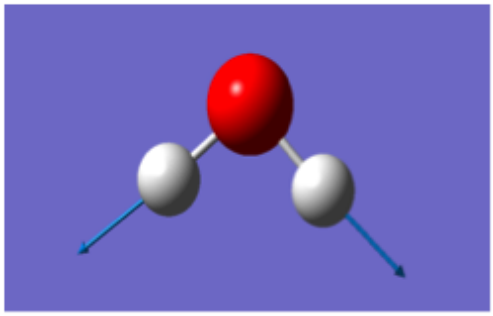

(c)

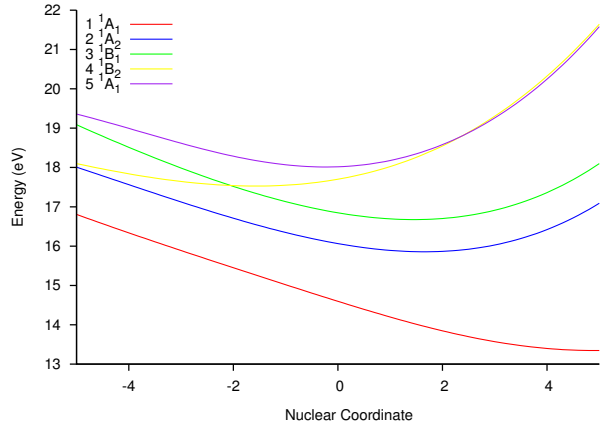

(d)

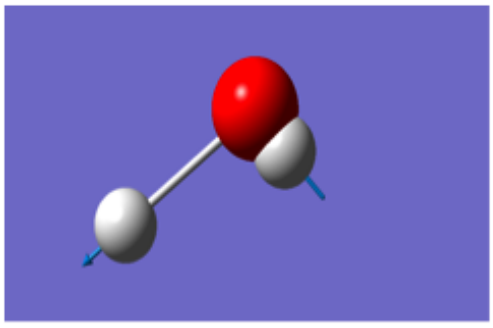

(e)

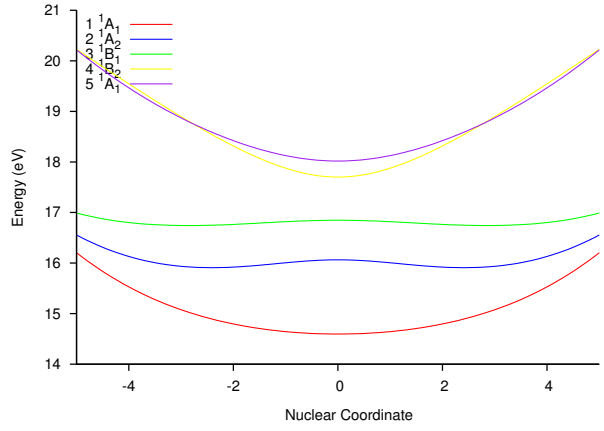

(f)

Figure 3.7: Adiabatic surfaces for the singlet states: (a,b): Bending Mode, (c,d): Symmetric Stretch, (e,f): Asymmetric Stretch

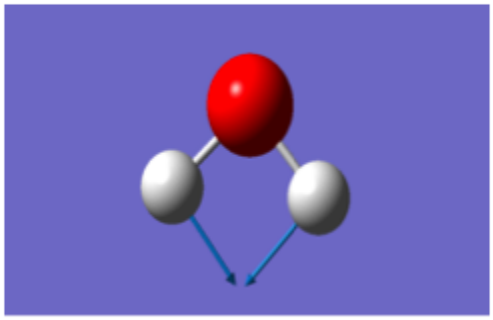

(a)

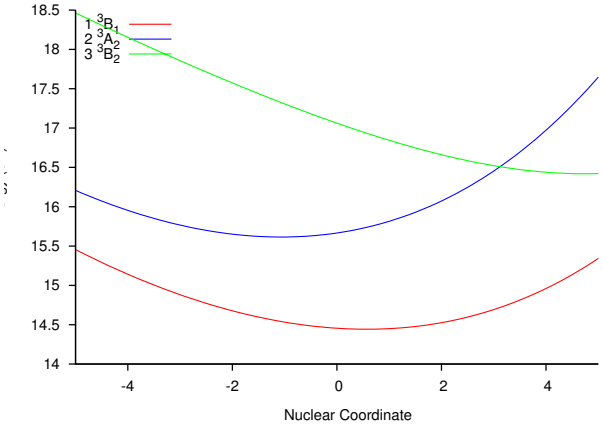

(b)

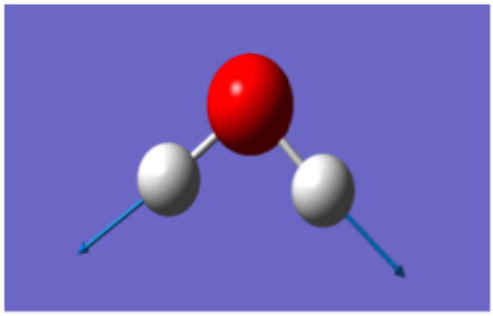

(c)

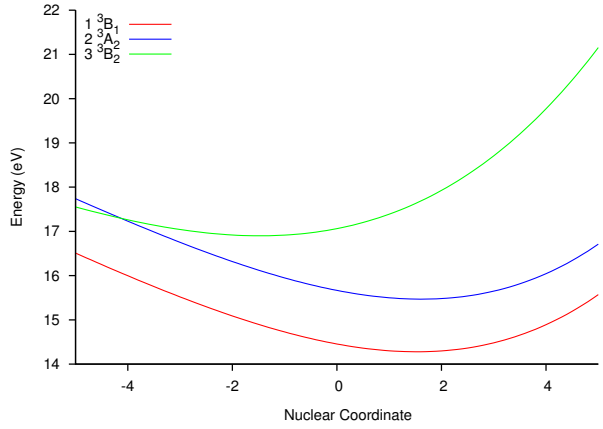

(d)

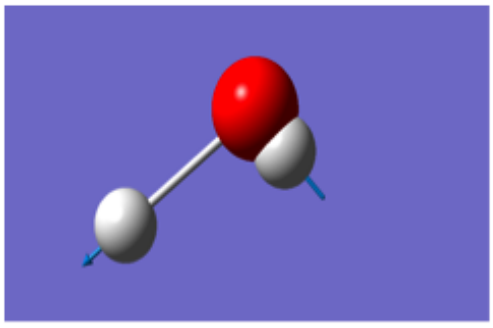

(e)

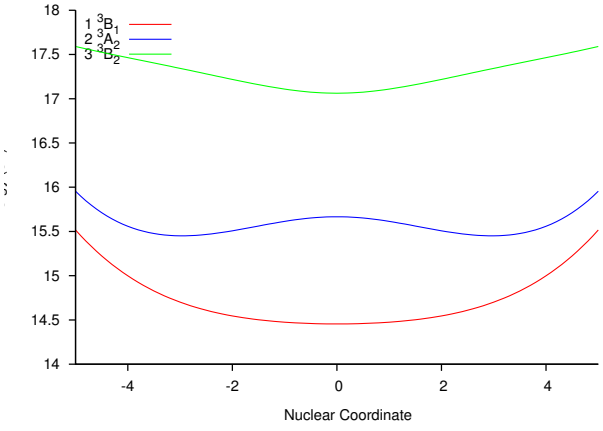

(f)

Figure 3.8: Adiabatic surfaces for the triplet states: (a,b): Bending Mode, (c,d): Symmetric Stretch, (e,f): Asymmetric Stretch

```
    0              ! units in eV
    6              ! Number of electronic states
    2              ! Number of symmetric normal modes
    1              ! Number of non-A1 normal modes
  500              ! Number of Lanczos iterations
  20   20
   0.099990    0.169741
  20
   0.160254
  0.100
  3.000
 auto

*vibron
 short_title=eig
 eigdirect=on
 max_setup=200
 cubic=on
 quartic=on
*eigdirect
 nroot=10
 nrestart=200
 maxiter=500
*end
```

Figure 3.9: VIBRON input file for the calculation of vibronic eigenstates of radical

```
    0              ! units in eV
    3              ! Number of electronic states
    2              ! Number of symmetric normal modes
    1              ! Number of non-A1 normal modes
  500              ! Number of Lanczos iterations
  20   20
   0.099990    0.169741
  20
   0.160254
  0.100
  3.000
 auto

*vibron
 short_title=abs
 special_seed=on
 cubic=on
 quartic=on
*end
```

Figure 3.10: VIBRON input file for the spectrum calculation

```
#########################################################################
###          NO2 Block-Improved-Relaxation                            ####
#########################################################################

RUN-SECTION
name = block_10 relaxation=0,olsen  precon=200
tfinal = 100.0   tout = all   tpsi= 100.0
psi=double gridpop  steps  orben split-rst
title = no2 block calculation
end-run-section

OPERATOR-SECTION
oppath = .
opname = COM
end-operator-section

SPF-BASIS-SECTION
packet=10, single-set
      v01         =  10
      v02         =  10
      v03         =  10
end-spf-basis-section

PRIMITIVE-BASIS-SECTION
    v01    HO     20   0.0     1.0     1.0
    v02    HO     20   0.0     1.0     1.0
    v03    HO     20   0.0     1.0     1.0
    el     el     12
end-primitive-basis-section

INTEGRATOR-SECTION
CMF      = 1.0, 3.0d-4
RK8/spf  = 1.0d-8, 0.1
RRDAV/A  = 100, 1.0d-9  # 720, 1.0d-9  ## 760, 1.0d-9
energyorb  eps_inv=1.d-9
end-integrator-section

INIT_WF-SECTION
build
  init_state=7
   v01   HO  0.2    0.0    1.00
   v02   HO  0.2    0.0    1.00
   v03   HO  0.1    0.0    1.00
end-build
   autoblock
end-init_wf-section

end-input
```

Figure 3.11: MCTDH input file for the calculation of vibronic eigenstates of radical

```
RUN-SECTION
name = all  propagate
tfinal= 500.0 tout = 0.1 tpsi = 1.0
psi auto=twice steps gridpop
title = no2 propagation singlet
end-run-section

OPERATOR-SECTION
oppath = .
opname = COM
end-operator-section

SPF-BASIS-SECTION
multi-set
     v01     = 7, 7, 7, 7, 7, 7, 7, 7, 7, %
               7, 7, 7
     v02,v03 = 7, 7, 7, 7, 7, 7, 7, 7, 7, %
               7, 7, 7
end-spf-basis-section

PRIMITIVE-BASIS-SECTION
    v01    HO   20  0.0   1.0   1.0
    v02    HO   20  0.0   1.0   1.0
    v03    HO   20  0.0   1.0   1.0
    el    el  12
end-primitive-basis-section

INTEGRATOR-SECTION
CMF/var = 0.5, 1.0d-05
BS/spf = 7, 1.0d-05, 2.5d-04
SIL/A = 5, 1.0d-05
end-integrator-section

INIT_WF-SECTION
  file=/home/p2goel/restart/no2_ip
  operate=Exprop
end-init_wf-section
end-input
```

Figure 3.12: MCTDH input file for the calculation of spectrum of singlet states

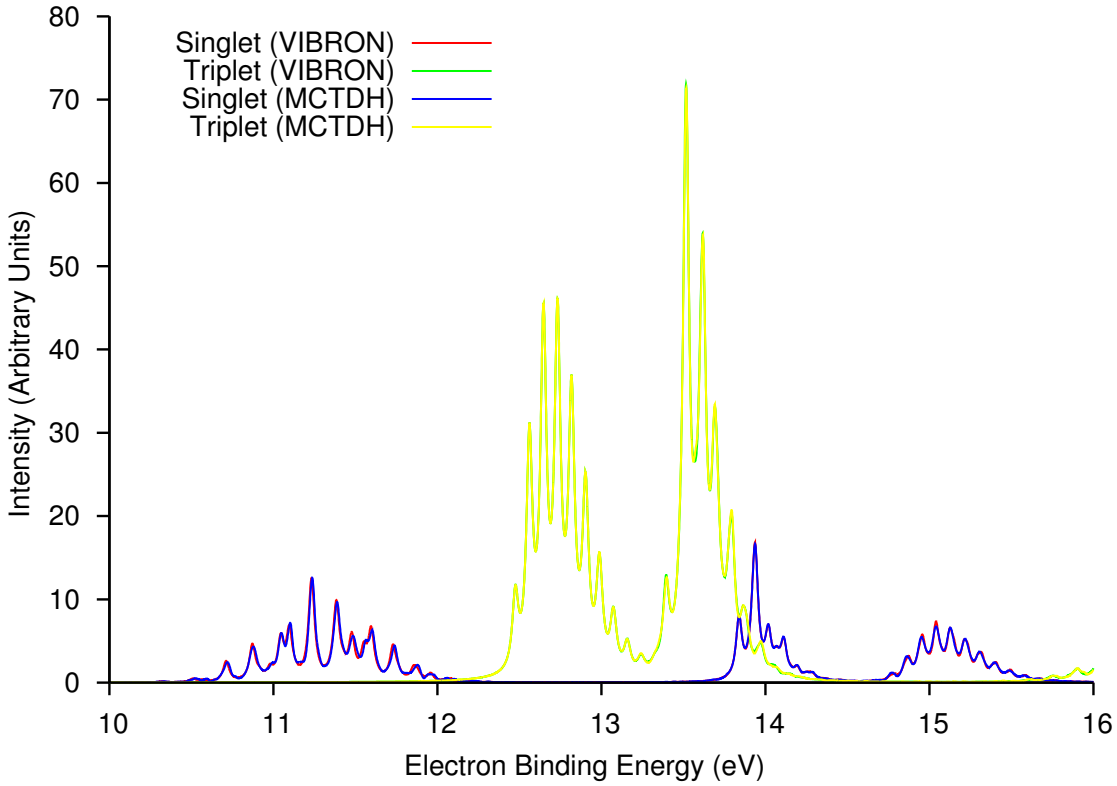

Figure 3.13: Photodetachment spectrum of the NO_2: MCTDH vs. VIBRON

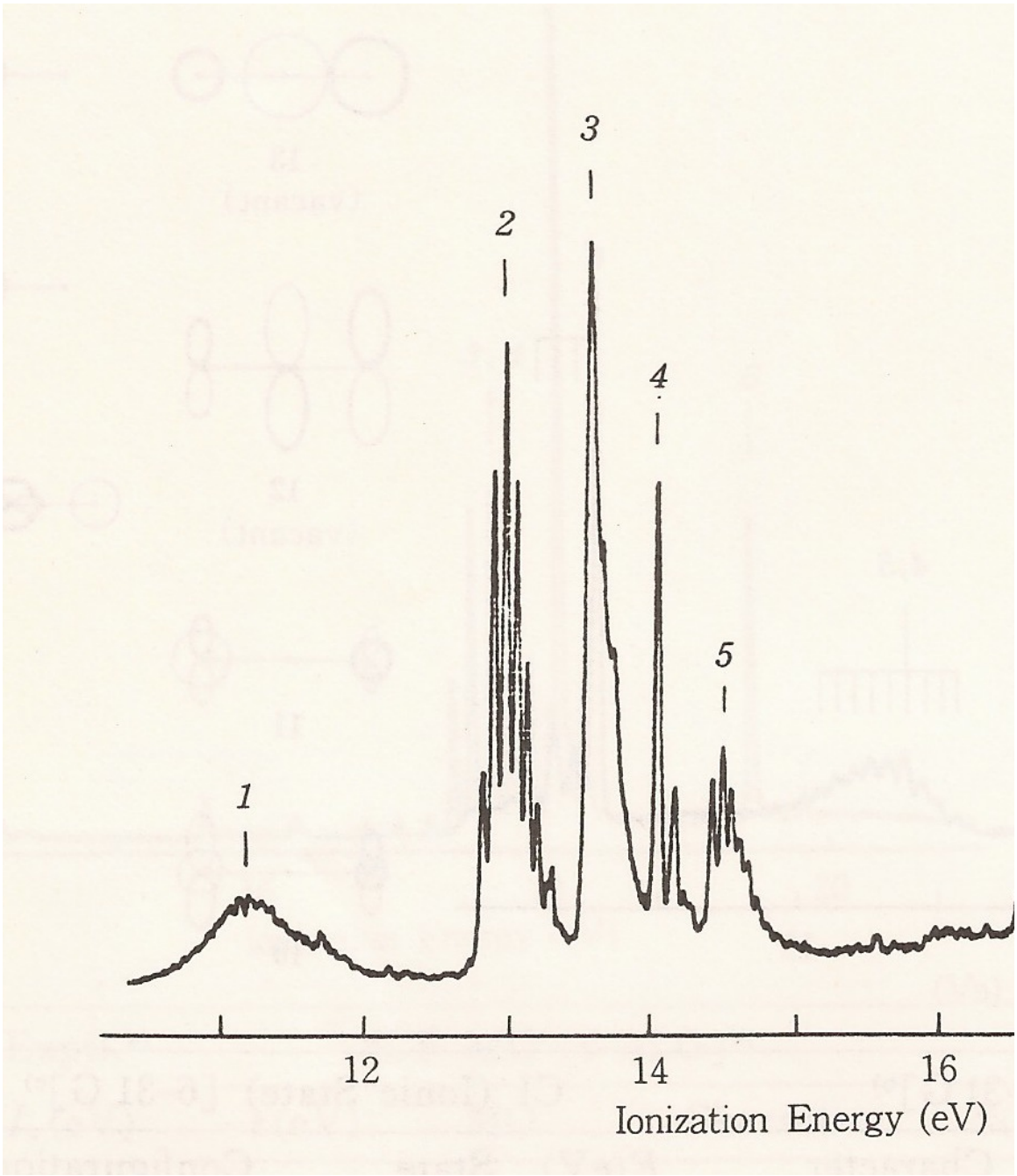

Figure 3.14: Photodetachment spectrum of the NO_2: MCTDH vs. VIBRON

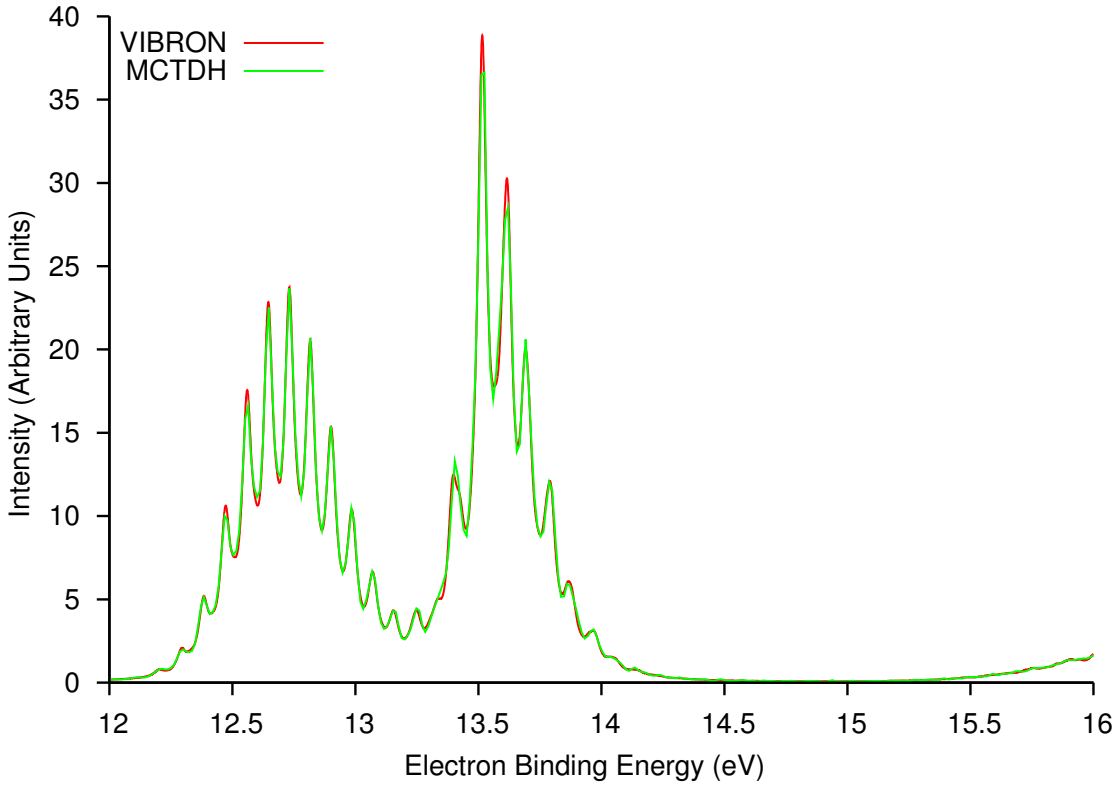

Figure 3.15: Hot band spectrum of triplet cation at 800K: MCTDH vs. VIBRON

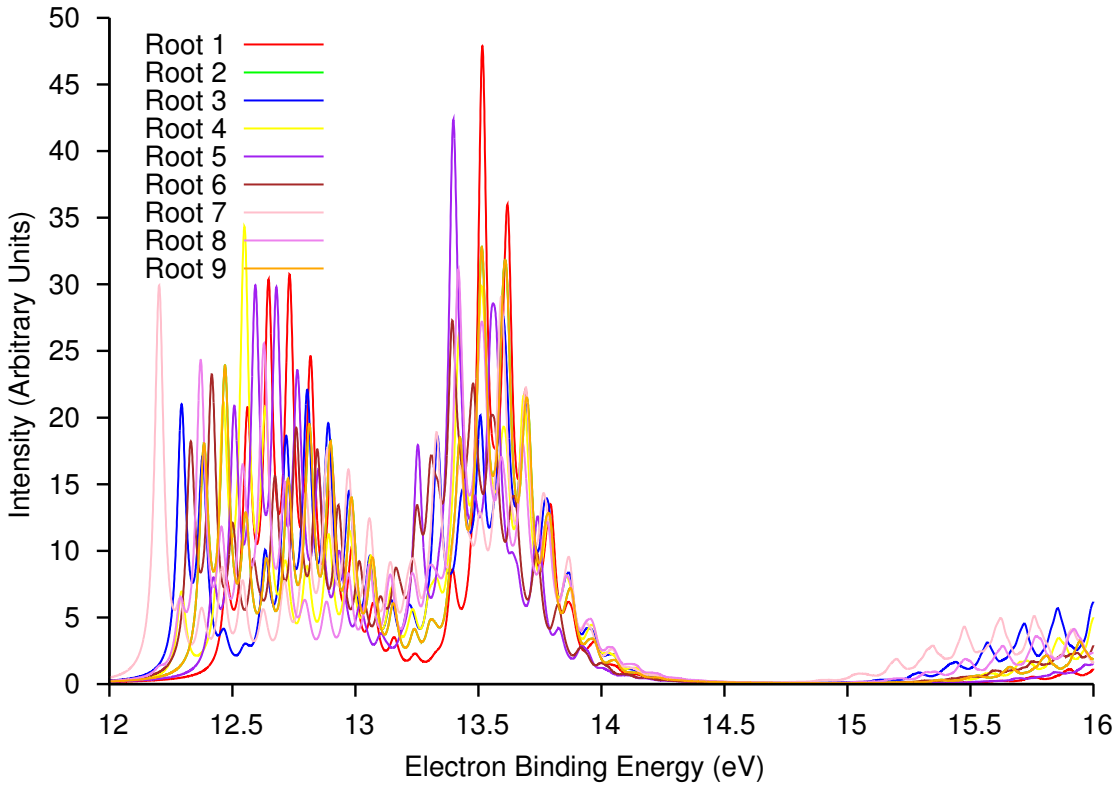

Figure 3.16: Hot band spectrum of triplet at 800K in VIBRON starting from different eigenstate

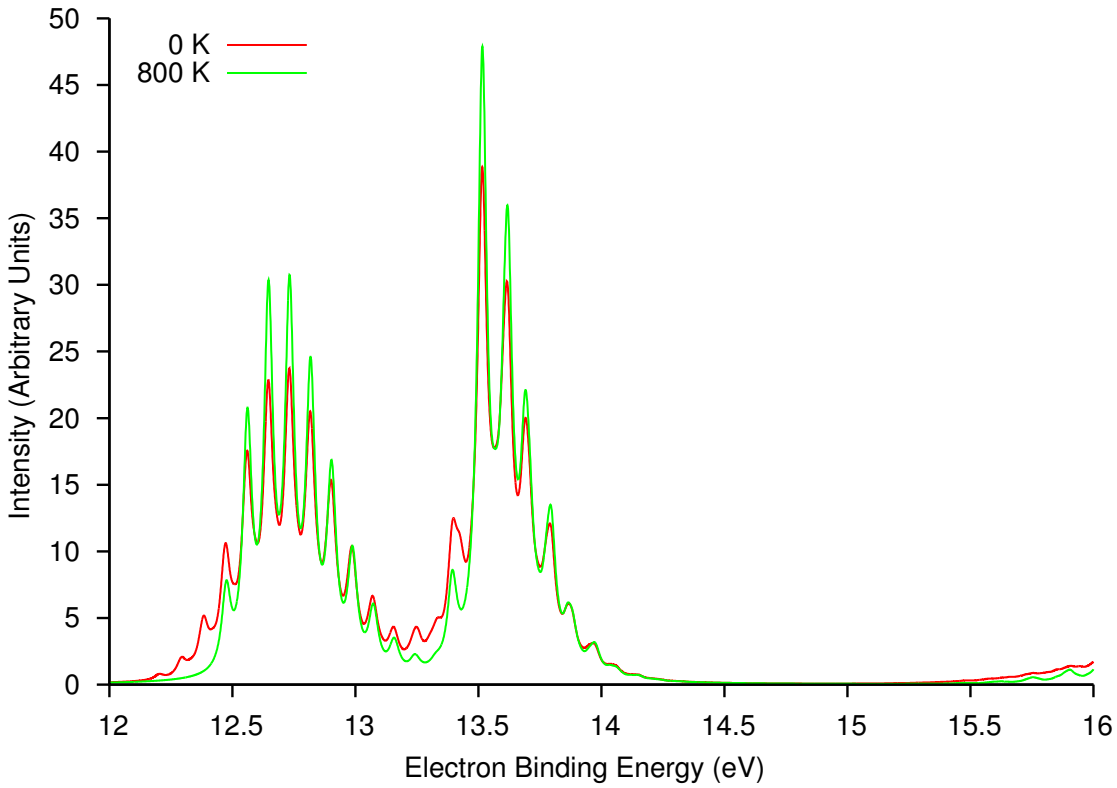

Figure 3.17: Comparison of spectrum at 0K vs. 800K in VIBRON

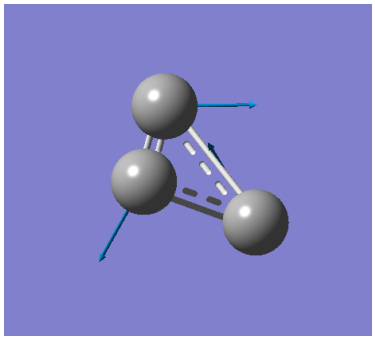

(a)

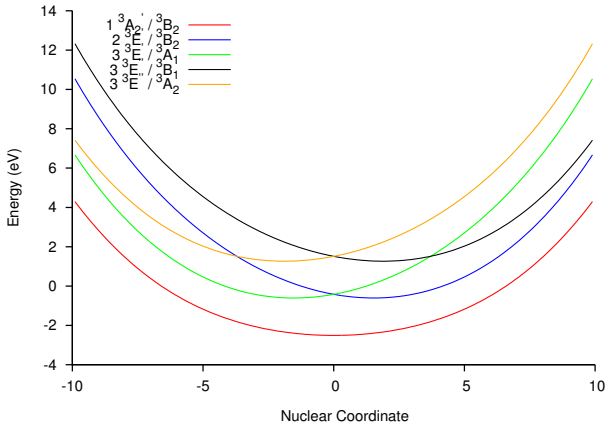

(b)

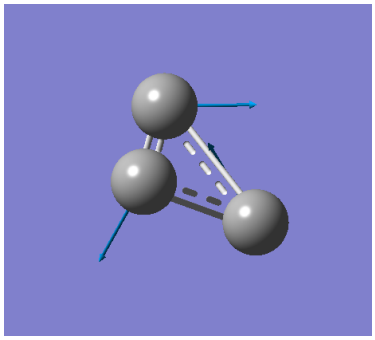

(c)

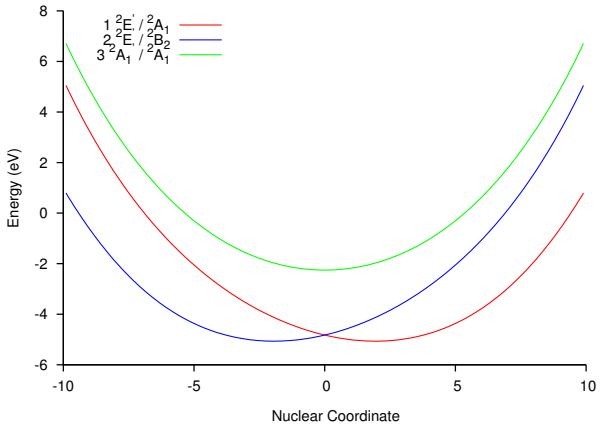

(d)

Figure 3.18: Adiabatic potential surfaces for Normal mode 3: Triplet C_3 and C_3^-

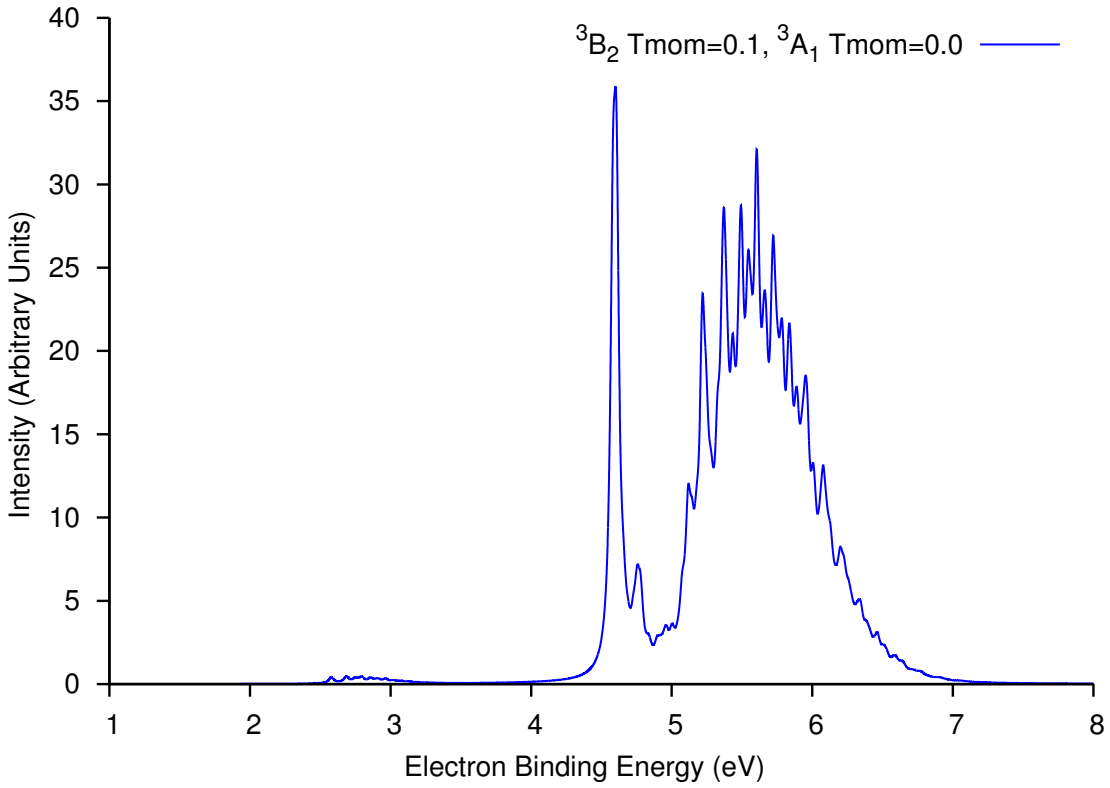

Figure 3.19: Case 1: Vertical excitation from nondegenerate ground anionic state to the first state ($^3B_2$) of JT pair

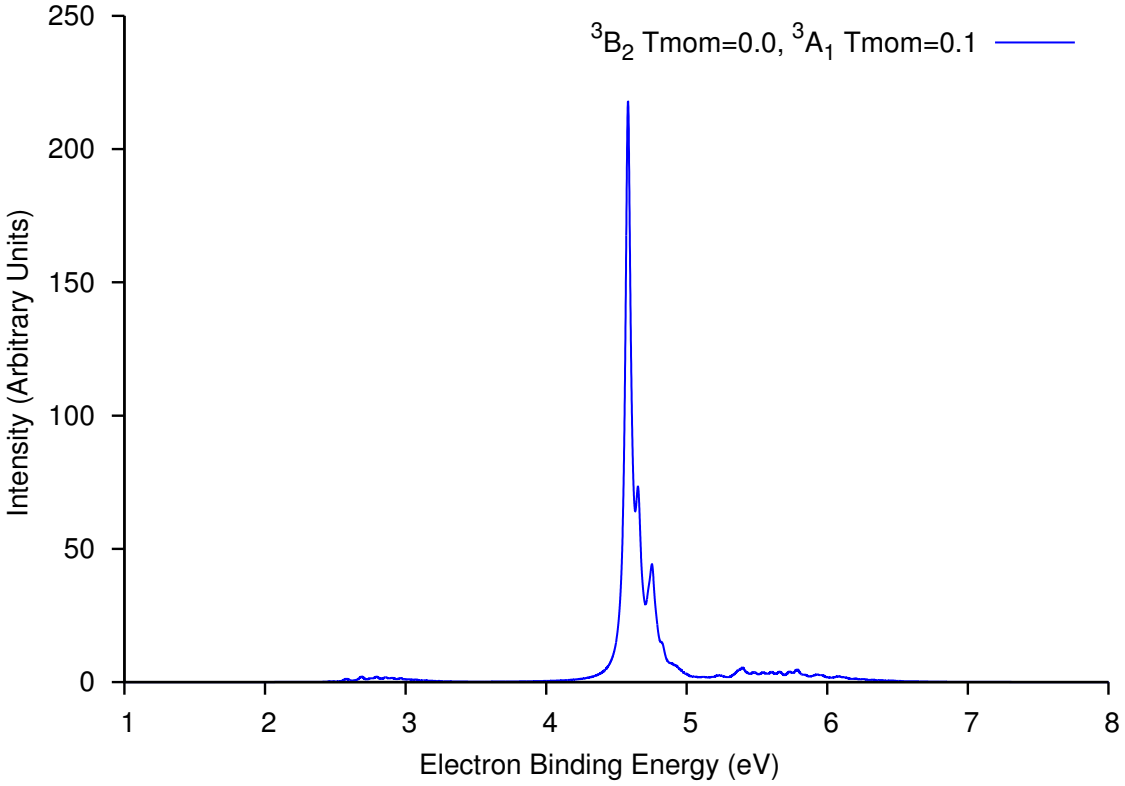

Figure 3.20: Case 2: Vertical excitation from nondegenerate ground anionic state to the second state ($^3A_1$) of JT pair

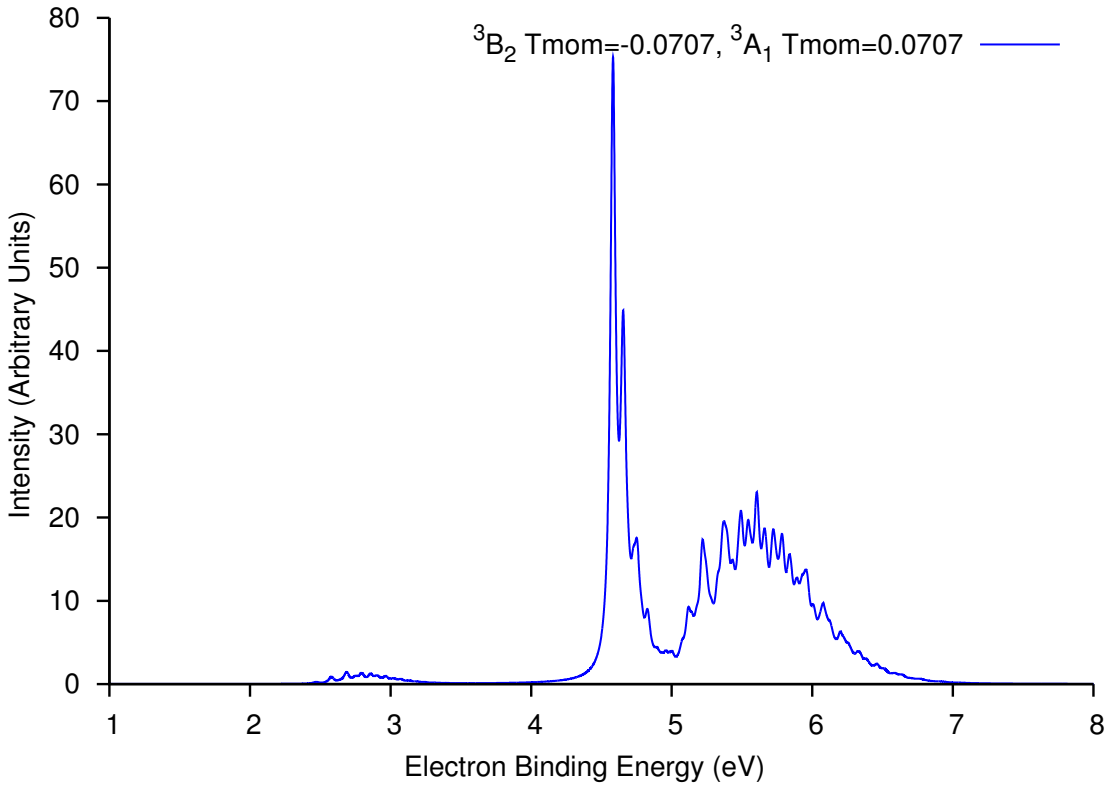

Figure 3.21: Case 3: Vertical excitation from nondegenerate ground anionic state to an asymmetric linear combination of ($^3B_2$) and ($^3A_1$)

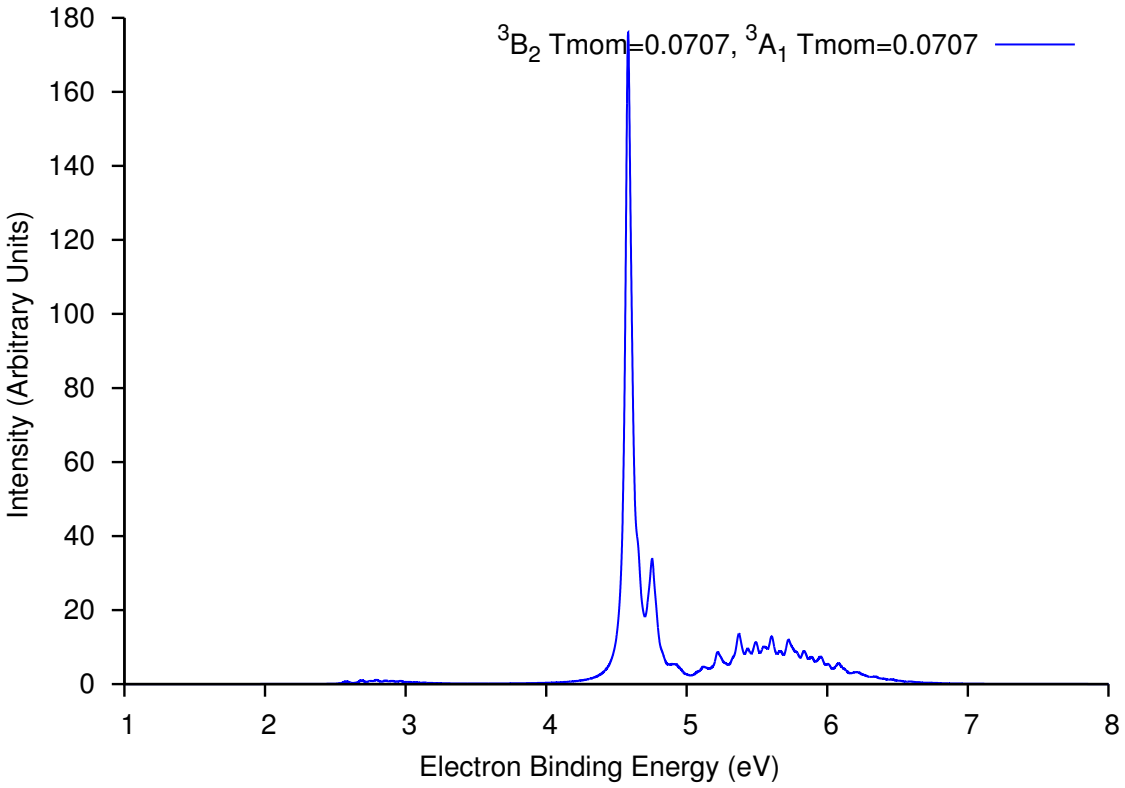

Figure 3.22: Case 4: Vertical excitation from nondegenerate ground anionic state to the symmetric linear combination of ($^3B_2$) and ($^3A_1$)

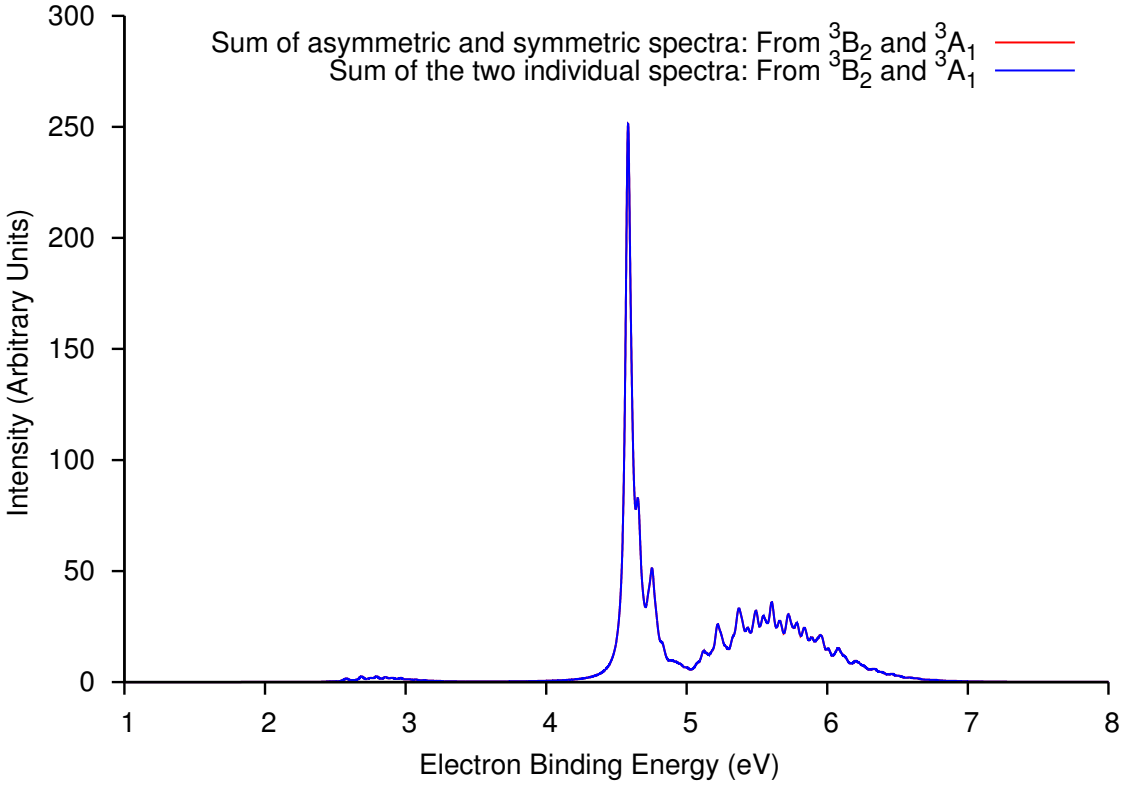

Figure 3.23: The sum of spectra for case 1 (3.19 and 3.20) and for case 2 (3.21 and 3.22) although being very different from individual spectra, remains invariant for two cases

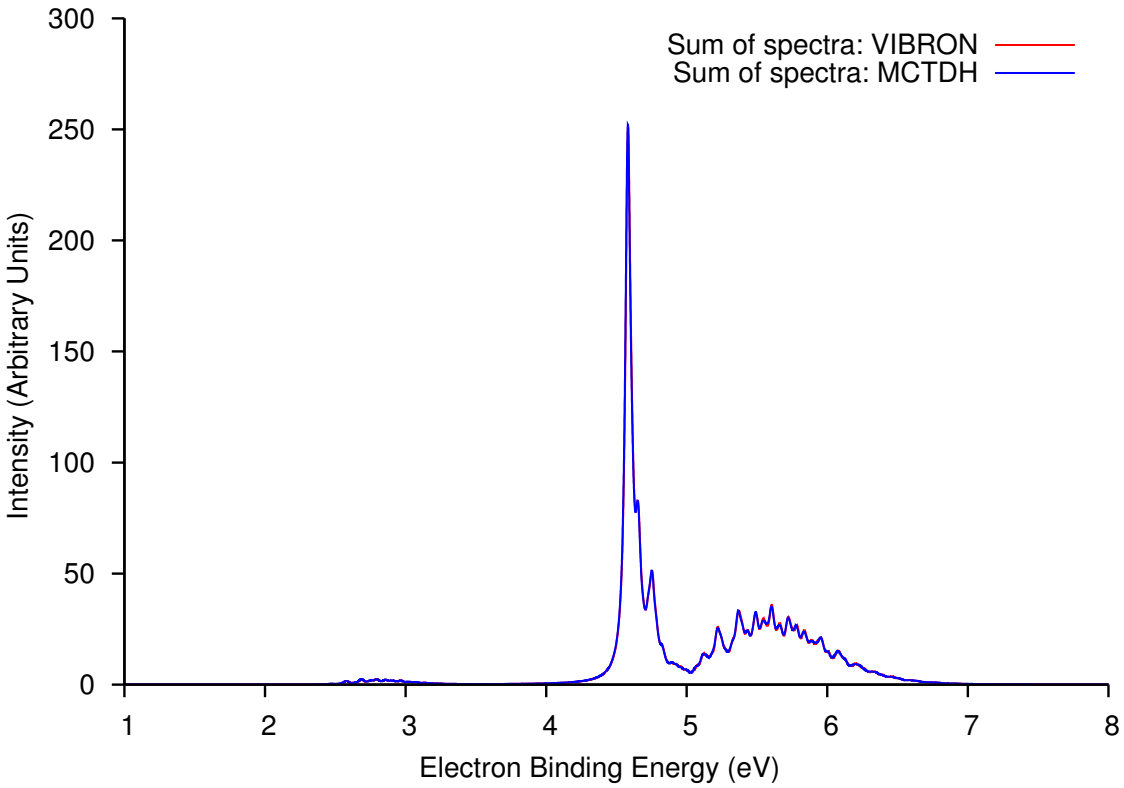

Figure 3.24: Comparison of total spectrum: VIBRON vs. MCTDH

Chapter 4

Nitrate Radical

4.1 Introduction

The nitrate free radical (NO_3) has continued to be a challenging system to study for both experimentalists and theoreticians equally. It's importance in atmospheric chemistry is well known. Much debate has taken place in the literature over the "symmetry breaking" problem for the ground state of neutral NO_3 as well as about the cation, NO_3^+, whether the symmetry of each ground state belongs to D_{3h} or C_{2v} point group. The symmetry breaking of the electronic wavefunction in NO_3 has almost become a textbook example. [22]

Very few studies have attempted to consider the excited states of NO_3^+ , which is a biradical system. The motivation behind such theoretical analysis came from the two experimental studies of NO_3 ionization spectrum in the mid 1990s. In the first study performed in 1994, Monks *et al.* [23] carried out the photoionization experiment of NO_3, in which they determined the first principal IP at 12.57 eV which was attributed to the lowest vertical ionization, i.e. NO_3^+ $(^1A_1^{'})$ $\longleftarrow$ NO_3 $(^2A_2^{'})$ in D_{3h} symmetry. In the second study performed in 1997, Wang *et al.* [24] reported the first photodetachment spectrum of NO_3, in which they observed five distinct bands. Their analysis also questioned the results obtained by Monks *et al.*. Although the first principal IP (12.55 eV) was in close agreement, Wang *et al.* obtained several higher IPs which were not found by Monks *et al.*.

Two important theoretical studies took place in the year 2002, interestingly at the same time, attempting to explore these issues in detail with the use of high-level *ab initio* calculations. In the first study by Eisfeld and Morokuma [25] , the vertical ionization spectrum of NO_3 was calculated using CASSCF and MRCI methods. They calculated and characterized 15 ionic singlet and triplet states of NO_3^+, for D_{3h} geometries. Also, they obtained equilibrium geometries and harmonic frequencies for the controversial higher principal ionization and adiabatic ionization potentials were obtained. In the second study by Wladyslawski and Nooijen [26], the ionization spectrum of NO_3 radical and the ground and excited states of the NO_3^+ cation were examined by the DIP-STEOM-CCSD method.

Both of the aforementioned theoretical studies obtained good agreement with the experiment for the first principal IP, but saw major disagreements for the higher transitions. The two studies did not support the experimentally assigned features at 14.05 eV. The features between 13.25 eV to 13.51 eV also became a matter of controversy and no clear assignments were made in this region of the spectrum. Wladyslawski and Nooijen also pointed out the presence of a conical intersection for states $^3E'$ and $^3A_2{}'$ and strong non-adiabatic effects are expected in the vibrational spectra associated with these states.

The two theoretical studies proposed a reassignment of the photodetachment spectrum of Wang *et al.* by performing a full vibronic analysis of the low triplet surfaces in order to verify the suggestions made therein and resolve some of the controversies. In fact, Eisfeld and Morokuma proposed to carry out such a study in the second paper of the series, but surprisingly such a study has never been reported to date. To the best knowledge of the author, no such study has been reported in the literature by anyone else either.

In this chapter, a full vibronic spectrum of NO_3 radical is calculated in the range of 12 to 15 eV, using the methodology and tools discussed in previous chapters. The study presented here tries to verify some of the suggestions and attempts to resolve some of the issues associated with the assignment of the spectrum.

4.2 Methodology

Two sets of vibronic model will be created for the radical as well as the singlet and triplet cation NO_3 species. For both sets, three vibronic models will be created. One model for the NO_3 radical and two models, one for each singlet and triplet states of NO_3^+, will be created centered at the geometry of the NO_3 radical ground state. We call this the *Single Model* scheme and from here onwards it will be referred as *Model 1*. Similarly, in the second set, three vibronic models, one for the NO_3 radical and one for each singlet and triplet states of NO_3^+ will be created at the the optimized ground state geometry of the closed-shell anion NO_3^-. This model will be referred as *Model 2*. While calculating the photodetachment spectrum using *Model 1*, we will not use the radical vibronic model and the ground state of NO_3 radical will be treated within harmonic approximation. The primary purpose of such analysis is to show the importance of having a vibronic model for the parent state (in this case the NO_3 radical) in order to correctly represent the potential energy surface and to get a correct ground state wavefunction. The electronic states and vibronic model parameters are obtained from IP-EOMCC and DIP-STEOM calculations.

Most of the analysis and comparison to the experiment and previous studies will be made using the results obtained by Model 2. The calculation of spectrum is performed using the same techniques as described in Chapter 3, using both MCTDH and VIBRON.

Once again, a comparison will also be made between these two approaches to make sure we are on the right track!

All the electronic structure calculations are performed at the CCSD level of theory using the TZ2P basis set.

4.3 Results & Discussions

The optimized geometry and the harmonic vibrational frequencies of the closed-shell anion as well as the neutral radical are shown in table 5.1 and 5.2.

Table 4.1: Optimized geometry for the closed-shell anion and neutral radical

Parameter	Anion	Radical
$R(NO)$	$1.2546852A^0$	$1.2301654A^0$

The ionization and double ionization energies of the closed-shell anion NO_3^- have been calculated using IP-EOMCC/DIP-STEOMCC at both of the reference geometries. It is evident that the singlet $^1A_1'$ is the ground state of the cation NO_3^+. The four excited states of singlet spin form JT pairs, while the low lying states of triplet also form two JT pairs

Table 4.2: Vibrational normal modes for the closed-shell anion and neutral radical

Normal Mode	Description	Frequency Anion (cm^{-1})	Frequency Radical (cm^{-1})
1 (A_1')	Symmetric Stretch	1079.44	1132.75
2 (E')	ONO Bending	723.93	248.71
3 (E')	ONO Bending	723.93	248.71
4 (E')	Asymmetric Stretch	1413.54	1113.21
5 (E')	Asymmetric Stretch	1413.54	1113.21
6 (A_2'')	Torsion Mode	877.15	814.25

and lie within a very close energetic proximity of each other. In total, 11 states of the NO_3^+ have been calculated as the vertical ionization of NO_3 which are ordered in energy in table 4.5 and the values are compared to those obtained by experiment as well as the CASSCF and MRCI methods. The agreements between the values is generally very good. The first principle IP has been shifted to the value of 12.55 eV to make a direct comparison to the experimental values.

Two sets of vibronic models are created using the $GRID = 3$ scheme by making a selection of states from the manifold of calculated ionized states of NO_3 radical and cation.

Table 4.3: Ionization energies of the anion calculated using IP-EOM-CCSD at two geometries

State (D_{3h}/C_{2v})	IP Model 1 (eV)	IP Model 2 (eV)
$^2A_2'/\ ^2B_2$	3.61	3.74
$^2E''/\ ^2A_2$	4.99	4.98
$^2E''/\ ^2B_1$	4.99	4.98
$^2E'/\ ^2A_1$	5.84	5.80
$^2E'/\ ^2B_2$	5.84	5.80

Model 1

Reference Geometry: NO_3 radical ground state

NO_3: 5 lowest states

Singlet NO_3^+: 3 lowest states

Triplet NO_3^+: 5 lowest states

Model 2

Reference Geometry: NO_3^- anion ground state

NO_3: 5 lowest states

Singlet NO_3^+: 3 lowest states

Table 4.4: Double ionization energies of the anion calculated using DIP-STEOM-CCSD at two geometries

State (D_{3h}/C_{2v})	DIP Model 1 (eV)	DIP Model 2 (eV)
$^1A_1'/\ ^1A_1$	15.94	16.06
$^1E''/\ ^1B_1$	16.67	16.69
$^1E''/\ ^1A_2$	16.67	16.69
$^1E'/\ ^1A_1$	18.71	18.98
$^1E'/\ ^1B_2$	18.71	18.98
$^3E''/\ ^3B_1$	16.57	16.67
$^3E''/\ ^3A_2$	16.57	16.67
$^3E'/\ ^3B_2$	16.96	17.02
$^3E'/\ ^3A_1$	16.96	17.02
$^3A_2'/\ ^3B_2$	16.78	17.09
$^3A_2''/\ ^3B_1$	18.24	18.18

Triplet NO_3^+: 5 lowest states

After obtaining the coupling constants, the potential energy surfaces are generated for all these six models. The surfaces are shown for the Model 1. It is observed that the radical

Table 4.5: Electronic states of NO_3^+, and vertical ionization potentials (in eV) of NO_3 from various calculations

No	State (D_{3h}/C_{2v})	Exp	STEOM 1	STEOM 2	CASSCF	MR-SDCI
1	$^1A_1'/\ ^1A_1$	12.55	12.55	12.55	12.55	12.54
2	$^3E''/\ ^3B_1$	13.18	13.18	13.16	13.21	13.36
3	$^3E''/\ ^3A_2$	13.18	13.18	13.16	13.21	13.36
4	$^1E''/\ ^1B_1$	14.05	13.28	13.18	13.25	13.37
5	$^1E''/\ ^1A_2$	14.05	13.57	13.18	13.25	13.37
6	$^3E'/\ ^3B_2$	13.62	13.57	13.51	13.61	13.62
7	$^3E'/\ ^3A_1$	13.62	13.57	13.51	13.61	13.62
8	$^3A_2'/\ ^3B_2$	-	13.39	13.58	13.70	14.02
9	$^3A_2''/\ ^3B_1$	-	14.85	14.67	15.01	14.73
10	$^1E'/\ ^1A_1$	15.54	15.32	15.47	15.01	15.12
11	$^1E'/\ ^1B_2$	15.54	15.32	15.47	14.55	15.12

ground state is very flat, for normal modes 2 and 3. Also, it can be seen that the potential surfaces for triplet are very close to each other and have complicated topologies. Two

dimensional surfaces can also be plotted to gain a better visual understanding. Since the potentials all look good, and are bound in nature, we can proceed towards the simulation of spectrum.

The spectrum for Model 1 is calculated trivially, using Lanczos algorithm for VIBRON and using wavepacket propagation for MCTDH, both starting from a harmonic ground state. For Model 2, the methodology used for NO_2 in previous chapter is followed. First the vibronic eigenstates are obtained for NO_3 radical (Table 4.7), and then the ground vibronic state will be read in as the absorbing state for the subsequent calculation. The computational setup of MCTDH is shown in table 5.5.

The calculated spectra are all shown along with the experimental spectrum as obtained by Wang *et al.*. For Model 2, three bands are seen in the calculated spectrum. The first band, which has a sharp peak, clearly belongs to the ground state singlet (12.55 eV). The second band between 13.25 to 13.51 eV is a superposition of $^1E''$ and $^3E''$ states, which nearly coincide with each other. The last band is result of superposition of JT states $^3E'$ with some contribution from the dark state $^3A_2{}'$. As suggested by Wladyslawski and Nooijen, there are strong nonadiabatic effects for these states as shown in figure 4.9, which is a superposition of two $^3E'$ and 4.10, which shows the full triplet spectrum along with the vibronic line structure for $^3E'$ states. However, contrary to what was suggested by Wladyslawski and Nooijen, there is not much of a vibronic interaction of the dark $^3A_2{}'$

state with the $^3E'$ state, and the weak, broad feature near the 14.05 eV is a Jahn-Teller effect from the $^3E'$ states, which is missing from the allowed vertical ionization results.

On another note, a comparison between the spectrum calculated from Model 1 and Model 2 is made and it is evident that the single model results are not accurate and the ground state of the NO_3 radical is correctly described with the use of a vibronic model.

4.4 Summary

The photodetachment spectrum of the NO_3 radical has been calculated successfully in the region of 12 to 15 eV. Many assignments have been made, some of which agree with the suggestions made by Wladyslawski and Nooijen, while some do not. The comparison with experiment is difficult, also because of the poor resolution of the experiment and the involvement of "stripping" of a strong NO_2 signal. It is worth mentioning that the combined spectrum of NO_3 and NO_2 was obtained from the pyrolysis of N_2O_5. A more refined experimental spectrum, at a high resolution, is desirable to perform a better comparison. At a theoretical level, we look forward to carry out the calculations using the $GRID = 10$ scheme in order to get a better representation of the complicated potential energy surfaces.

Table 4.6: Details of the MCTDH computational setup. Degenerate modes are combined together. Mode combinations are listed along with the primitive bases of these modes, and the number of SPFs used for the relaxation as well as for the propagation calculation. Vibrational normal modes in one bracket constitute single particles. The primitive basis is the number of harmonic-oscillator DVR functions. Each particle has a primitive basis consisting of $20 \times 20 \times 20 = 8000$ functions. The SPF basis is the number of single particle functions used for each electronic state. Only triplet SPFs are shown for Propagation.

Particle	Normal Modes	Primitive basis	SPF Basis (Relaxation)	SPF Basis (Propagation)
1	(1)	[20,20,20]	(5,5,5,5,5)	(5,5,5,5,5)
2	(2, 3)	[20,20,20]	(5,5,5,5,5)	(5,5,5,5,5)
3	(4, 5)	[20,20,20]	(5,5,5,5,5)	(5,5,5,5,5)
4	(6)	[20,20,20]	(5,5,5,5,5)	(5,5,5,5,5)

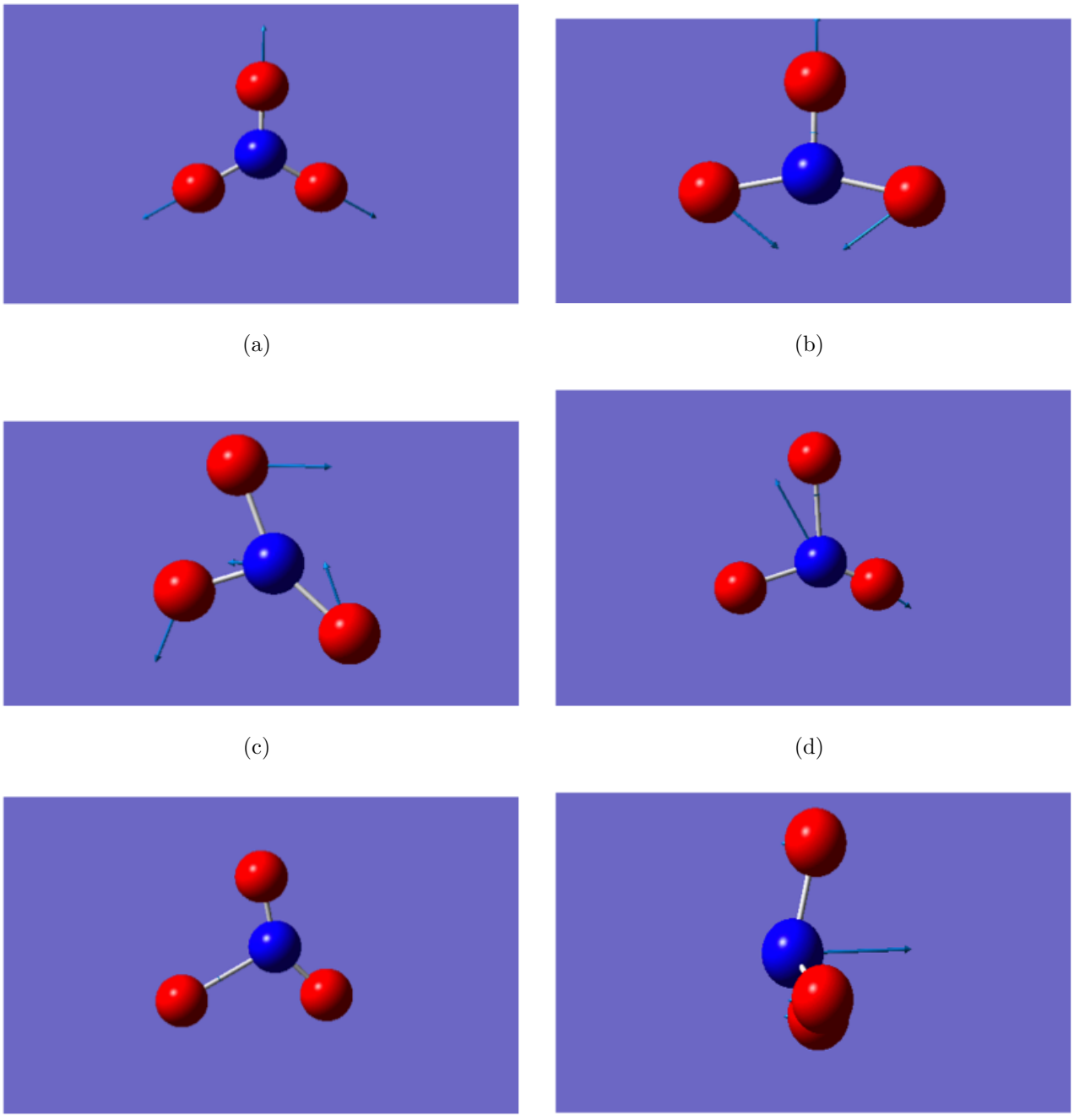

(a) (b) (c) (d) (e) (f)

Figure 4.1: Vibrational normal modes for NO_3: (a) Symmetric Stretch, (b) Bending, (c) Bending, (d) Asymmetric Stretch, (e) Asymmetric Stretch, (f) Torsion

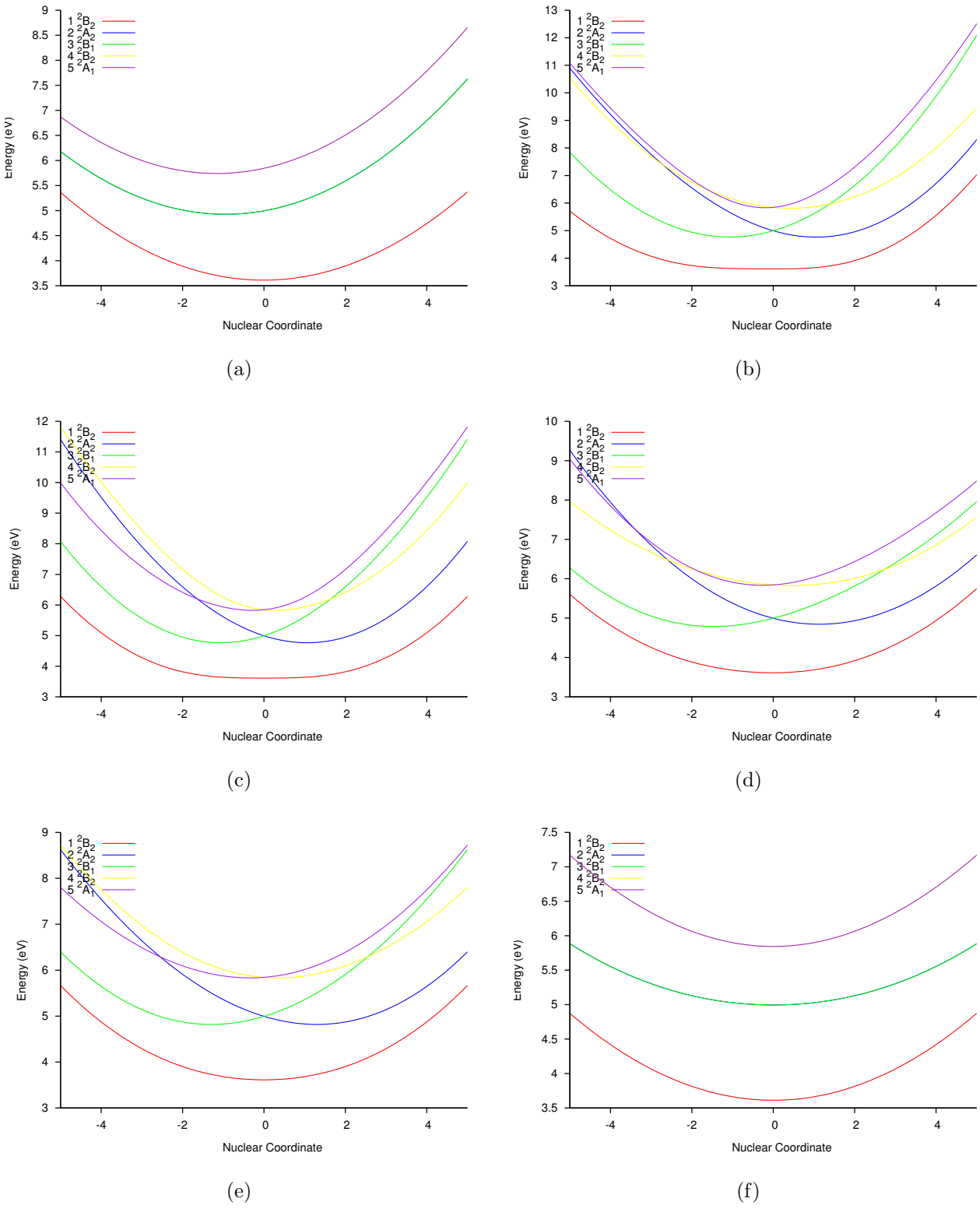

Figure 4.2: Adiabatic surfaces as calculated with Model 1 for the NO_3 radical for normal modes as shown in figure 5.1

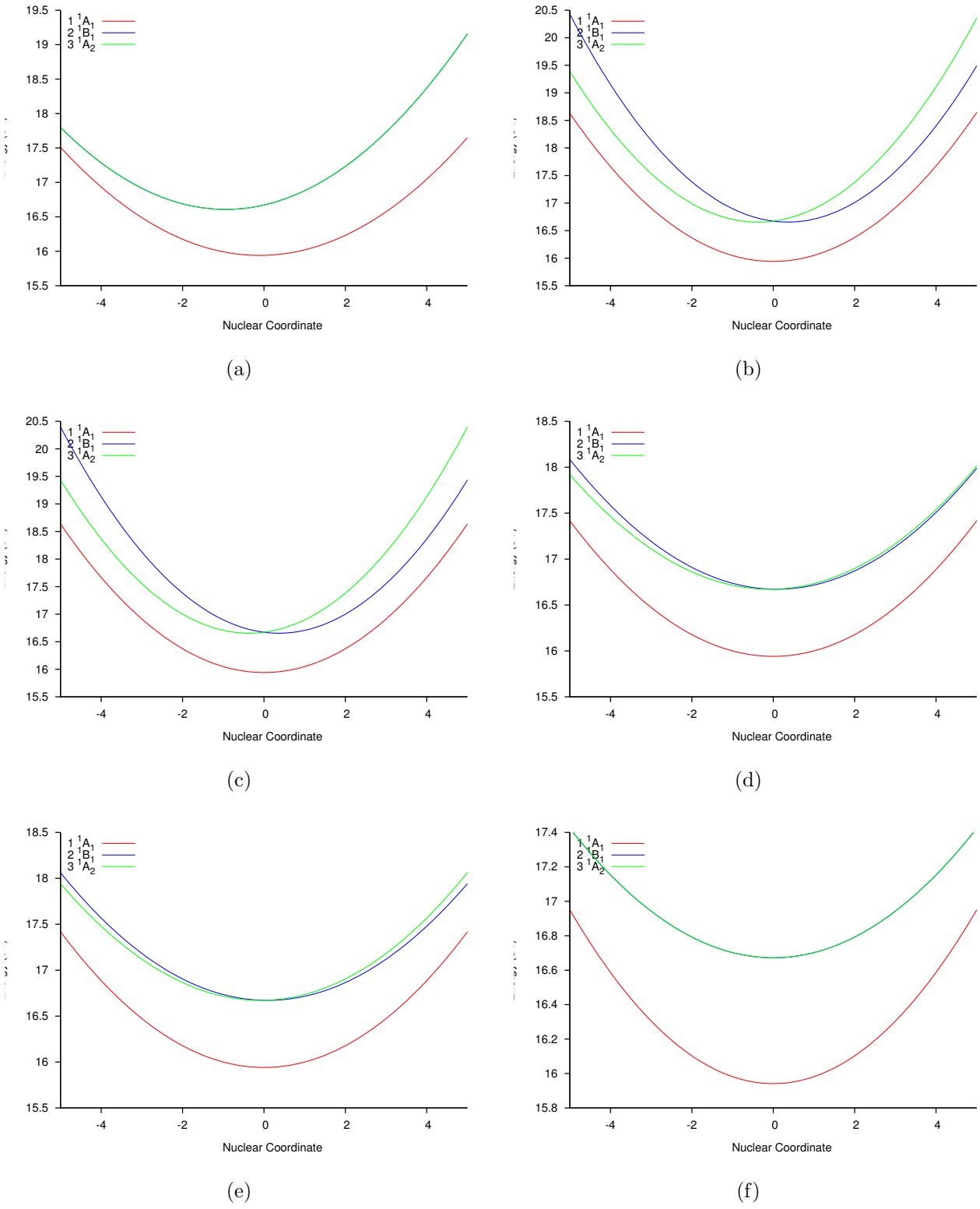

Figure 4.3: Adiabatic surfaces as calculated with Model 1 for the Singlet NO_3^+ for normal modes as shown in figure 5.1

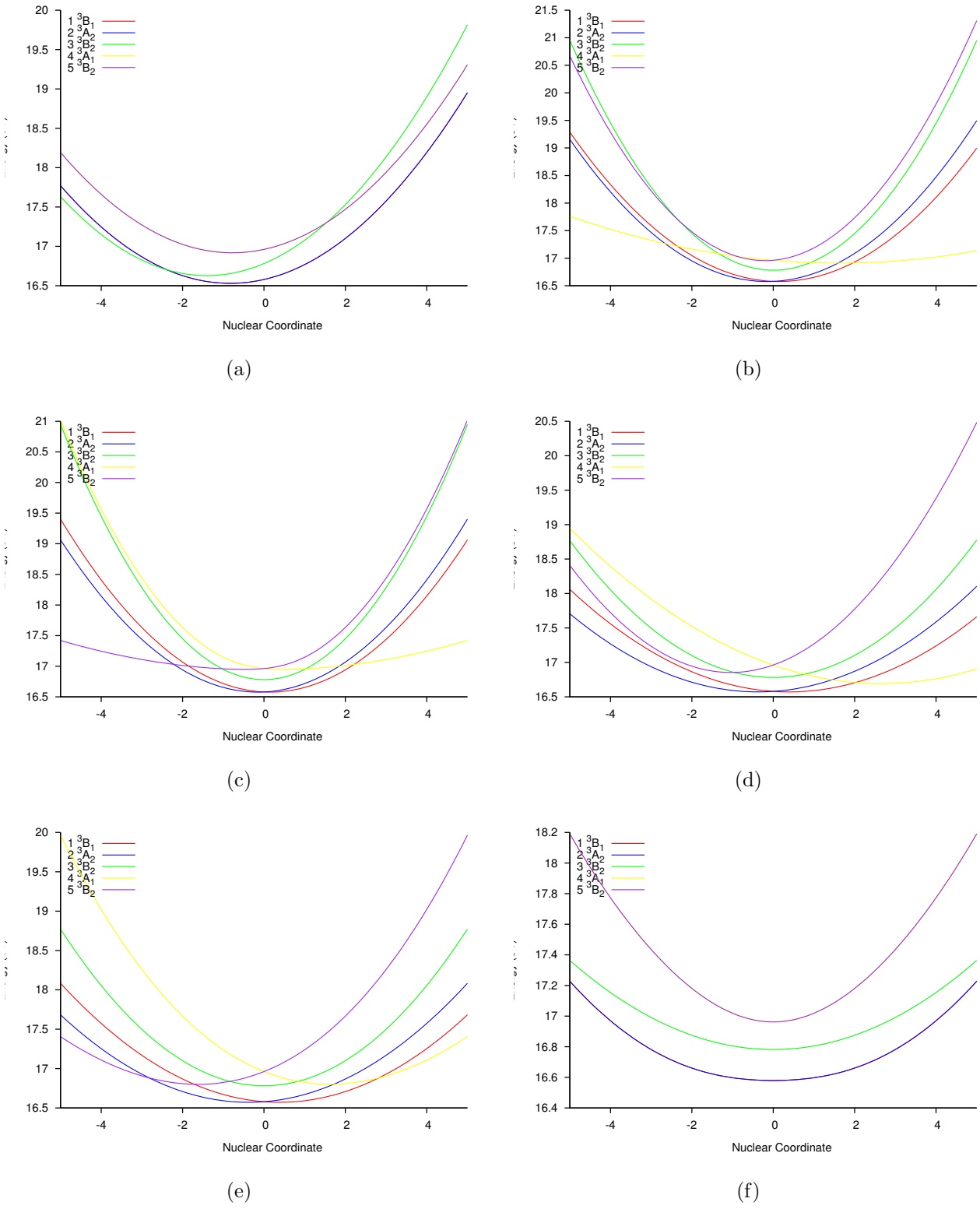

Figure 4.4: Adiabatic surfaces as calculated with Model 1 for the Singlet NO_3^+ for normal modes as shown in figure 5.1

Table 4.7: Three lowest vibronic eigenvalues of the NO_3 radical in VIBRON and MCTDH

Root	VIBRON (eV)	MCTDH (eV)	Relative Energy ($cm^{-}1$)
1	3.570	3.570	0.0
2	3.618	3.618	381.60
3	3.618	3.618	381.60

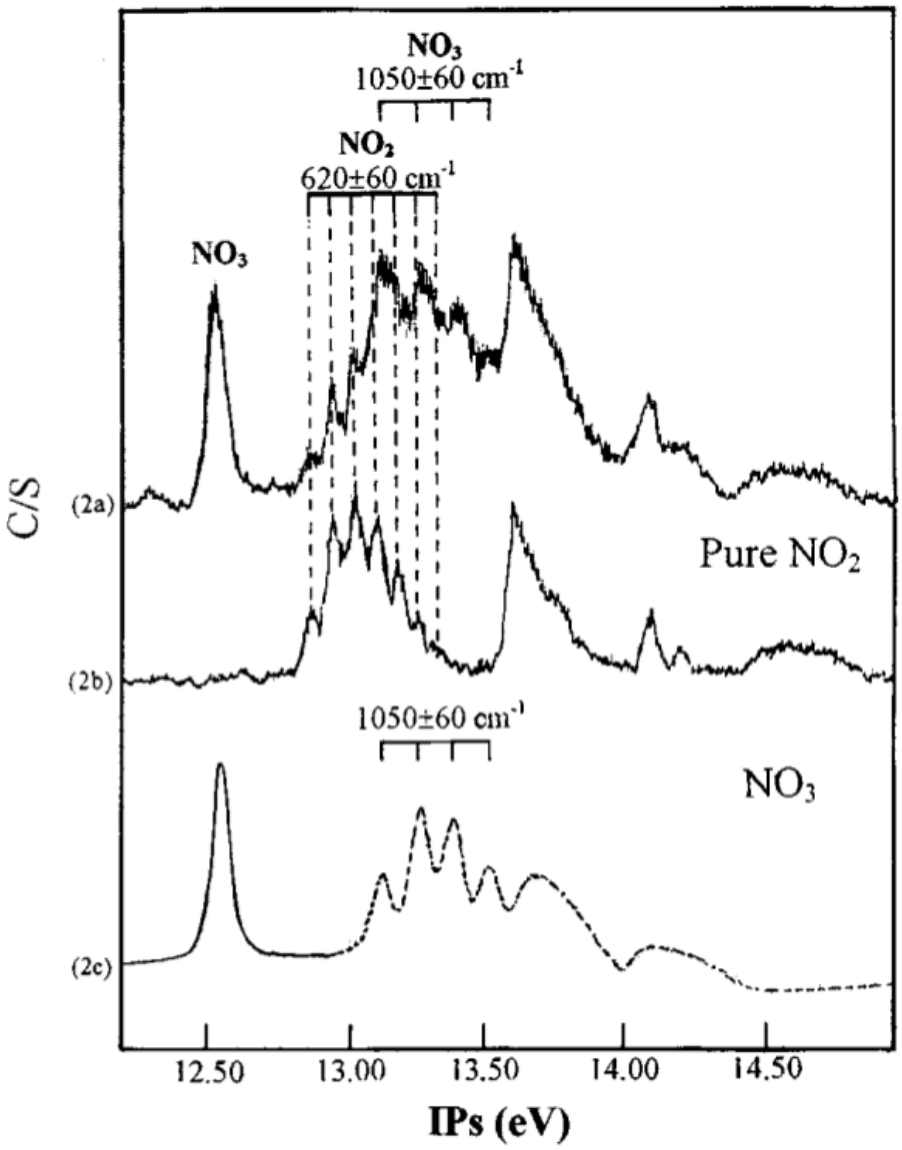

Figure 4.5: Experimental photodetachment spectrum of the NO_3: Reproduced from

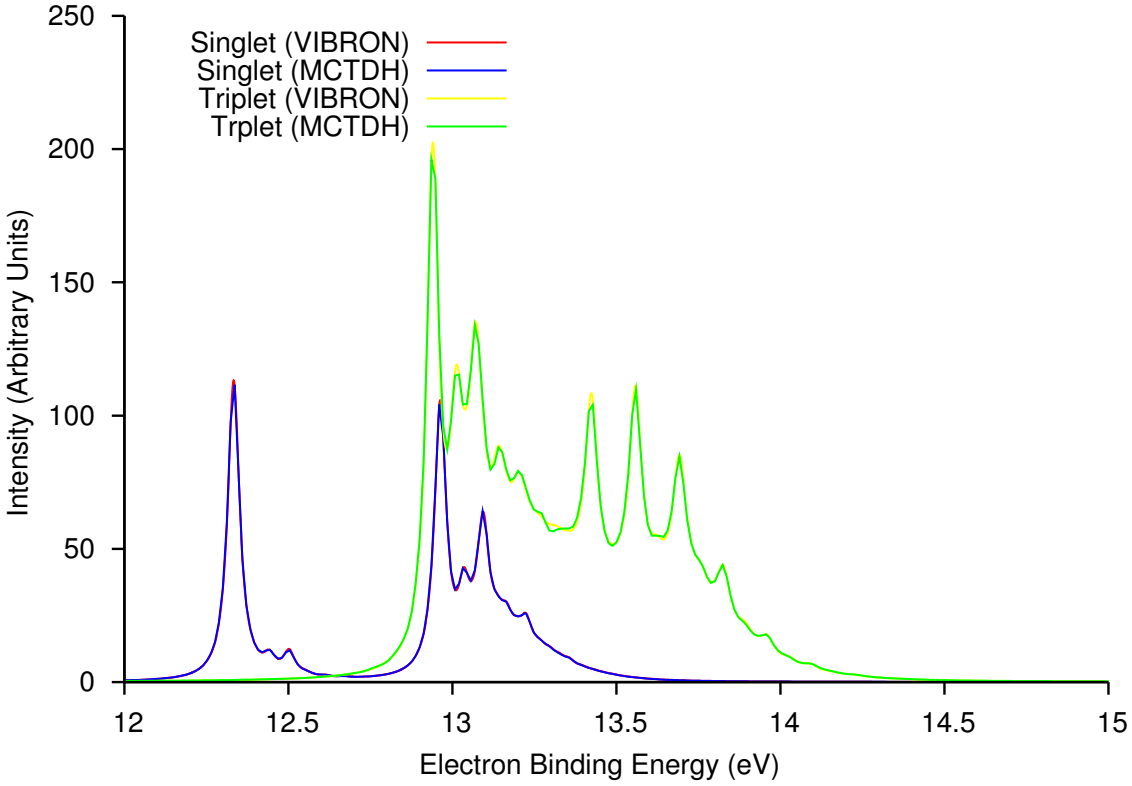

Figure 4.6: Calculated photodetachment spectrum of the NO_3 with multiple models (Model 2): Singlet and Triplet states on top of each other

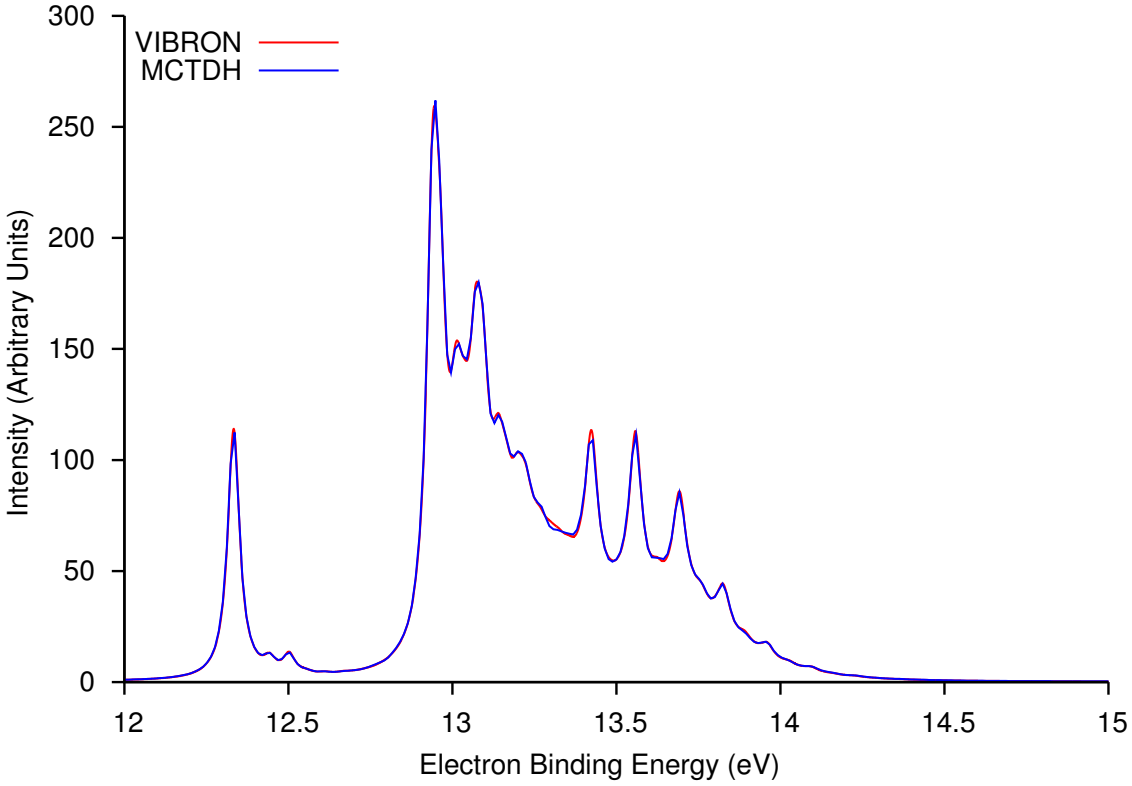

Figure 4.7: Calculated photodetachment spectrum of the NO_3 with multiple models (Model 2) as would be seen by experiment

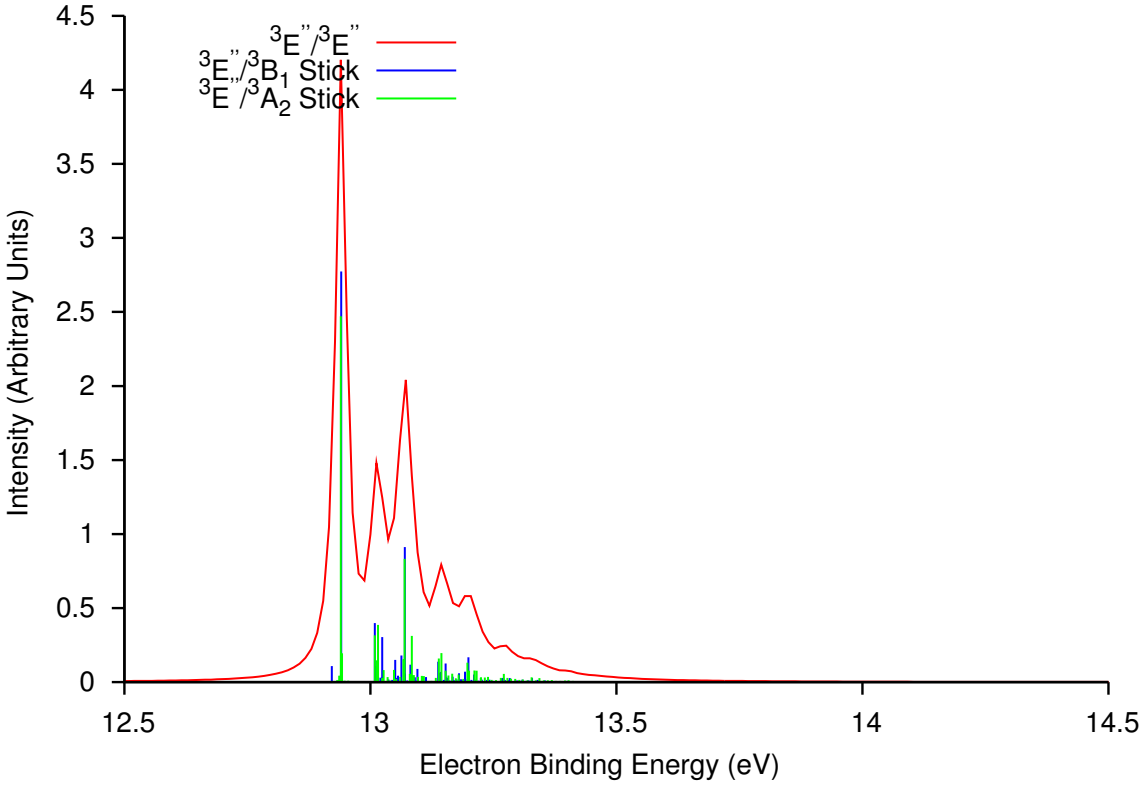

Figure 4.8: Calculated photodetachment spectrum of the $^3E''$ states (First JT pair) of NO_3 (Model 2) with stick spectrum, strong non-adiabatic effects are seen

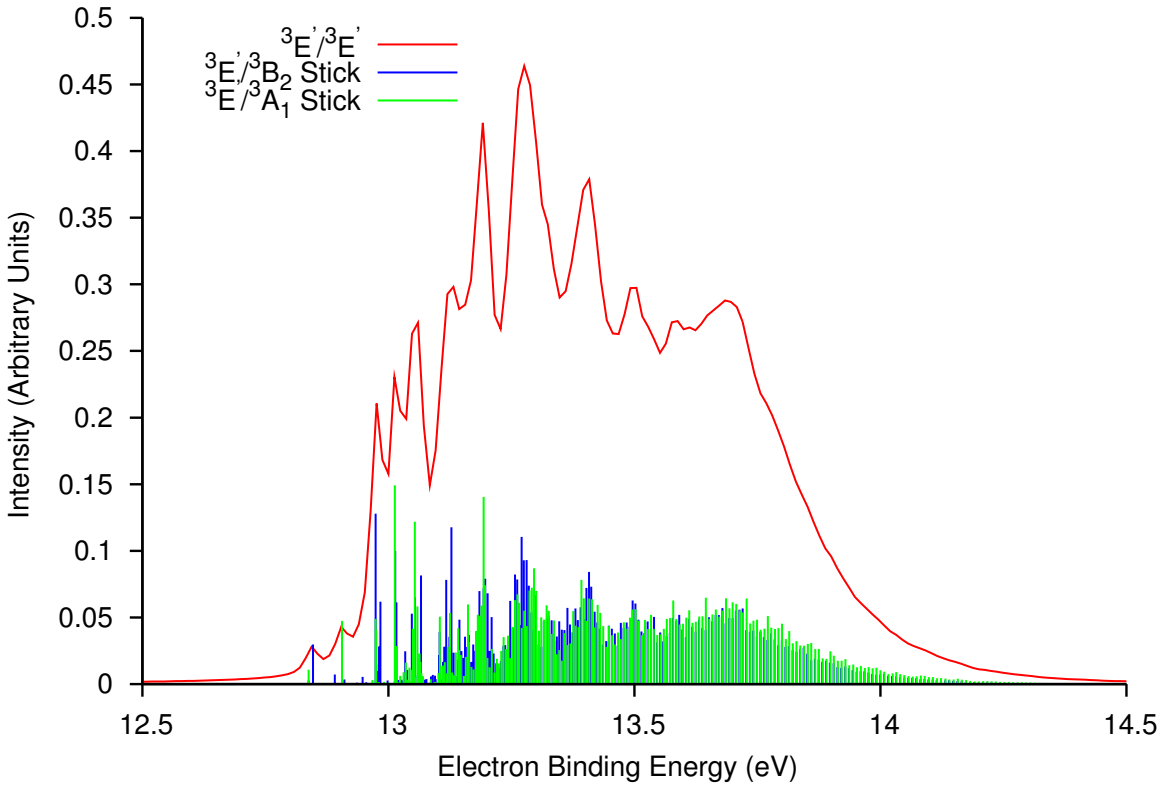

Figure 4.9: Calculated photodetachment spectrum of the $^3E'$ states (Second JT pair) of NO_3 (Model 2) with stick spectrum, strong non-adiabatic effects are seen

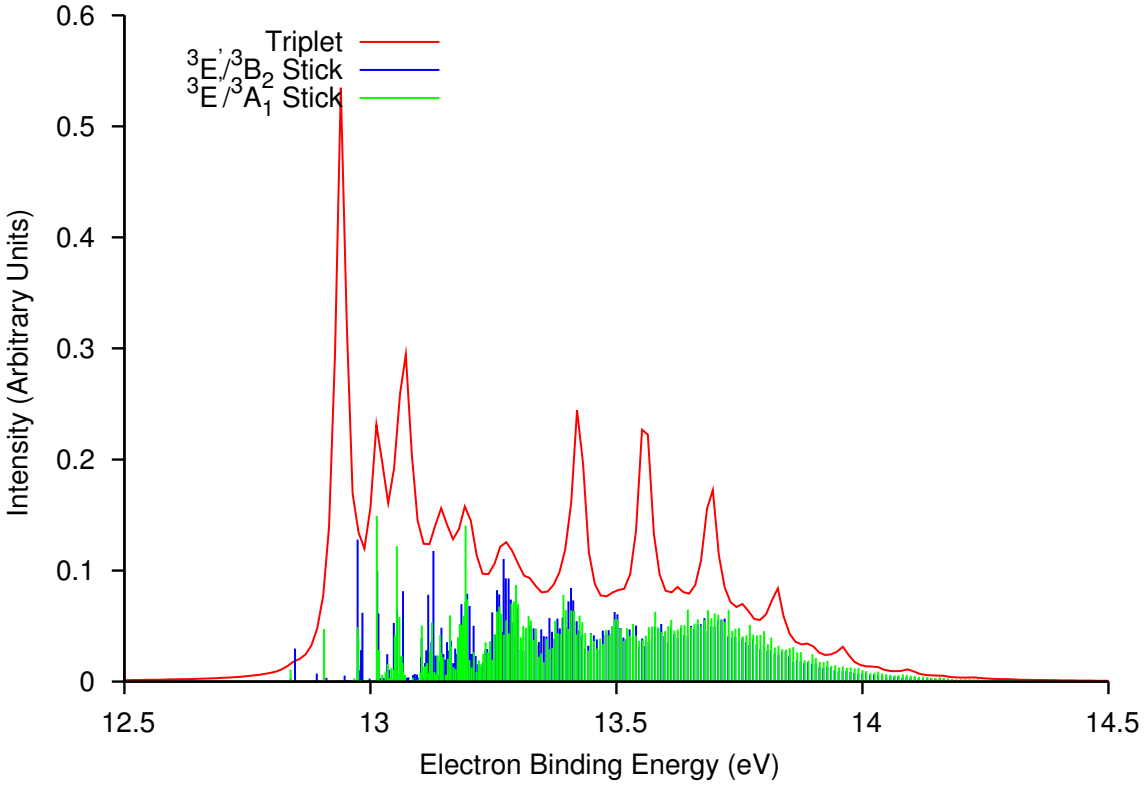

Figure 4.10: Calculated photodetachment spectrum of the 5 lowest triplet states of NO_3 (Model 2) with stick spectrum shown for $^3E''$ states, non-adiabatic effects are not so prominent in total spectrum

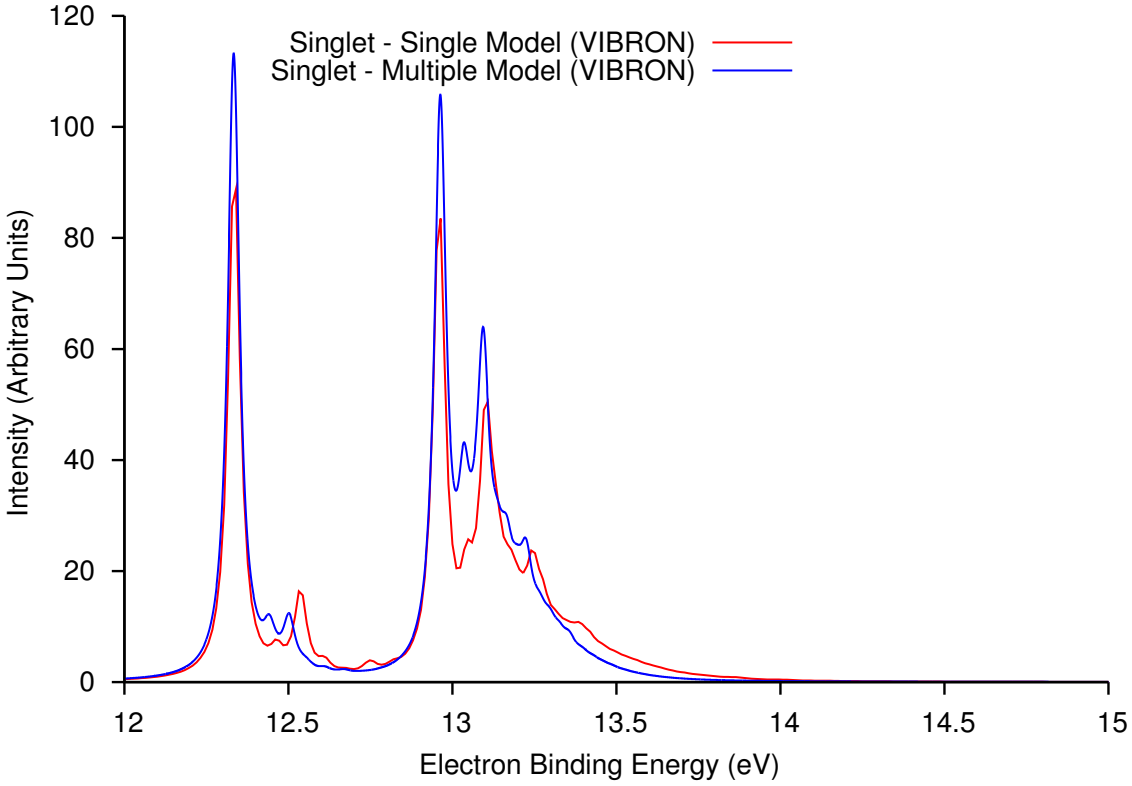

Figure 4.11: Calculated photodetachment spectrum of the Singlet NO_3 with single model (Model1) compared with multiple model (Model 2)

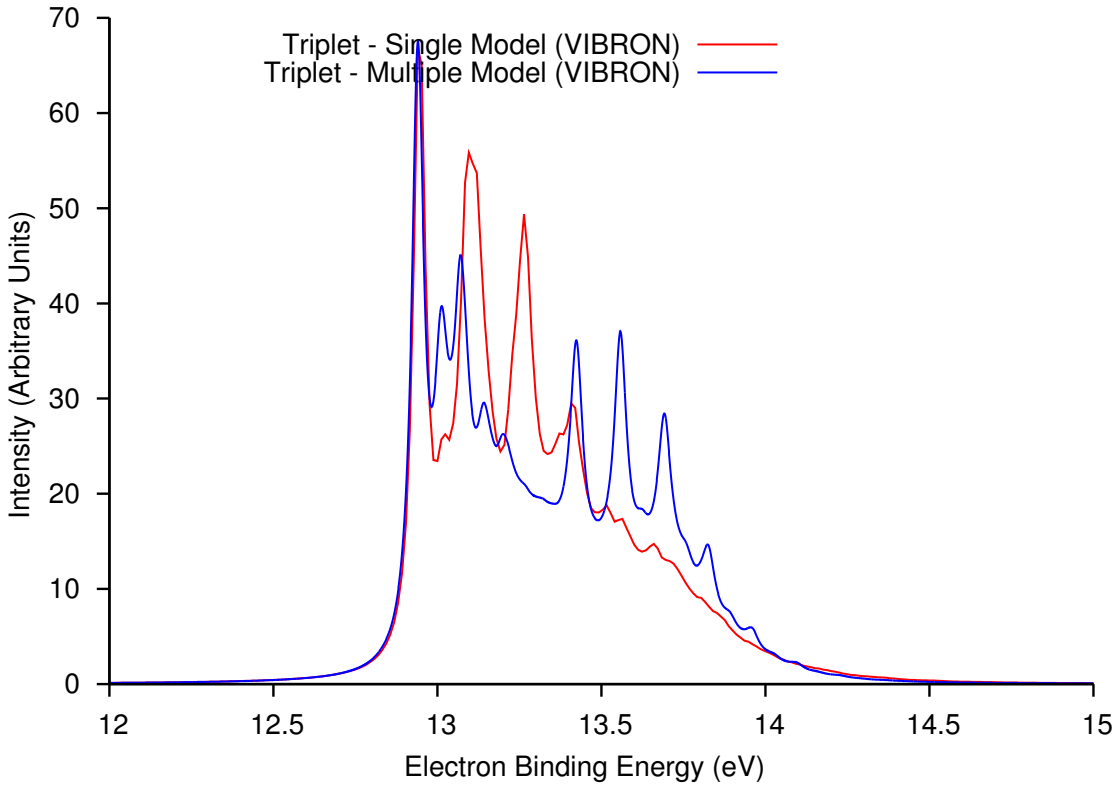

Figure 4.12: Calculated photodetachment spectrum of the Triplet NO_3 with single model (Model1) compared with multiple model (Model 2)

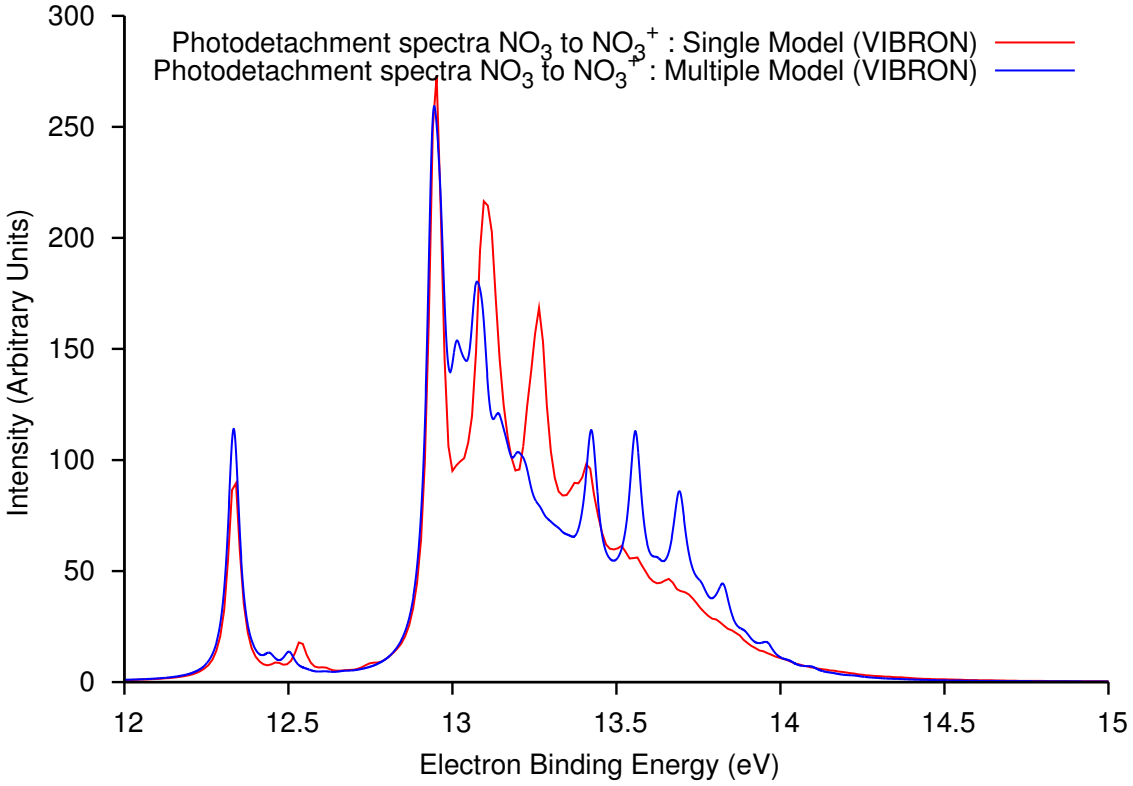

Figure 4.13: Calculated photodetachment spectrum of the NO_3 : Comparison of Single Model vs. Multiple Models

Chapter 5

Cyclobutadiene & Trimethylenemethane

Jahn-Teller systems were briefly discussed in Chapter 3 where we also looked at the prototype case of such systems, the C_3 molecule. In this chapter an attempt will be made to simulate the photodetachment spectra of cyclobutadiene and trimethylenemethane negative ions, leading to a characterization of two very challenging biradical systems - cyclobutadiene (C_4H_4) and trimethylenemethane (TMM), $C(CH_2)_3$.

It has been a challenge for theoretical chemists to elucidate the electronic structure of these two biradicals, in particular to determine the singlet-triplet energy gaps, to deter-

mine whether the singlet falls below the triplet in energy, or to determine the equilibrium geometry of the ground state.[27]

In addition to their complex electronic structure, these systems present a major challenge to the nuclear dynamics simulation not only due to the presence of Jahn-Teller distortion, but also due to the presence of a large number of vibrational degrees of freedom. While C_4H_4 has 18 ($3N-6, N=8$) degrees of freedom, TMM has of 24 ($3N-6, N=10$) degrees of freedom. While the time-independent methods of spectral simulations become out of the question at once for systems of this magnitude, to carry out full quantum dynamics simulation using the efficient time-dependent methods also start to hit the walls.

This chapter makes an attempt to simulate the photodetachment spectra for the negative ions of these two systems using the DIP-STEOM methodology to carry out the electronic structure calculations, while using the advanced features of the MCTDH program to perform the nuclear dynamics simulations. To the best of our knowledge, the studies performed in this chapter are first of their kind and there has not been any report in the literature to date. An important point to note here is that the emphasis of this chapter is not on answering the electronic structure questions to a great accuracy, but to be able to carry out simulations of photodetachment spectra using the methodology presented in this thesis. The DIP-STEOM methodology is fast and also accurate for excited state energies, but there are issues with this method in regards to application on biradical systems.[10]

The spectral simulation for $C_4H_4^-$ will be predictive in nature, as there has been no experiment reported in the literature on this system. We hope that this study can stimulate the experimental chemists to consider to perform this challenging experiment. On the other hand, a beautiful photodetachment spectrum for TMM^- exists, carried out by Wenthold et al. and a comparison will be made to our simulated spectrum.

5.1 Cyclobutadiene

Cyclobutadiene, an antiaromatic annulene containing 4π electrons, represents one of the classic cases where nonadiabatic effects play a vital role in its structure and stability. One would anticipate a square planar, D_{4h}, structure for this molecule, but it turns out that the equilibrium geometry for C_4H_4 is rectangular, D_{2h}. A CASSCF study has been performed [28] on cyclobutadiene discussing the molecular structures, vibrational frequencies and energies of the ground and low-lying excited states taking into account the pseudo Jahn-Teller effect, responsible for the symmetry lowering. A comparison will be drawn to the values calculated with our methods.

5.1.1 Method

As stated earlier, the methodological scheme to carry out the simulation is very much the same as described in chapter 3 for NO_2, the only difference being that there is no time-independent simulation of spectrum in this case. The reference geometry here is taken as the ground state geometry of triplet state of the neutral cyclobutadiene. At this geometry, the closed-shell dianion ($C_4H_4^{2-}$) is taken as the reference state for the EOMCC calculations, and the ionization and double ionization energies are calculated using the IP-EOMCC and DIP-STEOMCC methods respectively. Vibronic models are created for all the three systems – the anion, as well as the singlet and triplet states of the neutral cyclobutadiene using the $GRID = 10$ scheme. All the electronic structure calculations have been performed at the CCSD level of theory using the TZ2P basis set. The choice of TZ2P basis set is made due to it's small size to avoid the issues of diffuse basis set for the dianion.

For the simulation of spectra, first the vibronic eigenstates of the anion are calculated using the *block-improved-relaxation* technique for both the singlet and triplet cases. The spectrum is calculated as a weighted sum of spectrum starting from the two lowest eigenstates, which are degenerate/near-degenerate in energy. The mode combination technique is used to get the maximum efficiency in MCTDH calculations.

5.1.2 Results & Discussions

The optimized geometry of the neutral triplet state at the square planar geometry is given in table 5.1. The harmonic vibrational frequencies at this geometry are calculated at the UCCSD level and are compared to the MP2 values calculated using Gaussian09 as given in table 5.2.

Table 5.1: Optimized parameters for the neutral triplet cyclobutadiene

$R(CC)$	$1.44A^0$
$R(CH)$	$1.08A^0$

The energies of the lowest states for the anion as well as for the singlet and triplet states of the neutral are calculated using the aforementioned EOMCC methods. It can be seen that the ground state of the anion is degenerate where the two states $^2E_{1g}$ and $^2E_{1g}$ are equal in energy. The two highest occupied molecular orbitals in the closed-shell dianion are degenerate and creating two holes from these orbitals gives rise to four lowest states of the neutral, three singlets ($^1B_{2g}$, $^1B_{1g}$, $^1B_{1g}$) and one triplet ($^3B_{2g}$). From the table of energies, it can be seen that the ground state is the singlet $^1B_{2g}$, lying $4.93kcal/mol$ below the triplet. The singlet-triplet gap predicted by MCSCF calculation is $6.2kcal/mol$.[29] As

predicted by the MCSCF studies, our studies also confirm that singlet is the ground state for the neutral cyclobutadiene.

The vibronic model Hamiltonians are now set up for the anion (6 lowest states) as well as for the singlet (3 lowest states) and triplet (3 lowest states) for the neutral cyclobutadiene. The diabatic Hamiltonian is created and the coupling constants are calculated for all the three cases. The adiabatic potential energy surfaces are also generated for all the three systems. We can identify the important normal modes by looking at the coupling constants, in particular the linear coupling constants, as well as by looking at the behaviour of adiabatic potential surfaces.

Cyclobutadiene represents one of the simplest systems with a square-planar D_{4h} geometry in the high symmetry configuration and a doubly degenerate E term which results in a $E \otimes (b_1 + b_2)$ type of Jahn-Teller problem. For the anion, the ground state is doubly degenerate ${}^2E_{1g}$ term, the symmetrized direct product of which with itself can be decomposed as

$$E_{1g} \times E_{1g} = A_{1g} + B_{1g} + B_{2g} \tag{5.1}$$

According to the general theory [30] the Jahn-Teller active coordinates are of either b_{1g} or b_{2g} symmetry, which results in D_{2h} configurations of a rhombus or rectangle, respectively. By looking at frequency table and the adiabatic surfaces for the anion, it can be clearly

seen that for cyclobutadiene anion these modes are Normal mode 14 (B_{1g}), 16 (B_{2g}), and 17 (B_{2g}). Normal mode 1, 4, 5 are also important due to large anharmonicities and the double well kind of structure of the potential surfaces corresponding to these modes. The degenerate E vibrational modes (4-11) may be PJT active, rather than being JT active for cyclobutadiene as opposed to an $E \otimes e$ Jahn-Teller problem. Displacement diagrams for the important normal modes are shown in figure 5.1. Adiabatic surfaces corresponding to these normal modes are shown in figure 5.2. Very similar is the case for the neutral singlet and triplet cyclobutadiene and the adiabatic surfaces corresponding to the above mentioned 6 normal modes are shown in figure 5.3 and 5.4.

We are now in a position to calculate the photodetachment spectrum of $C_4H_4^-$. As a first step, the vibronic eigenstates and eigenfunctions of the anion are calculated using the *block-improved-relaxation* method. The 18 vibrational degrees of freedom are combined into eight particles involving either three, two or one DOF each, in order to reduce the computational cost of wavepacket propagation on the product primitive grid. The mode combination used are given in table 5.5. 10 primitive basis function are used for all the particles. Several SPFs are used for the first four particles, constituting the important modes, while a single SPF is used for the remaining particles.

Two such calculations are performed, for anion + singlet, as well as for anion + triplet after merging the operator files. Both the calculations produce the same set of eigenvalues

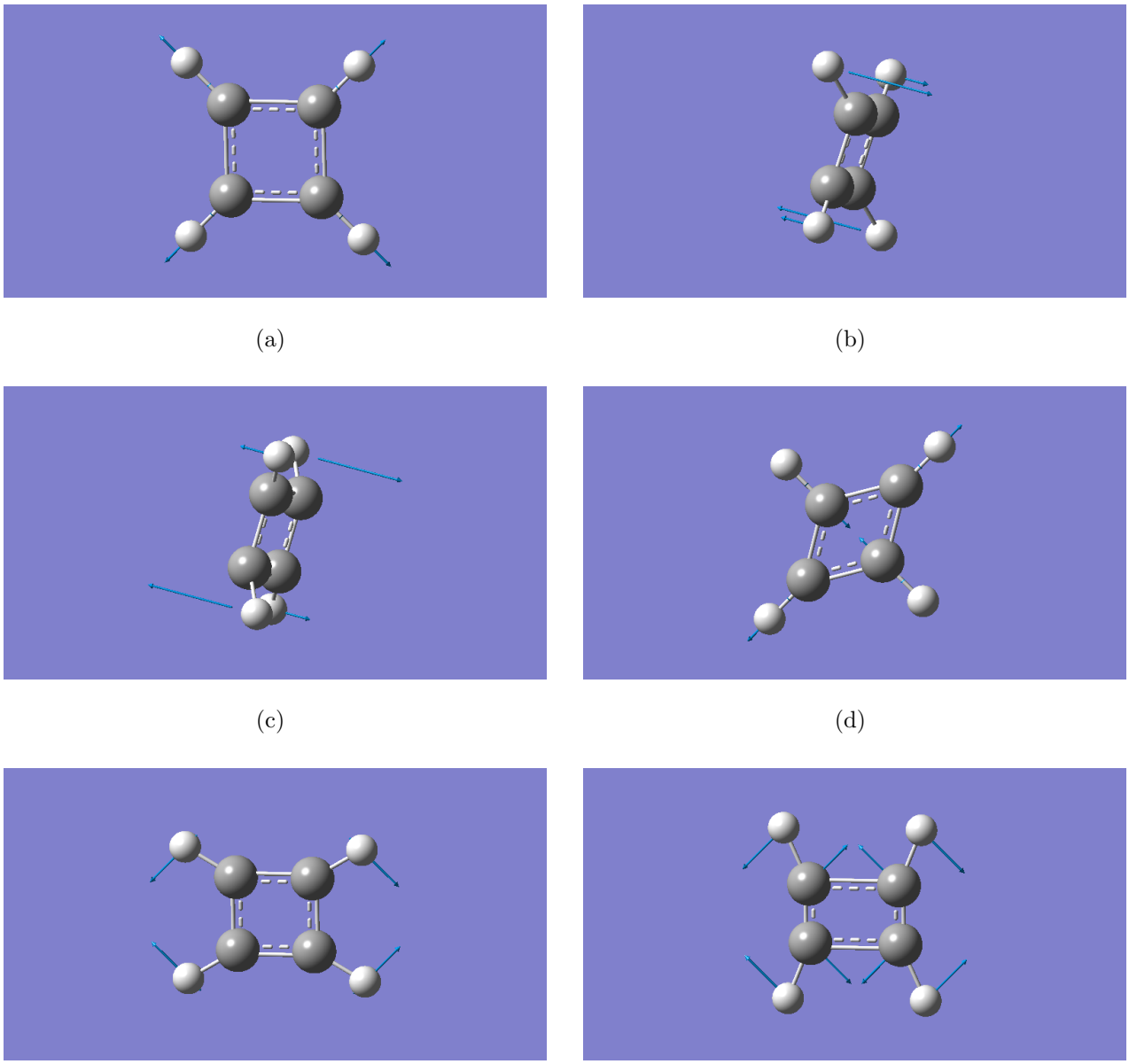

(a) (b) (c) (d) (e) (f)

Figure 5.1: The important normal modes for cyclobutadiene: Mode 1(A_{1g}, 1280.19$cm^{-}1$), 4(E_{1g}, 559.03$cm^{-}1$), 5(E_{1g}, 559.03$cm^{-}1$), 14(B_{1g}, 951.97$cm^{-}1$), 16(B_{2g}, 1026.00$cm^{-}1$), 17(B_{2g}, 1375.64$cm^{-}1$)

(as they should) and it can be seen that the lowest vibronic eigenstate is degenerate. The spectrum for both the singlet and triplet will be calculated starting from both the states.

The next step is to perform the dynamics of the neutral cyclobutadiene once the initial wavefunction has been generated. A vertical excitation corresponding to the instantaneous removal of an electron with no relaxation of nuclear framework is used to form the initial wavepacket. This is done by the help of an excitation operator which takes the lowest energy vibronic eigenfunction of the anion and places it into all of the diabatic states of the neutral. This step is repeated four times, two times for singlet where the two separate calculation takes place starting from the two lowest degenerate states of the anion and the similar procedure is repeated for the triplet. The photodetachment spectrum for the individual states are obtained first by taking the Fourier transform of the time correlation function, and then a Boltzmann averaged spectrum is calculated for both the singlet and triplet case using the `sumspec` program.

It is apparent that the contribution to the spectrum (for both singlet and triplet) from different roots of the vibronic degenerate eigenstates is quite different. A Boltzmann averaging is performed to get the total spectrum for singlet as well as triplet. Again, to get the total spectrum for the neutral cyclobutadiene, singlet and triplet spectra are combined with appropriate weighted sum i.e. 1 and 3 respectively. A predictive experimental spectrum is presented in figure 5.10.

5.1.3 Summary

The methodology for calculating the photodetachment spectrum described in the earlier chapters has been successfully applied to the cyclobutadiene molecule. Unfortunately, there is no experimental spectrum to which a comparison can be made. It is important to note that convergence can be an issue for MCTDH calculations, and further calculations need to be performed in order to make sure that convergence is reached for both stages – whether finding the initial wavefunction or performing the dynamics to calculate the spectrum. Another meaningful comparison can be made with a spectrum simulated using the models created at a different GRID, let us say for GRID=3, which can show the importance (or lack thereof) of the higher order coupling constants in the representation of PESs as well as in the simulation of spectrum. We look forward to carry out these calculations in near future.

5.2 TMM

In our studies of biradicals, the last molecule we are going to look at is Trimethylenemethane (TMM), a notorious biradical. The photodetachment spectrum of the negative ion of the TMM has been reported by Lineberger et al [31] . This non-Kekule conjugated hydrocarbon has continued to be a challenging subject for electronic structure calculations

for many years now and a wide variety of electronic structure methods have been employed in it's study, including the sophisticated multireference methods such as Spin-Flip Equation of Motion Coupled Cluster (SF-EOMCC)[32] and Reduced Multireference Coupled Cluster (RMR CC) [33] methods. The four π electrons in neutral TMM are delocalized over four π MOs. Orbital occupation gives rise to a ${}^3A_2^{'}$ state of D_{3h} symmetry, which is the ground state, and a ${}^1E'$ state undergoing JT distortion leading to two singlets, ${}^1A_1$ and ${}^1B_2$, with C_{2v} geometries. Considerable efforts have been put in the studies of equilibrium geometry, energies and vibrational frequencies of these states in the above mentioned references, as well as to determine the singlet-triplet energy gaps.

The goal in this section is to simulate the photodetachment spectra of TMM^-, which is a challenging task not only due to the presence of JT and PJT couplings in the anion as well as the neutral TMM, but also due to the large number of vibrational degrees of freedom this molecule has (24!). At the electronic structure level, it can be a daunting task to find a meaningfully compact representation of such complicated surfaces also due to the presence of large amplitude motions. On the other hand, at the nuclear dynamics level, while the computational expense grows exponentially, it also becomes a challenge to get a converged spectrum. We employ the computational tools discussed in this thesis so far to reach this goal, and a reasonable agreement with experiment has been obtained. It is worthwhile to mention that such a theoretical study for TMM has not been reported in

the literature till date. We hope to refine our analysis and send these results for a journal publication.

5.2.1 Method

A similar procedure to that used for C_4H_4 in the last section will be followed here. The reference geometry is taken as the triplet ground state geometry the neutral TMM. The DIP-STEOM methodology is used to calculate the ionization energies starting from the closed-shell dianion ($TMM2-$). Vibronic models are created for all the three systems – the anion, as well as the singlet and triplet states of the neutral TMM using the $GRID = 10$ scheme. All the electronic structure calculations have been performed at the CCSD level of theory using the TZ2P basis set.

In order to perform nuclear dynamics, as a first step the vibronic eigenstates of the anion are calculated using the *block-improved-relaxation* method for both the singlet and triplet cases, as discussed in Chapter 3. The spectrum is calculated as a weighted sum of spectrum starting from the two lowest eigenstates, which are degenerate/near-degenerate in energy. Normal modes are combined in order to get the maximum efficiency in MCTDH calculations.

5.2.2 Results & Discussions

The optimized parameters of the neutral triplet state at the D_{3h} geometry is given in table 5.7. The harmonic vibrational frequencies are calculated at the UCCSD level and are given in two tables, 5.8 and 5.8, for degenerate and non-degenerate modes respectively.

The energies of several low-lying excited states for the anion as well as for the singlet and triplet states of the neutral are calculated using the aforementioned EOMCC methods. It is observed that the ground state of the anion is degenerate by symmetry ($^2E''$). Moreover, the ground state of the singlet TMM also forms a degenerate pair of $^1E'$ symmetry. From the table of energies, it can be clearly observed that the ground state of the neutral TMM is the triplet $^3A_2{}'$, lying $1.08eV$ below the singlet, at the triplet optimized geometry.

Two deferent sets of vibronic models are created using the $GRID = 10$ scheme:

Model-1:

TMM^-: 3 lowest states

Singlet TMM: 3 lowest states

Triplet TMM: 3 lowest states

Model-2:

TMM^-: 6 lowest states

Singlet TMM: 6 lowest states

Triplet TMM: 3 lowest states

Adiabatic potential surfaces are created for all the six cases. In TMM, the degeneracy of E'' and E' electronic states are lifted by the coupling with normal modes of E' symmetry as predicted by the Jahn-Teller theorem, and leads to a symmetry lowering (from D_{3h} to C_{2v}). This can be seen in the potential surfaces diagrams, and also large linear coupling constants can be seen in the model Hamiltonian parameters. Normal modes of E' and E'' symmetry are shown in figure 5.11 and 5.12. Adiabatic potential surfaces corresponding to these modes for Model-1 are shown in figure 5.13 and 5.14 for anion, 5.15 and 5.16 for singlet, and 5.17 and 5.18 for triplet.

For Model-2, some of the adiabatic surfaces represent unbound potentials (figure 5.19. This might be due to the increased active space (number of states in IP) or also due to the presence of large amplitude motions (rotation of CH_2 groups) in singlet. This is a limitation of vibronic model Hamiltonians, where the calculated potentials might not be the true representation of real potential energy surfaces. The extra states (4-6) in the model seem to be causing the problem.

The photodetachment spectrum of TMM^- is simulated using the vibronic models from Model-1. Vibronic eigenstates and eigenfunctions of the TMM^- are calculated using the

block-improved-relaxation method. The 24 vibrational degrees of freedom are combined into eight particles involving either two, three or four DOF each, in order to reduce the computational cost of wavepacket propagation on the product primitive grid. The mode combination used is given in table 5.12. 10 primitive basis function are used for all the particles. SPFs used for each particle are also mentioned in the table 5.12.

Two such calculations are performed, for anion + singlet, as well as for anion + triplet after merging the operator files. Both the calculations produce the same set of eigenvalues (as they should) and it can be seen that the lowest vibronic eigenstate is degenerate. The spectrum for both the singlet and triplet will be calculated starting from both the states.

Once the initial wavefunctions have been generated, the next step is to perform the dynamics of the neutral TMM. Once again, a vertical excitation corresponding to the instantaneous removal of an electron with no relaxation of nuclear framework is used to form the initial wavepacket. This is done by the help of an excitation operator which takes the lowest energy vibronic eigenfunction of the anion and places it into all of the diabatic states of the neutral. This step is repeated four times, two times for singlet where the two separate calculation takes place starting from the two lowest degenerate states of the anion and the similar procedure is repeated for the triplet. The photodetachment spectrum for the individual states are obtained first by taking the Fourier transform of the time correlation function, and then a Boltzmann averaged spectrum is calculated for both

the singlet and triplet case using the `sumspec` program.

The simulated spectrum comprised of 3 low lying singlet as well 3 low lying triplet states is shown in figure 5.20. The spectrum between the range of 0 to 3 eV is shown in figure 5.21 along with the experimental spectrum in figure 5.22. There is a reasonable agreement between the experimental and simulated spectrum. The first band (lower energy) corresponds to the ground state triplet while the second band corresponds to the lowest singlet state. The triplet region of the spectrum is expanded where a good agreement with simulation (figure 5.23) and experiment (figure 5.24) is seen.

5.2.3 Summary

The photodetachment spectra of TMM^- has been simulated successfully using the computational tools discussed and a reasonable agreement with the experiment has been observed. Most certainly, there are issues with convergence in MCTDH and more accurate calculations with increased number of Primitive bases and SPFs need to be carried out. These calculations also tend to become expensive very quickly and a careful monitoring of the convergence is required. Nonetheless, the analysis performed in this chapter shows that the methodology discussed is quite useful for simulating the complicated vibronic spectrum of biradicals of larger size.

Table 5.2: Vibrational normal modes for the neutral triplet cyclobutadiene

Normal Mode	Description	Frequency CCSD (cm^{-1})	Frequency MP2 (Gaussian)(cm^{-1})
1 (A_{1g})		1280.19	1303.04
2 (A_{1g})		3303.52	3311.13
3 (A_{2g})		1223.43	1217.33
4 (E_{1g})		559.03	481.5
5 (E_{1g})		559.03	481.5
6 (E_{1u})		875.68	1093.23
7 (E_{1u})		875.68	1093.23
8 (E_{1u})		1326.69	1824.57
9 (E_{1u})		1326.69	1824.57
10 (E_{1u})		3276.44	3303.66
11(E_{1u})		3276.44	3303.66
12(B_{2u})		467.68	335.83
13(B_{2u})		625.07	531.03
14 (B_{1g})		951.97	949.26
15 (B_{1g})		3262.95	3273.21
16 (B_{2g})		1026.00	1036.30
17 (B_{2g})		1375.64	1378.79
18 (A_{2u})		556.87	470.20

Table 5.3: Ionization energies of the anion calculated using IP-EOM-CCSD

State	Ionization Energy (eV)
$^2E_{1g}$	-6.23
$^2E_{1g}$	-6.23
$^2A_{2u}$	-1.10
$^2E_{1u}$	-0.20
$^2E_{1u}$	-0.20
$^2B_{2g}$	0.18

Table 5.4: Double ionization energies of the anion calculated using DIP-STEOM-CCSD

State	Ionization Energy (eV)
$^1B_{2g}$	-6.72
$^1B_{2g}$	-5.12
$^1B_{1g}$	-4.22
$^3B_{2g}$	-6.51
$^3E_{1u}$	-1.32
$^3E_{1u}$	-1.32

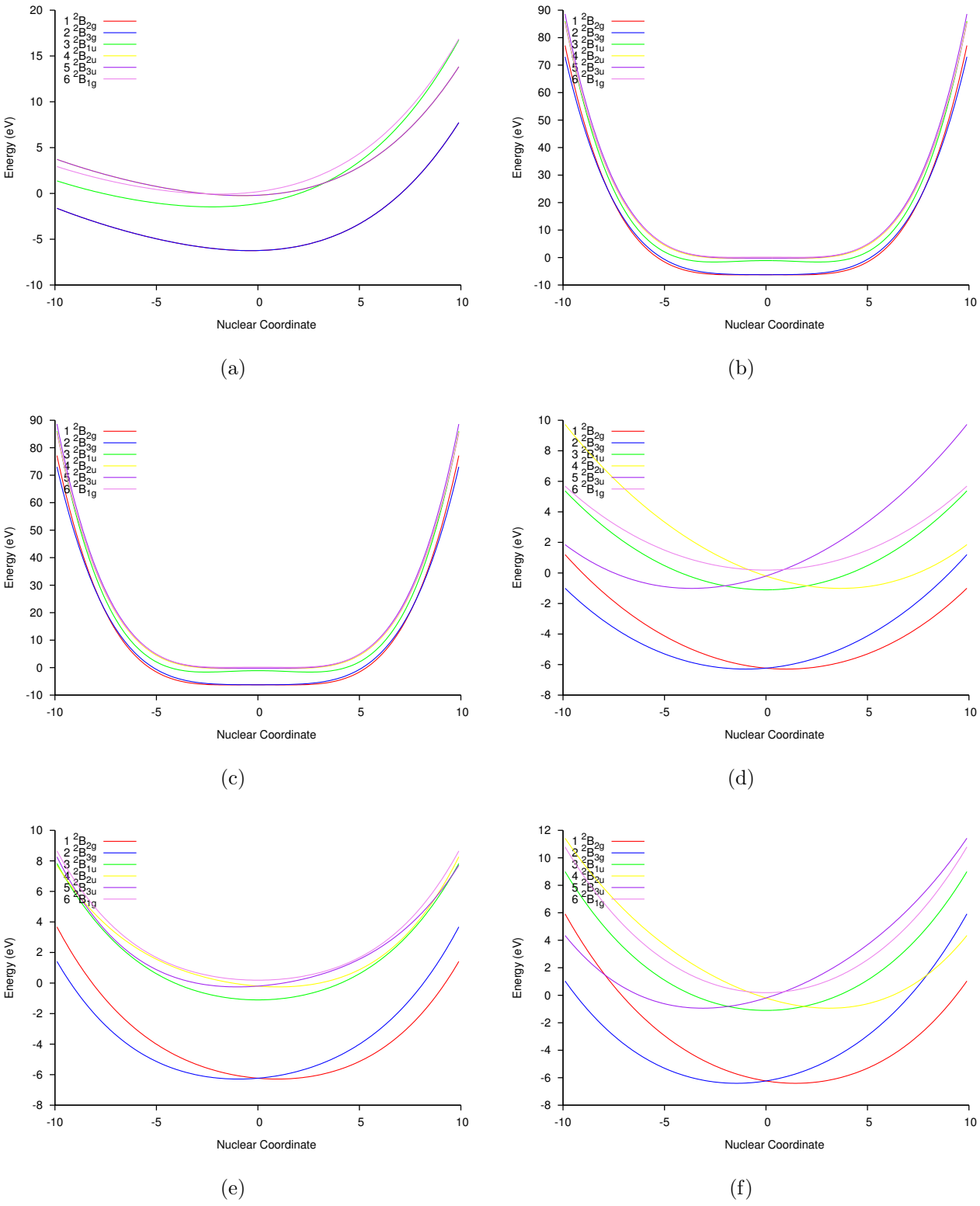

(a) (b)

(c) (d)

(e) (f)

Figure 5.2: Adiabatic surfaces for the anion cyclobutadiene: Mode 1, 4, 5, 14, 16, 17

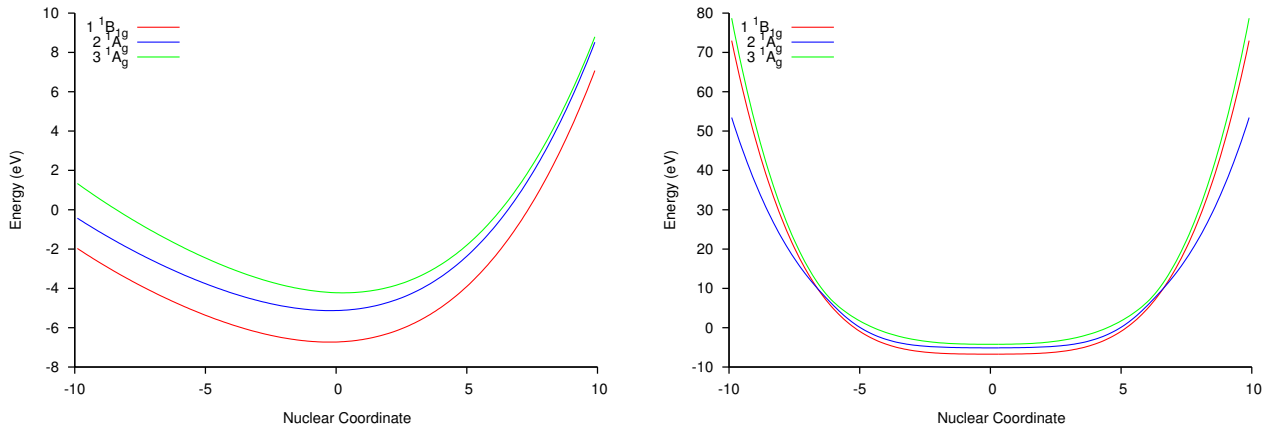

(a)

(b)

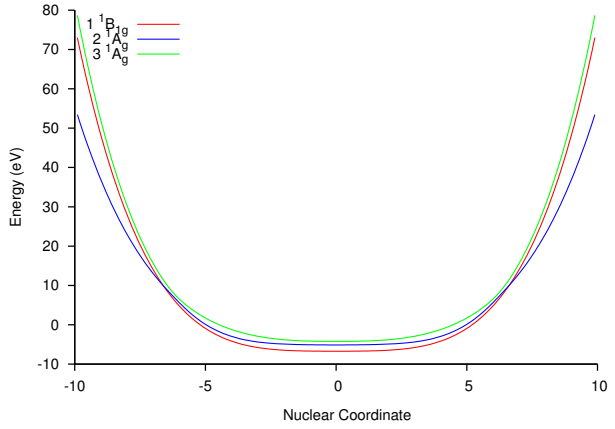

(c)

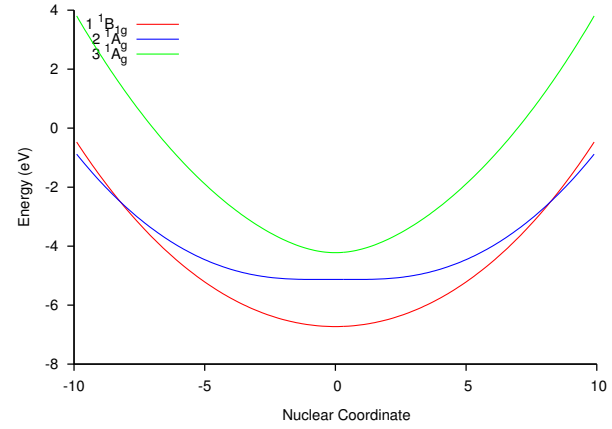

(d)

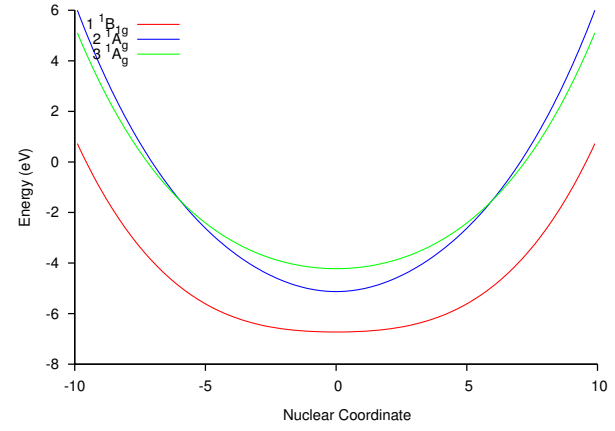

(e)

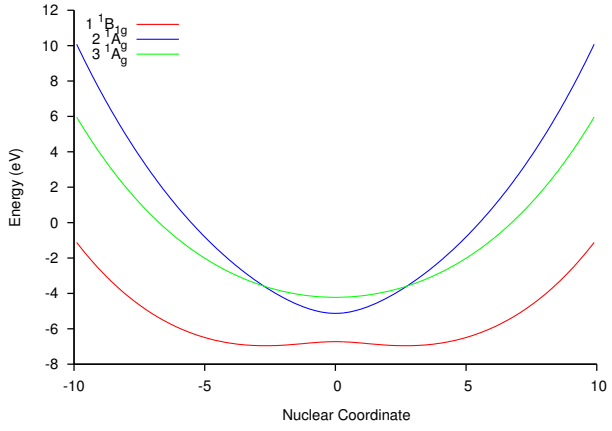

(f)

Figure 5.3: Adiabatic surfaces for the singlet neutral cyclobutadiene: Mode 1, 4, 5, 14, 16, 17

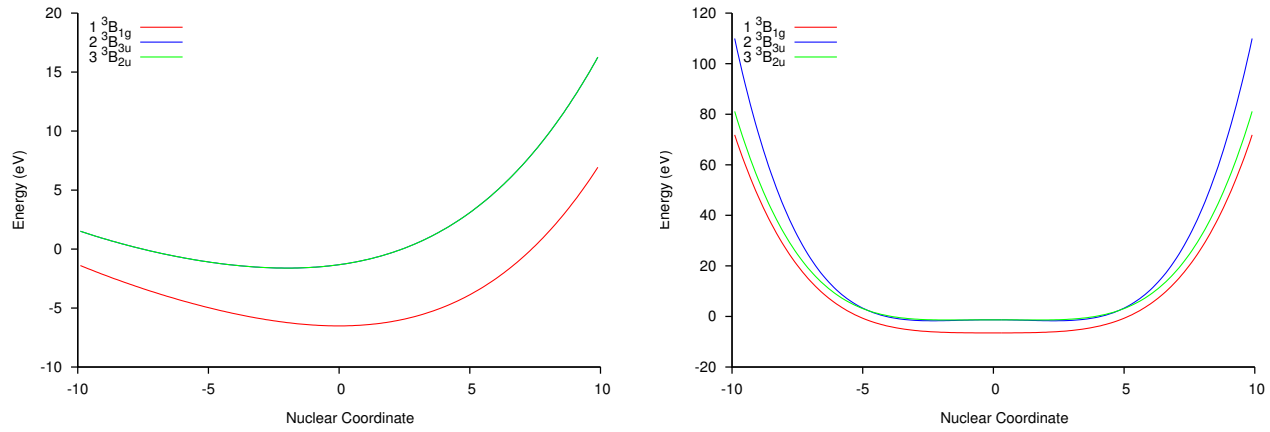

(a)

(b)

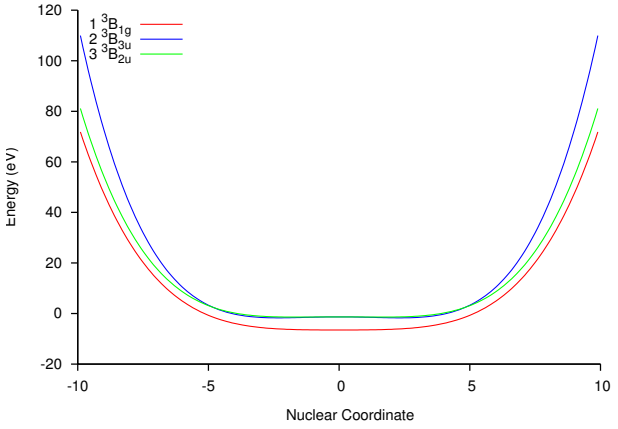

(c)

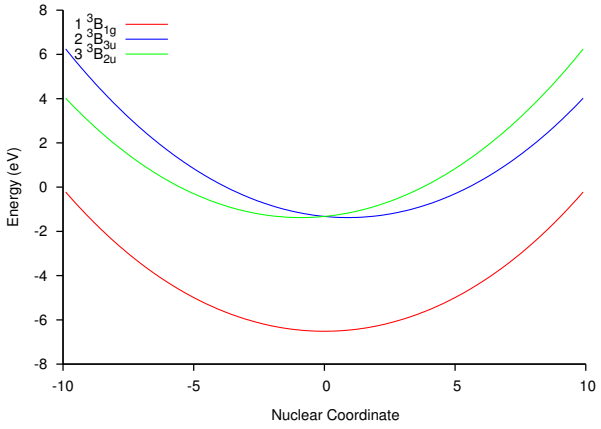

(d)

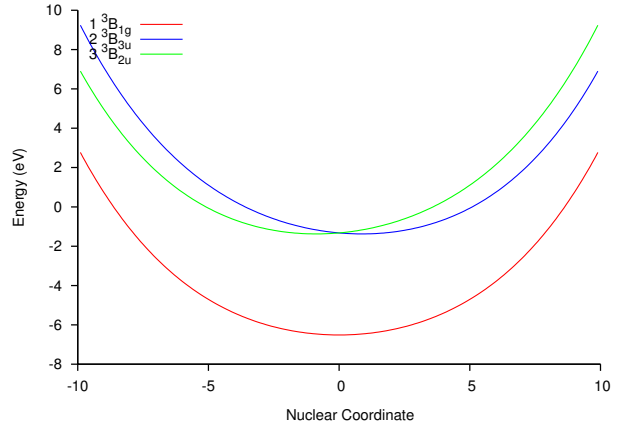

(e)

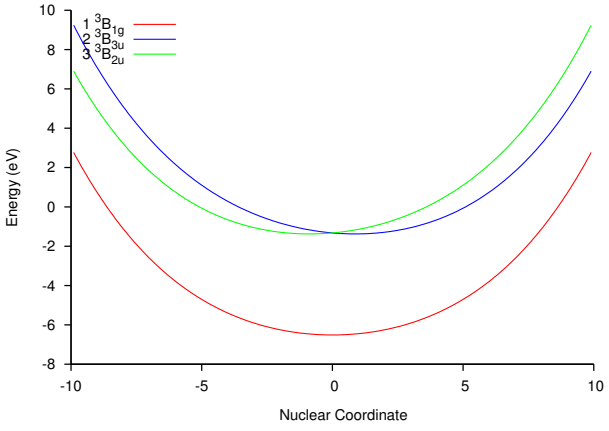

(f)

Figure 5.4: Adiabatic surfaces for the triplet neutral cyclobutadiene: Mode 1, 4, 5, 14, 16, 17

Table 5.5: Details of the MCTDH computational setup. Mode combinations are listed along with the primitive bases of these modes, and the number of SPFs used for the relaxation as well as for the propagation calculation. Vibrational normal modes in one bracket constitute single particles. The primitive basis is the number of harmonic-oscillator DVR functions. Each particle has a primitive basis consisting of $10 \times 10 \times 10 = 1000$ functions. The SPF basis is the number of single particle functions used for each electronic state (being a single-set calculation).

Particle	Normal Modes	Primitive basis	SPF Basis (Relaxation)	SPF Basis (Propagation)
1	(4, 5, 14)	[10,10,10]	7	10
2	(1, 16,17)	[10,10,10]	7	10
3	(13, 18)	[10,10,10]	7	10
4	(8, 9)	[10,10,10]	7	10
5	(10, 11, 15)	[10,10,10]	1	2
6	(6, 7, 12)	[10,10,10]	1	2
7	(2)	[10,10,10]	1	2
8	(3)	[10,10,10]	1	2

Table 5.6: Vibronic eigenvalues of the cyclobutadiene anion as MCTDH with block-improved-relaxation method

Root	Energy (eV)	Energy ($cm^{-}1$)
1	0.0	0.0
2	0.0	0.0
3	0.036	290.03
4	0.040	322.25
5	0.058	467.27
6	0.059	475.32
7	0.064	515.61
8	0.064	515.61
9	0.065	523.66
10	0.065	523.66

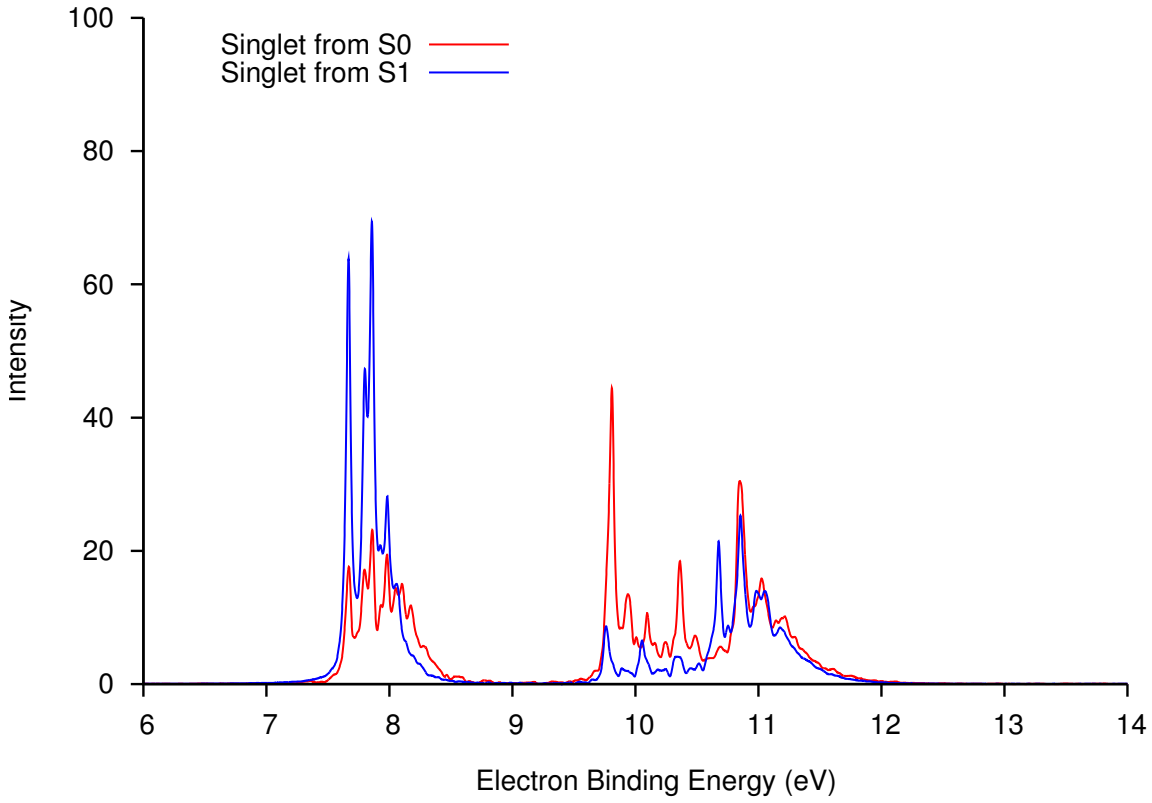

Figure 5.5: Photodetachment spectrum of the $C_4H_4^-$: singlet states contribution from two lowest eigenstates of anion

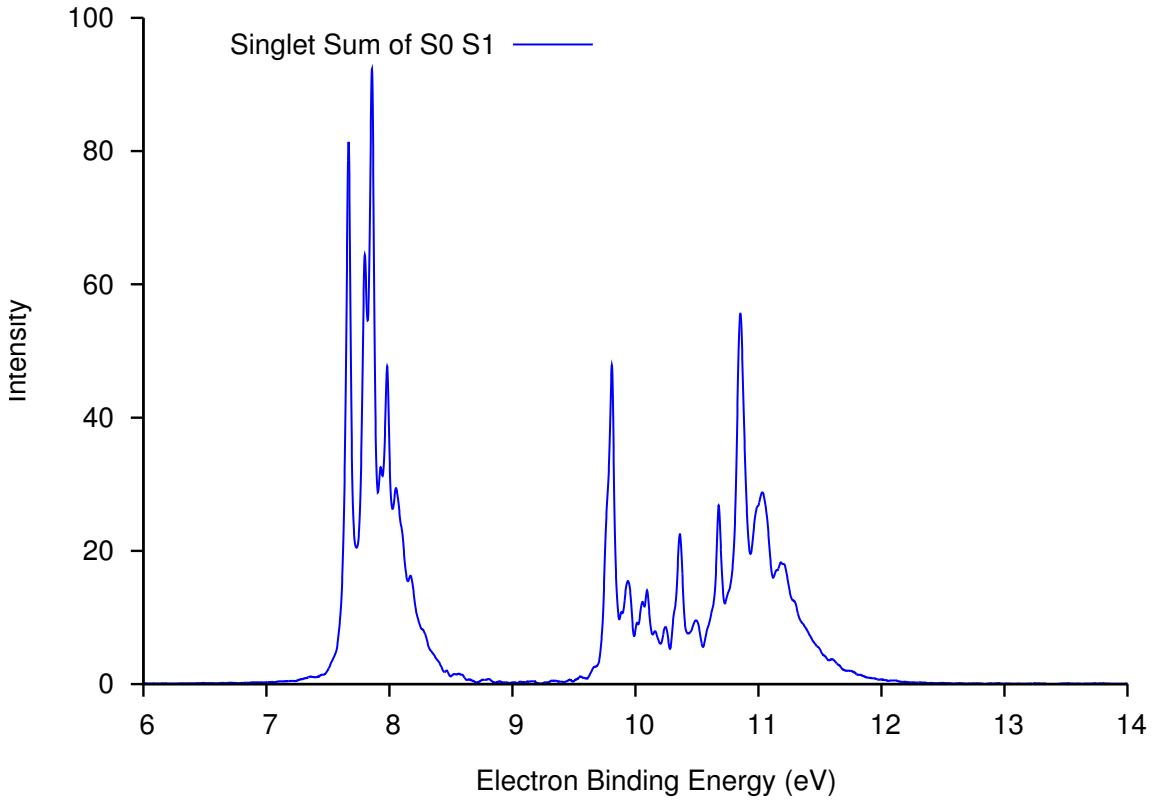

Figure 5.6: Photodetachment spectrum of the $C_4H_4^-$: Boltzmann averaged total singlet spectrum

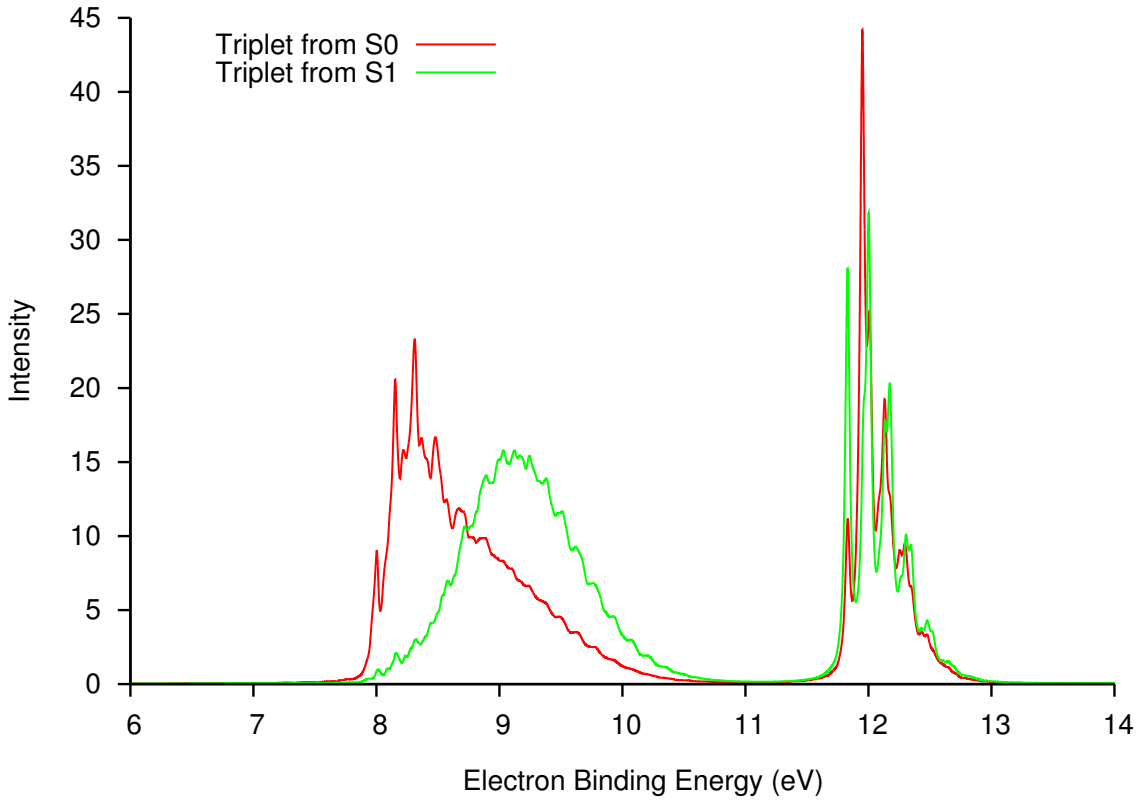

Figure 5.7: Photodetachment spectrum of the $C_4H_4^-$: triplet states contribution from two lowest eigenstates of anion

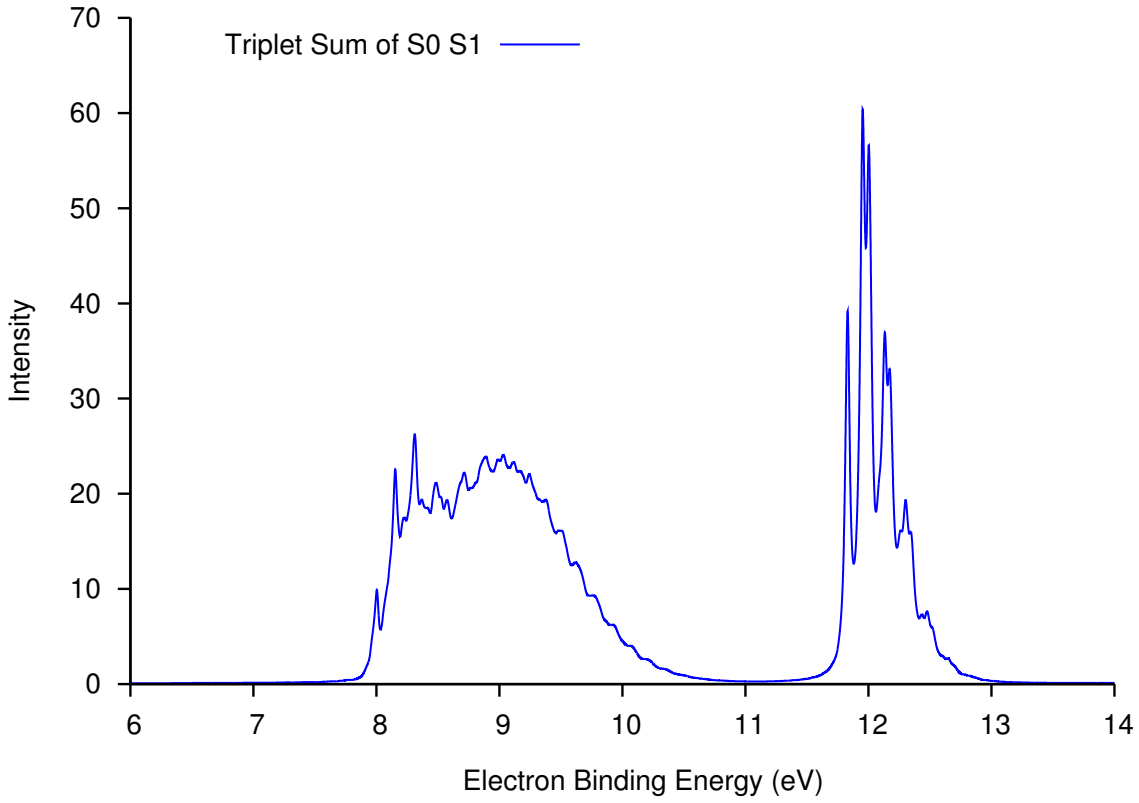

Figure 5.8: Photodetachment spectrum of the $C_4H_4^-$: Boltzmann averaged total triplet spectrum

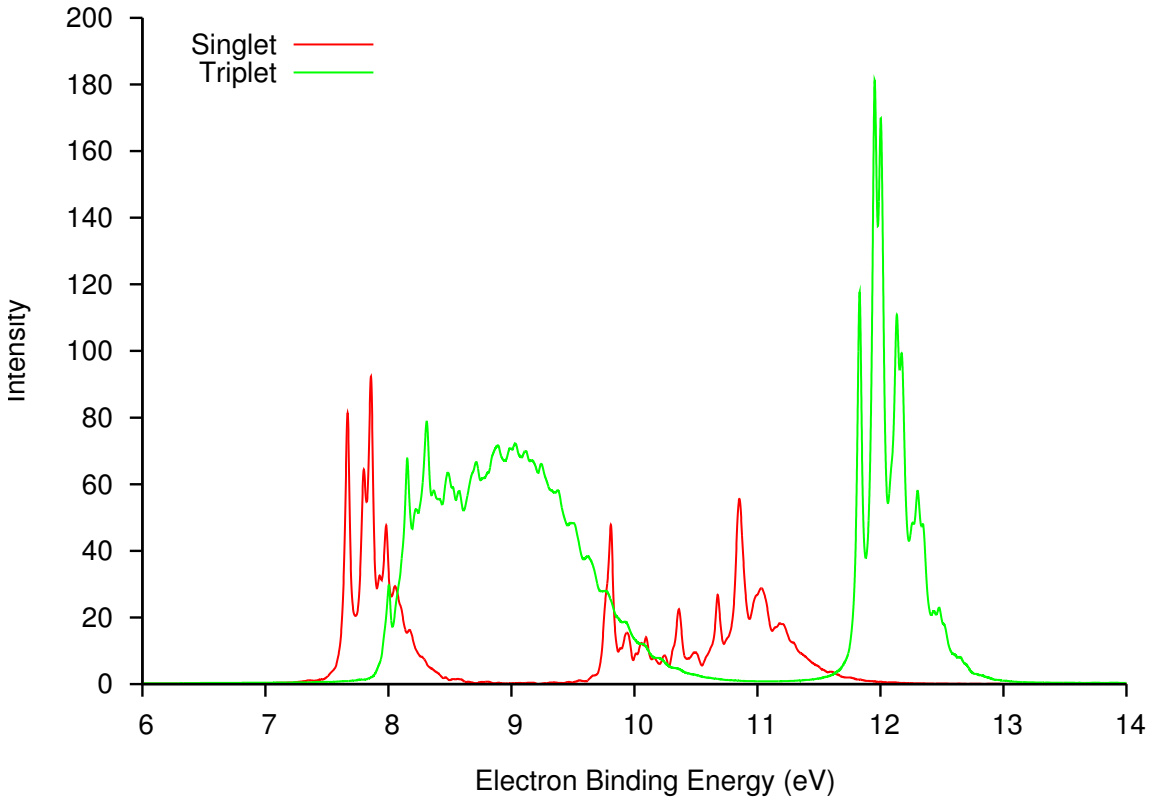

Figure 5.9: Photodetachment spectrum of the $C_4H_4^-$: Total spectrum showing individual singlet and triplet contributions

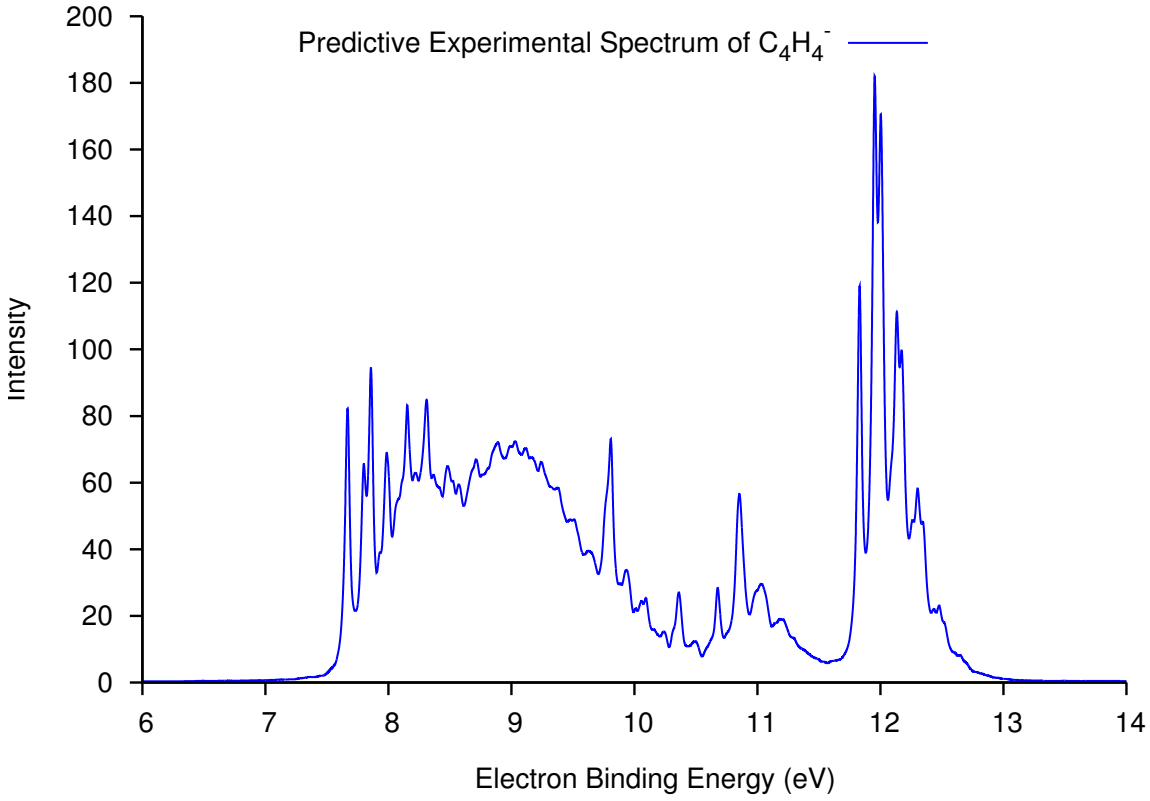

Figure 5.10: Predictive Experimental Photodetachment Spectrum of the $C_4H_4^-$

Table 5.7: Optimized geometry for the neutral triplet TMM

$R(CC)$	$1.4130214941A^0$
$R(CH)$	$1.0792693355A^0$
$A(HCC)$	120.8567816223^0

Table 5.8: Vibrational normal modes for the neutral triplet TMM: Degenerate Modes ($E^{''}$) and ($E^{'}$)

Normal Mode	Frequency CCSD (cm^{-1})
1 ($E^{''}$)	476.91
2 ($E^{''}$)	476.91
3 ($E^{''}$)	698.61
4 ($E^{''}$)	698.61
5 ($E^{'}$)	429.61
6 ($E^{'}$)	429.61
7 ($E^{'}$)	1029.54
8 ($E^{'}$)	1029.54
9 ($E^{'}$)	1362.11
10 ($E^{'}$)	1362.11
11 ($E^{'}$)	1518.55
12 ($E^{'}$)	1518.55
13 ($E^{'}$)	3184.61
14 ($E^{'}$)	3184.66
15 ($E^{'}$)	3294.32
16 ($E^{'}$)	3294.32

Table 5.9: Vibrational normal modes for the neutral triplet TMM: Non-degenerate Modes

Normal Mode	Frequency CCSD (cm^{-1})
1 ($A_1^{'}$)	937.50
2 ($A_1^{'}$)	1539.21
3 ($A_1^{'}$)	3191.88
4 ($A_1^{''}$)	470.96
5 ($A_2^{'}$)	971.24
6 ($A_2^{'}$)	3291.37
7 ($A_2^{''}$)	498.75
8 ($A_2^{''}$)	739.15

Table 5.10: Ionization energies of the anion calculated using IP-EOM-CCSD

State	Ionization Energy (eV)	Symmetry (D_{3h})	Symmetry (C_{2v})
1	-4.97	$^2E''$	$^2B_1$
2	-4.97	$^2E''$	$^2A_2$
3	-0.34	$^2A_2''$	$^2B_1$
4	1.15	$^2E'$	$^2B_2$
5	1.15	$^2E'$	$^2A_1$
6	1.92	$^2A_2{}'$	$^2B_2$

Table 5.11: Double ionization energies of the anion calculated using DIP-STEOM-CCSD

State	Ionization Energy (eV)	Symmetry (D_{3h})	Symmetry (C_{2v})
1	-3.99	$^1E'$	$^1A_1$
2	-3.99	$^1E'$	$^1B_2$
3	-0.97	$^1A_1'$	$^1A_1$
4	1.75	$^1A_1''$	$^1A_2$
5	1.78	$^1E''$	$^1A_2$
6	1.78	$^1E''$	$^1B_2$
7	-5.07	$^3A_2'$	$^3B_2$
8	0.33	$^3E'$	$^3A_1$
9	0.33	$^3E'$	$^3B_2$

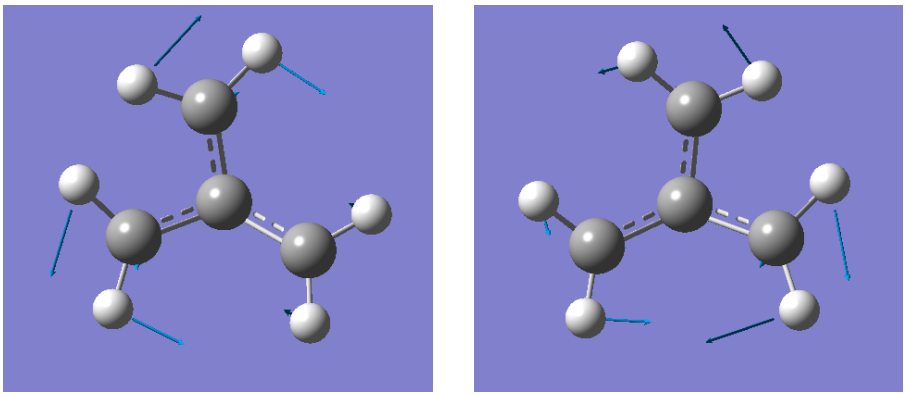

(a) (b)

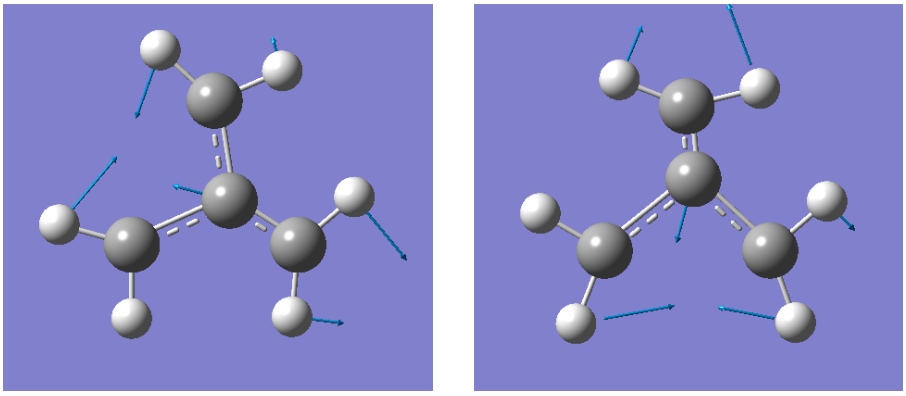

(c) (d)

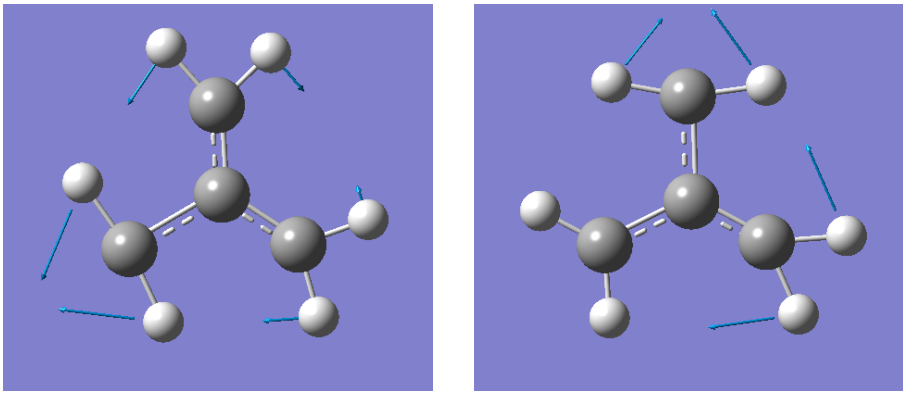

(e) (f)

Figure 5.11: The $E^{'}$ JT active modes for TMM: Mode 5, 6 ($429.61cm^{-}1$), 9, 10 ($1362.11cm^{-}1$), 11, 12 ($1518.55cm^{-}1$)

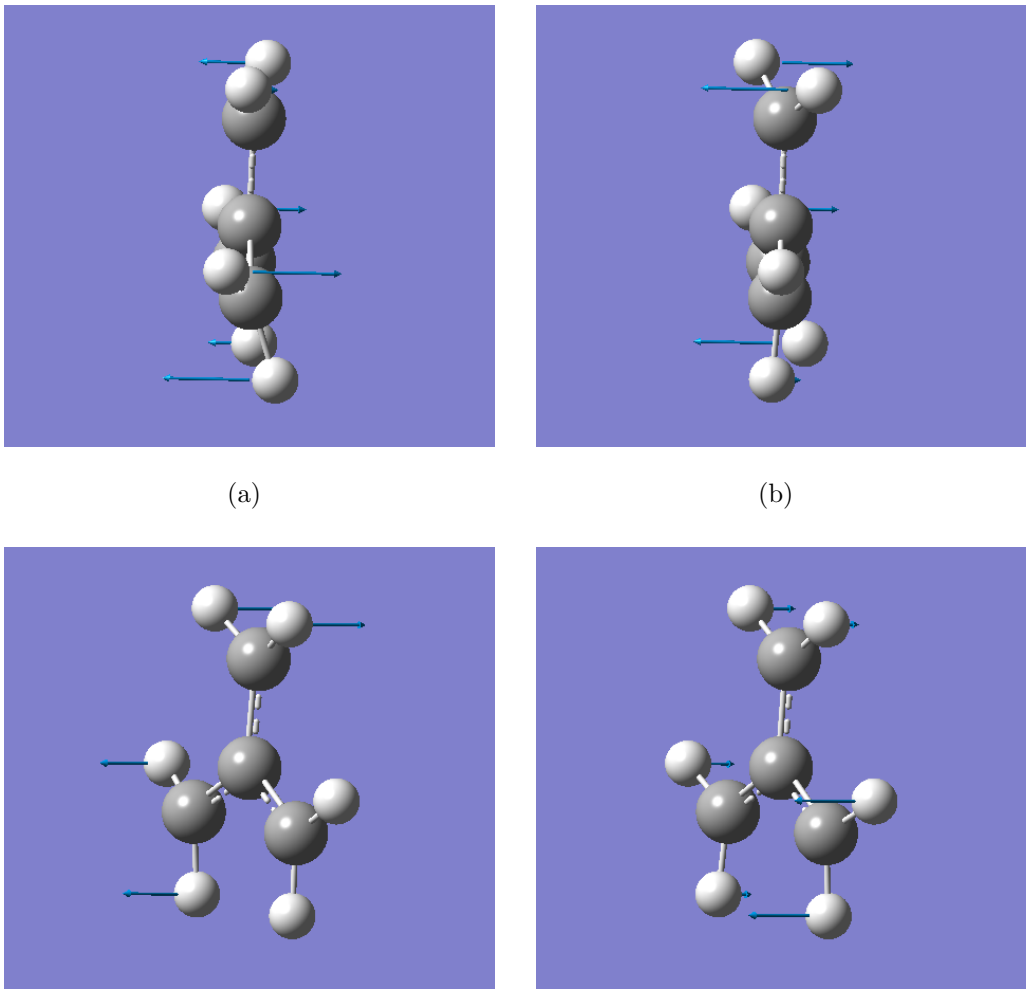

(a) (b)

(c) (d)

Figure 5.12: The E'' degenerate modes for TMM: Mode 1,2 ($476.91cm^{-}1$), 3,4 ($698.61cm^{-}1$)

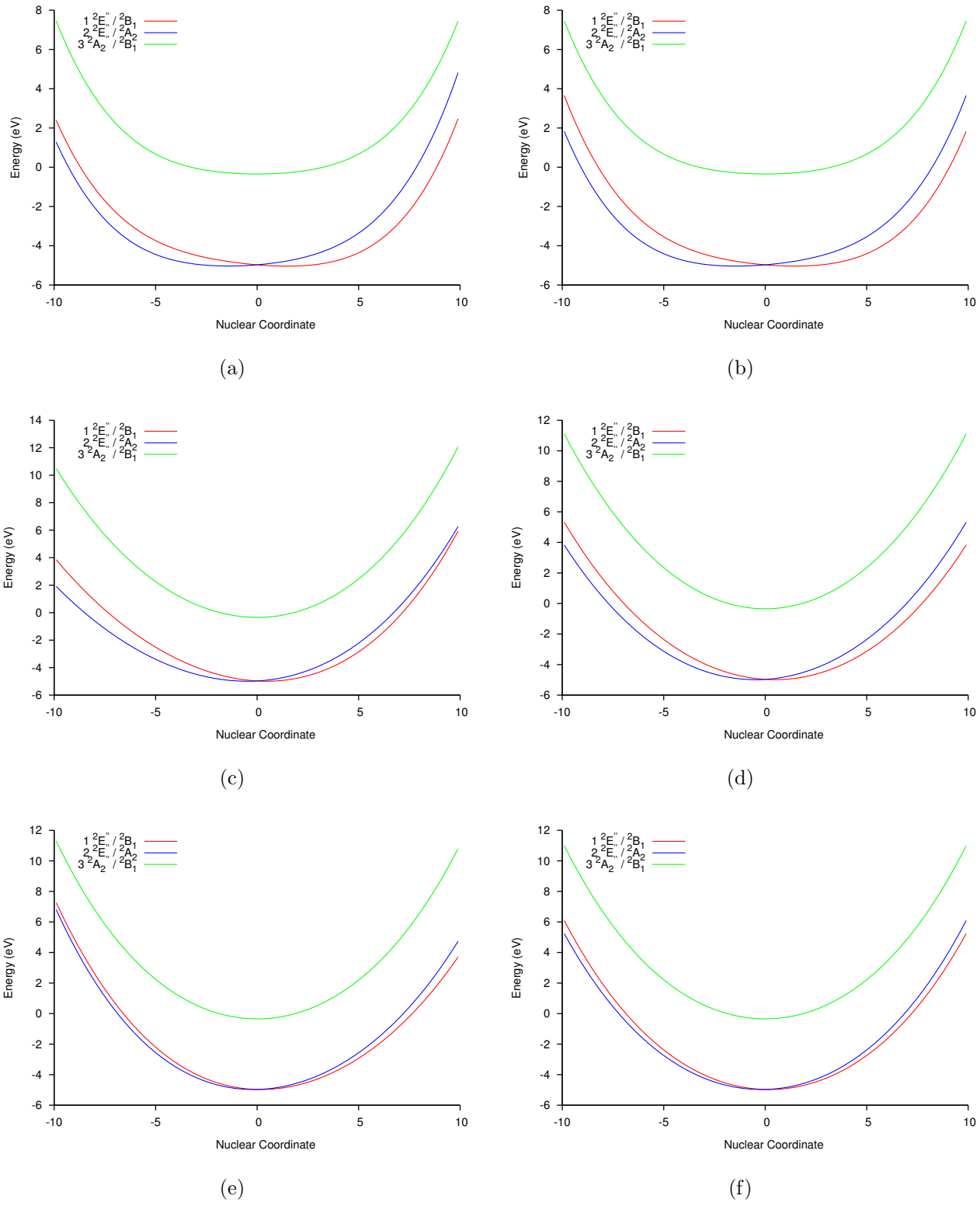

Figure 5.13: Adiabatic surfaces for the TMM^{-}: For modes shown in figure 5.11

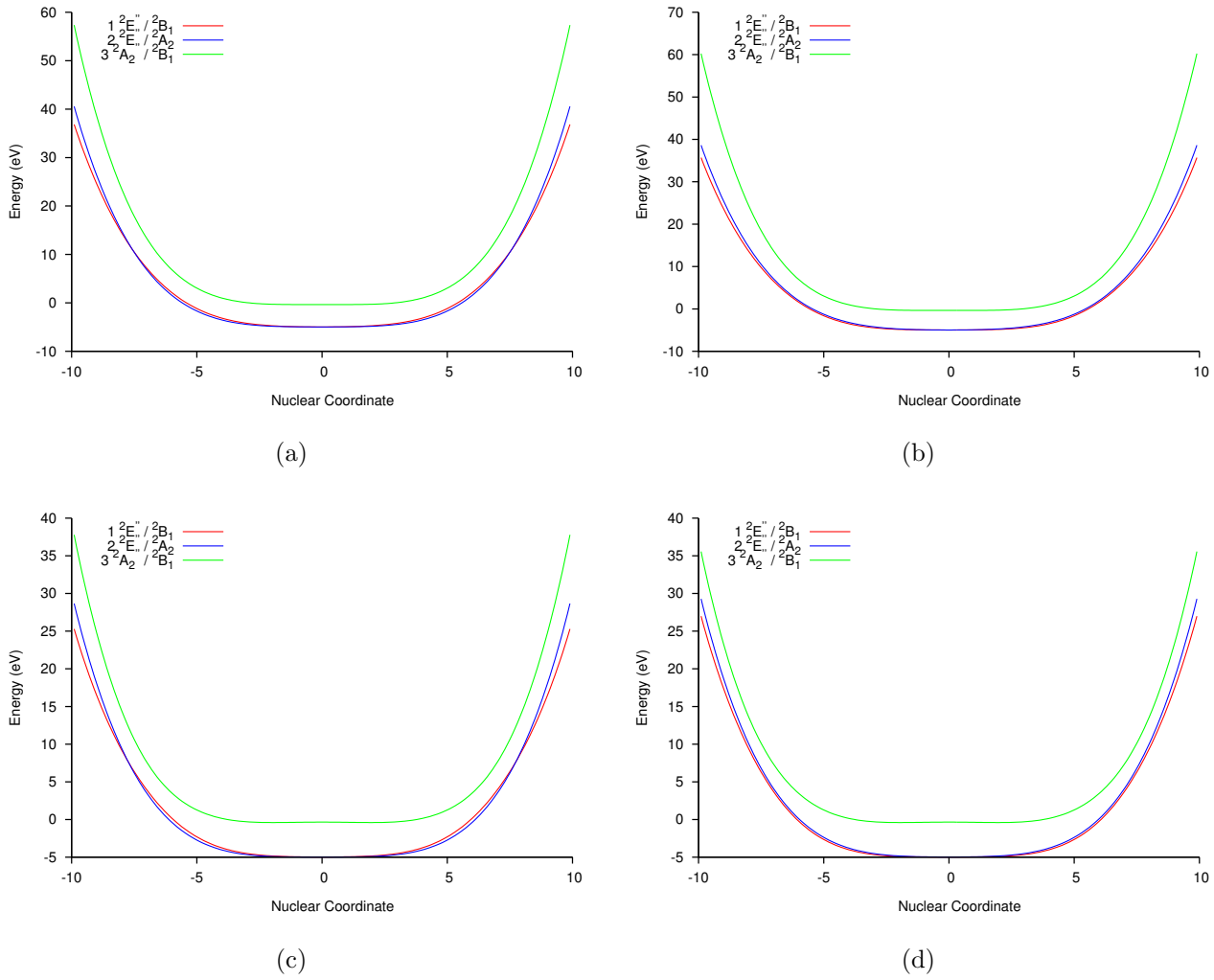

Figure 5.14: Adiabatic surfaces for the TMM^{-}: For modes shown in figure 5.12

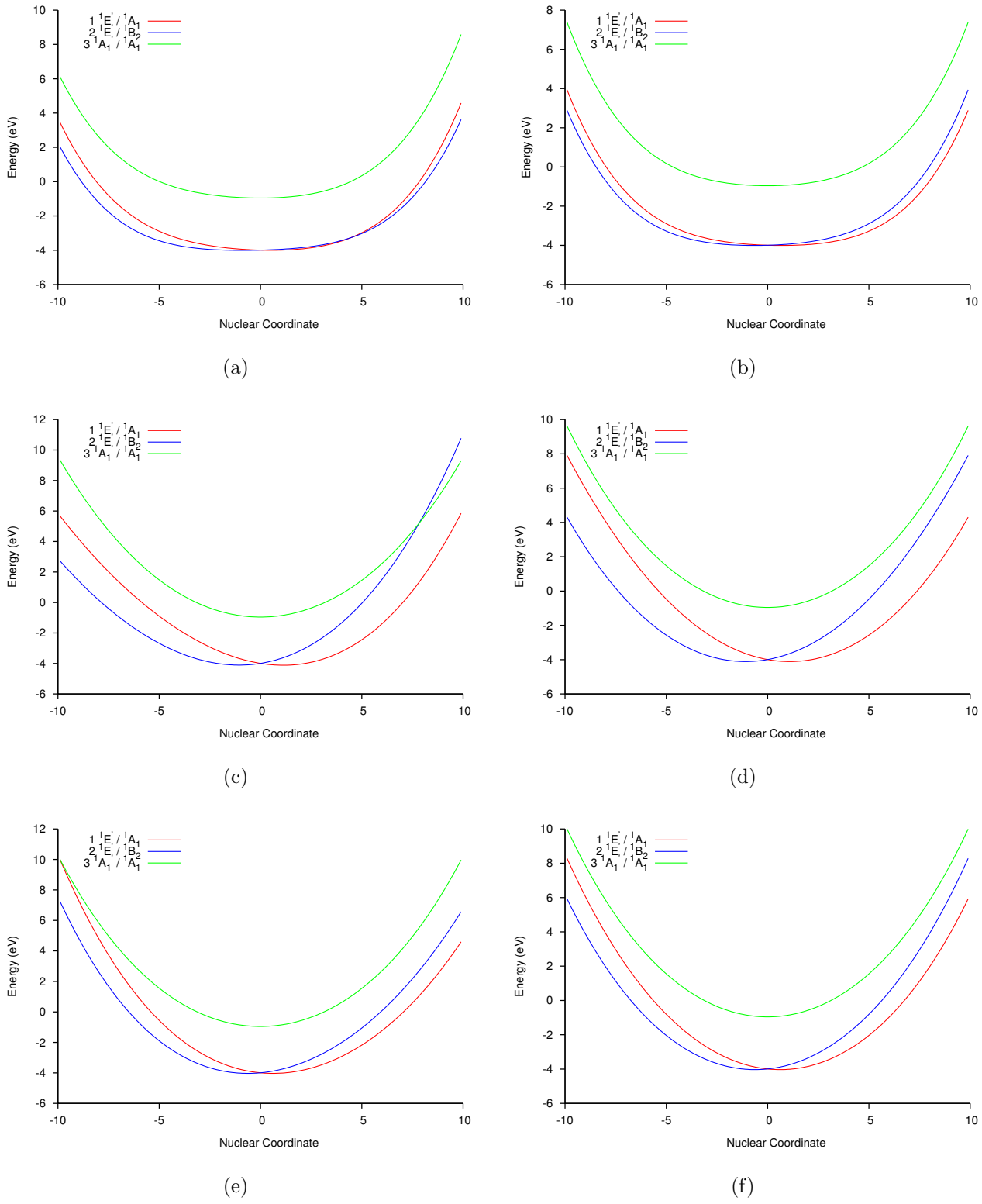

Figure 5.15: Adiabatic surfaces for the Singlet TMM: For modes shown in figure 5.11

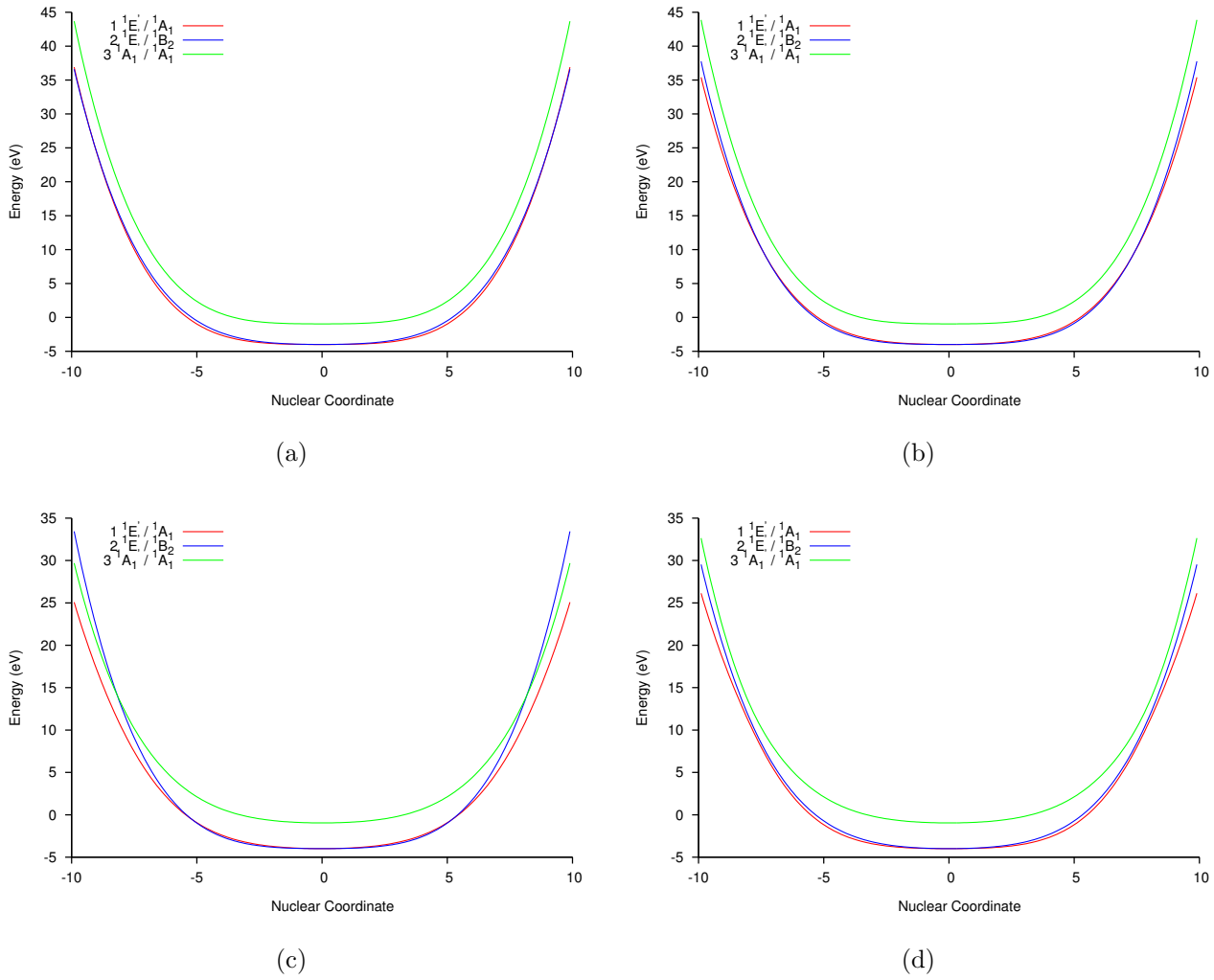

Figure 5.16: Adiabatic surfaces for the Singlet TMM: For modes shown in figure 5.12

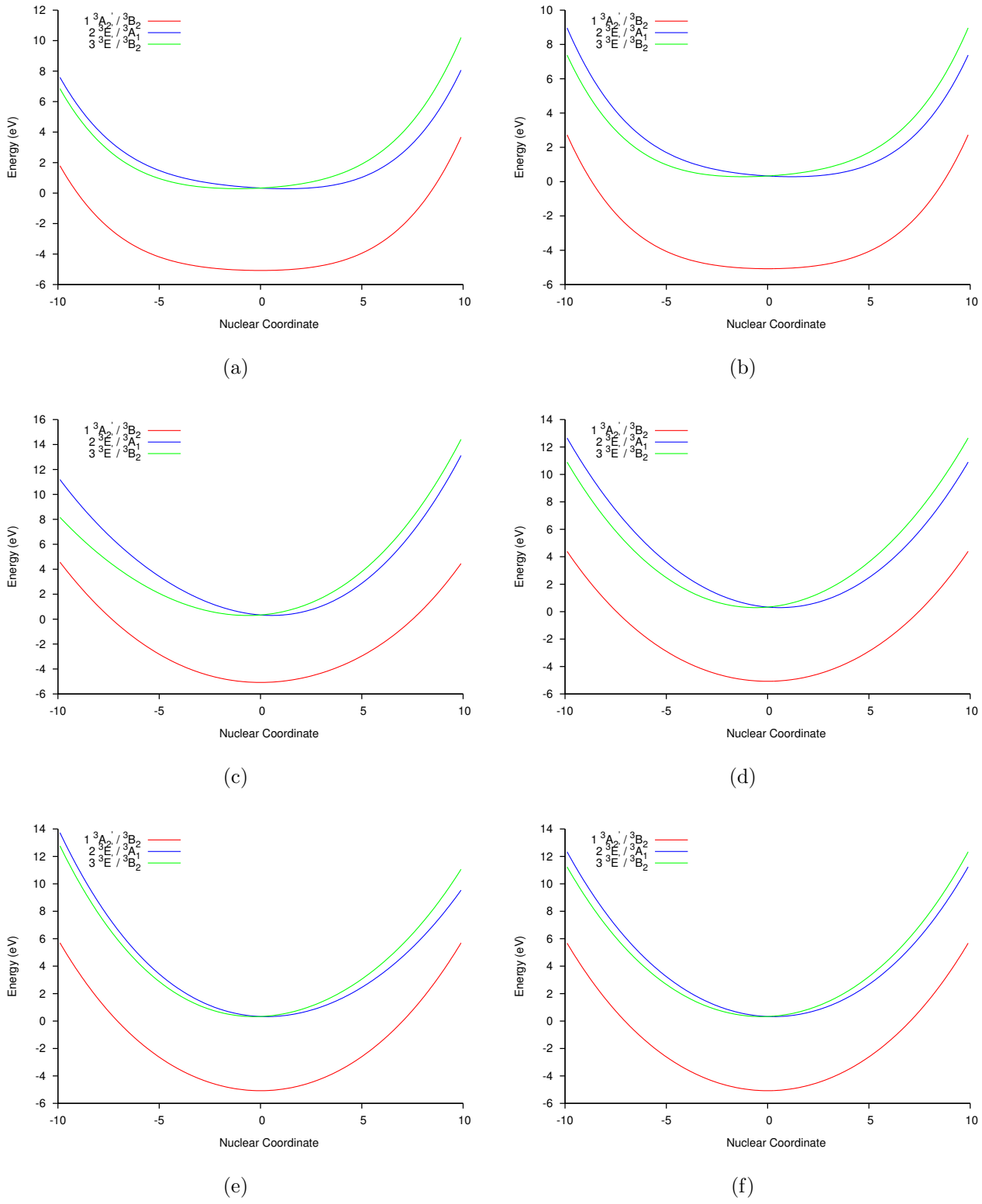

Figure 5.17: Adiabatic surfaces for the Triplet TMM: For modes shown in figure 5.11

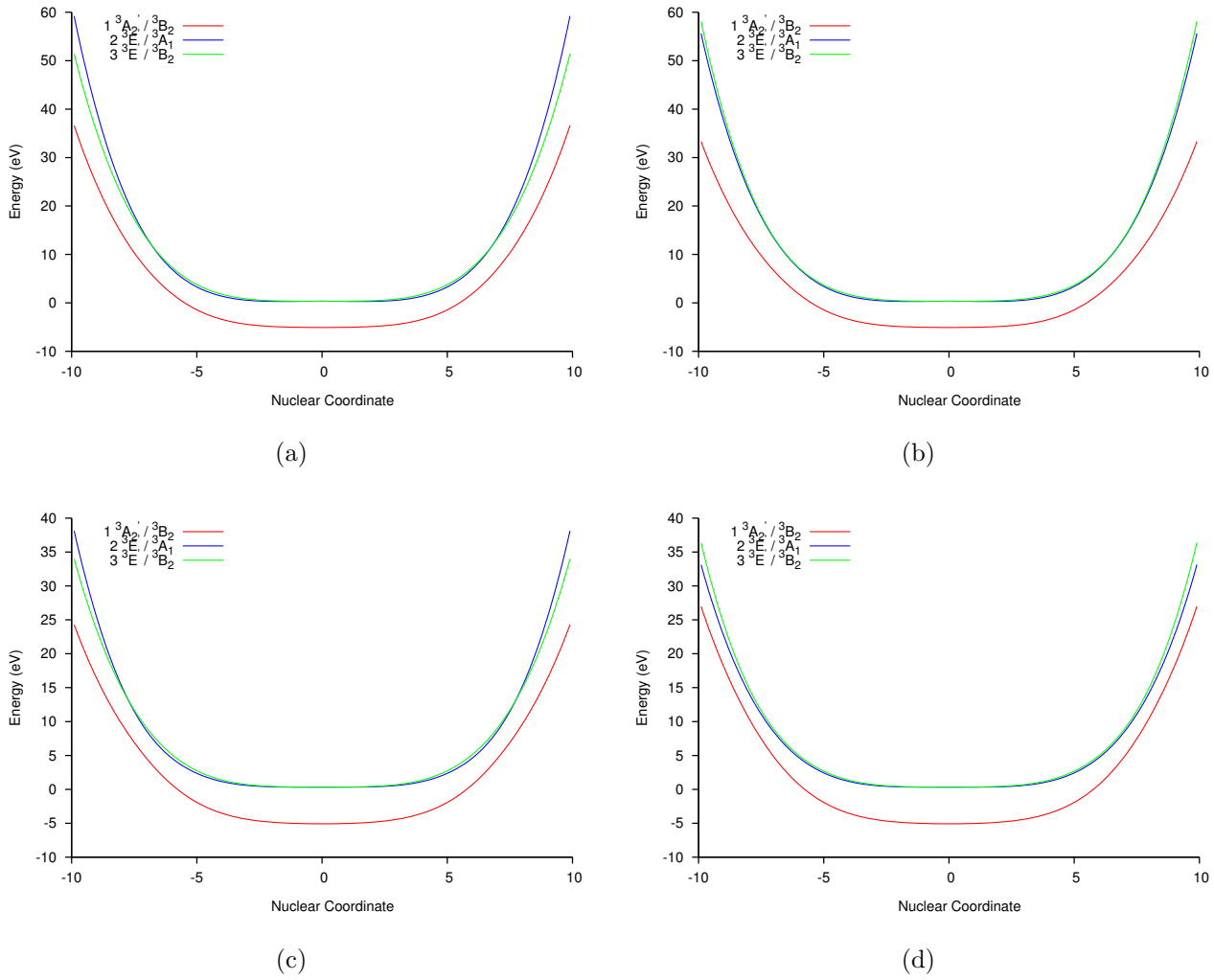

Figure 5.18: Adiabatic surfaces for the Triplet TMM: For modes shown in figure 5.12

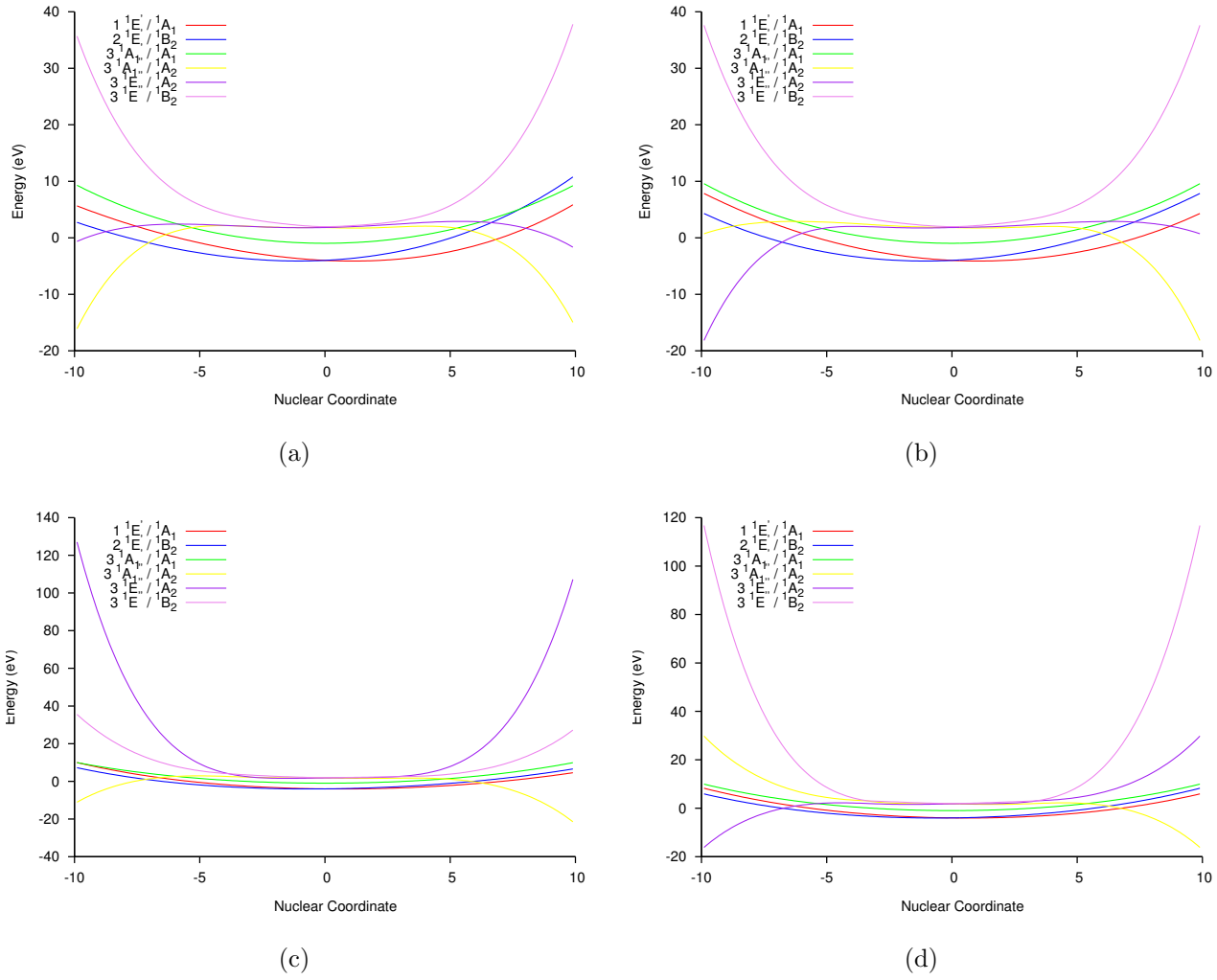

Figure 5.19: Adiabatic surfaces for selected JT modes of the Singlet TMM: Model-2, unbound potentials

Table 5.12: Details of the MCTDH computational setup. Mode combinations are listed along with the primitive bases of these modes, and the number of SPFs used for the relaxation as well as for the propagation calculation. Vibrational normal modes in one bracket constitute single particles. The primitive basis is the number of harmonic-oscillator DVR functions. Each particle has a primitive basis consisting of $10 \times 10 \times 10 = 1000$ functions. The SPF basis is the number of single particle functions used for each electronic state (being a single-set calculation).

Particle	Normal Modes	Primitive basis	SPF Basis (Relaxation)	SPF Basis (Propagation)
1	(1, 11, 12)	[10,10,10]	7	7
2	(2, 13, 14)	[10,10,10]	7	7
3	(3, 15, 16)	[10,10,10]	7	7
4	(17, 18, 19)	[10,10,10]	7	7
5	(4, 7, 8)	[10,10,10]	5	5
6	(5, 6)	[10,10,10]	2	2
7	(9, 10, 23, 24)	[10,10,10,10]	5	5
8	(20, 21, 22)	[10,10,10]	2	2

Table 5.13: Vibronic eigenvalues of the TMM anion as MCTDH with block-improved-relaxation method

Root	Energy (eV)	Energy ($cm^{-}1$)
1	0.0	0.0
2	0.0	0.0
3	0.024	193.35
4	0.030	241.69
5	0.050	402.81
6	0.050	402.81
7	0.058	467.27
8	0.061	491.44
9	0.065	523.66
10	0.066	531.72

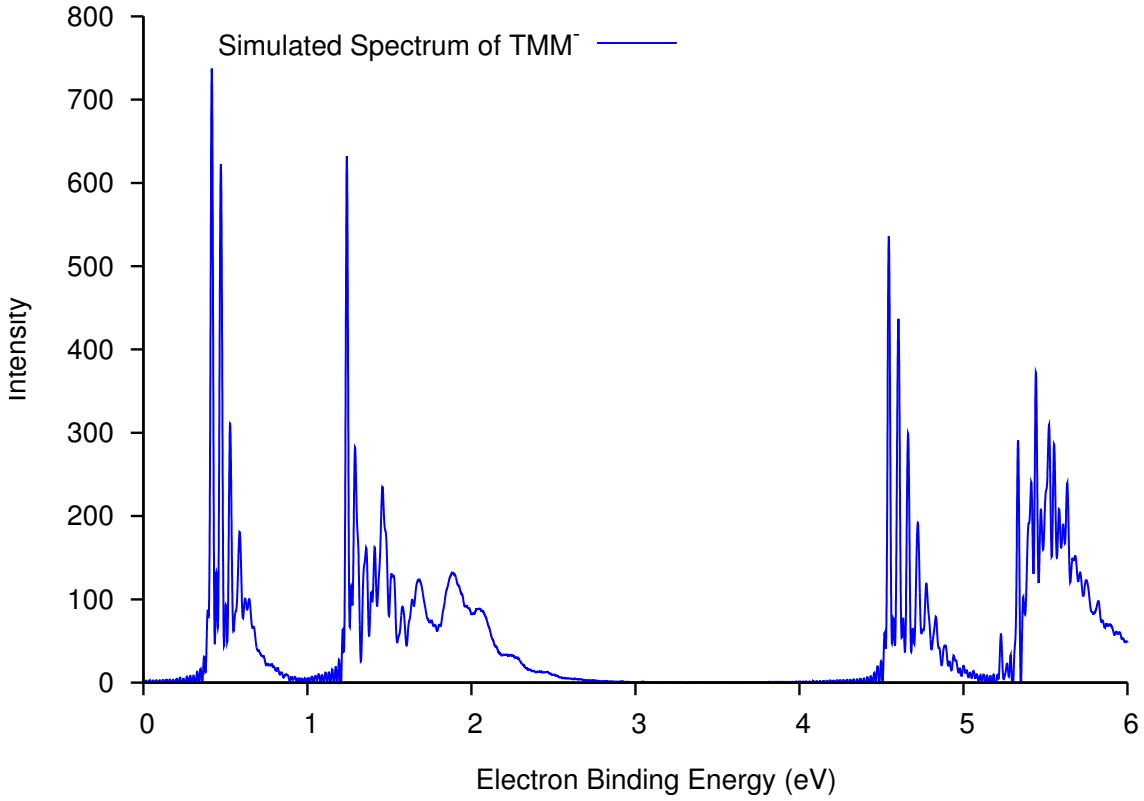

Figure 5.20: Simulated Photodetachment Spectrum of TMM^-

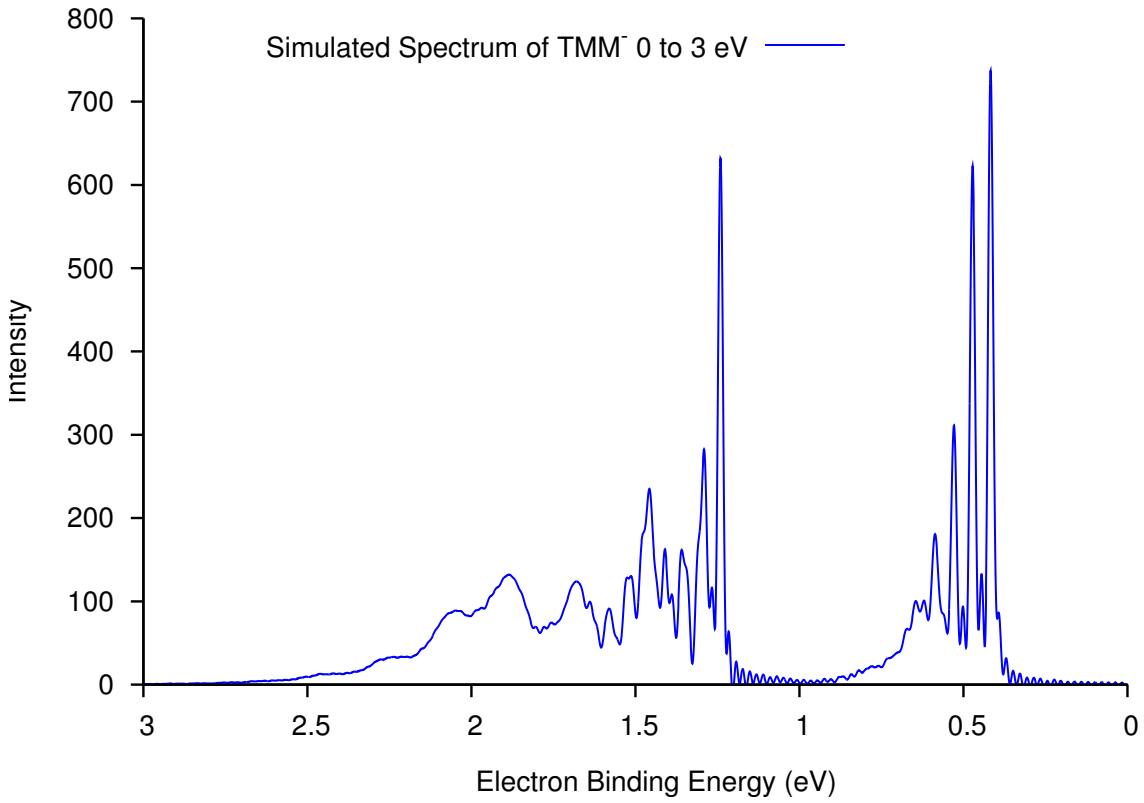

Figure 5.21: Simulated Photodetachment Spectrum of TMM^{-} : 0 to 3 eV

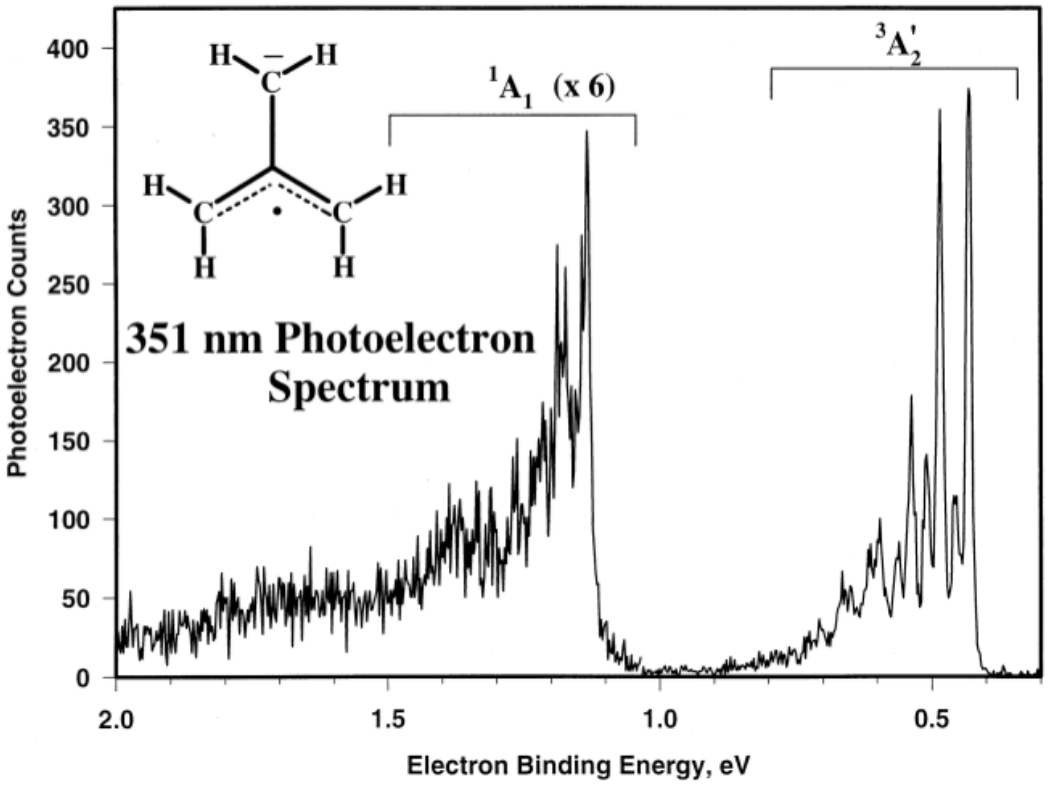

Figure 5.22: Experimental Photodetachment Spectrum of TMM^-

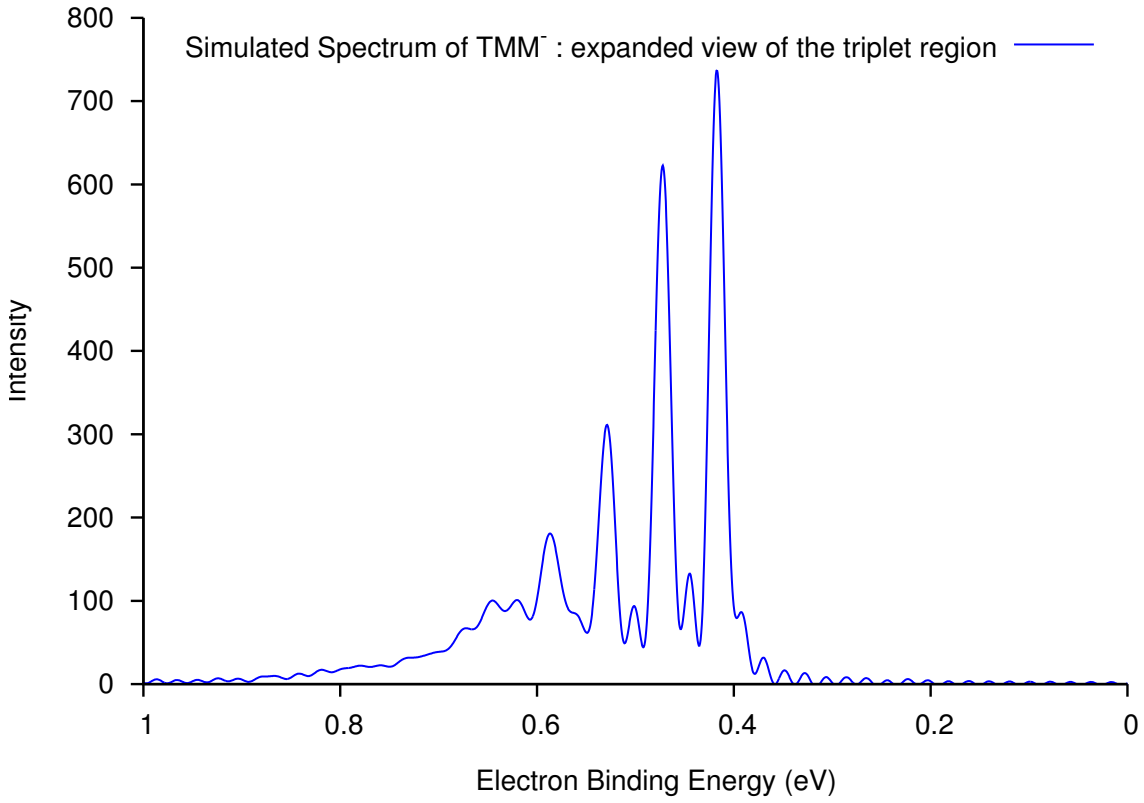

Figure 5.23: Expanded view of the simulated triplet region of the photodetachment spectrum

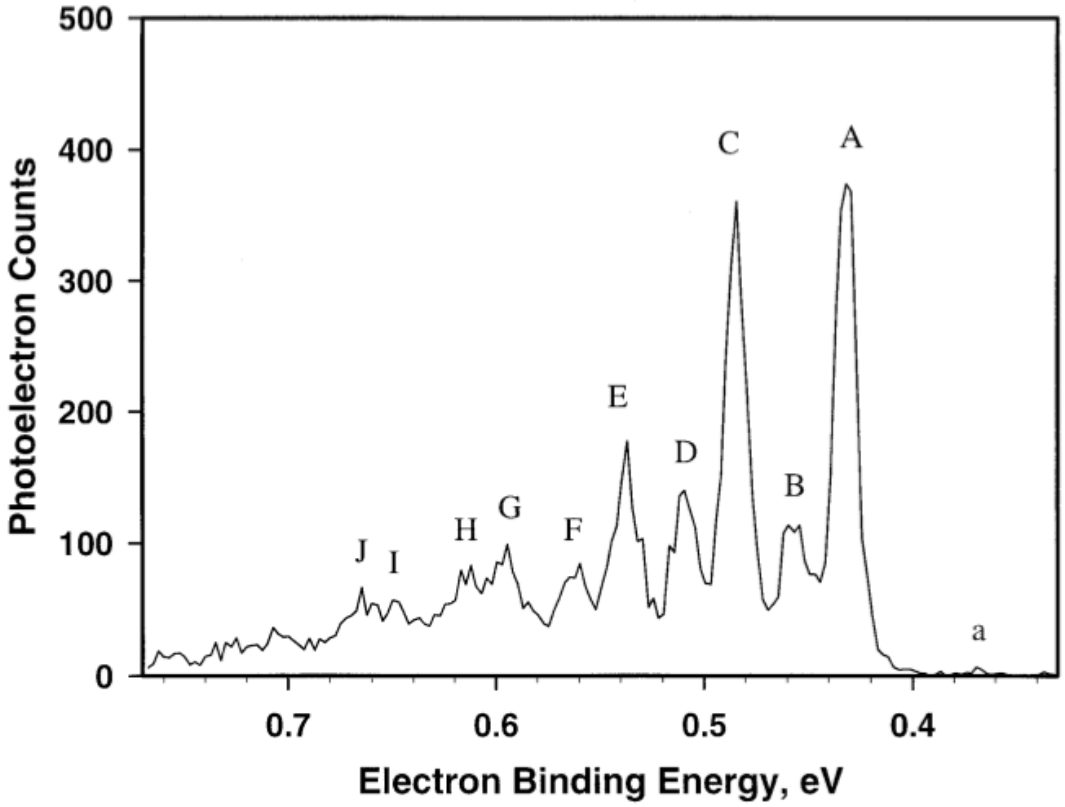

Figure 5.24: Expanded view of the simulated triplet region of the photodetachment spectrum

Chapter 6

Conclusions

Vibronic model Hamiltonians are a very good starting point for the studies of nonadiabatic systems, which can provide a compact representation of complicated coupled potential energy surfaces. The construction of vibronic models for small-to-medium sized molecule is a routine procedure with the computational tools and methods available in our group. A large number of vibronic models have been constructed successfully for radicals and biradicals, the characterization of which still remain a challenge for theoretical chemistry. In this work, photodetachment spectra of selected biradicals have been successfully simulated starting from first principles, with systems including up to 24 vibrational degrees of freedom. For systems, where the anionic ground state is also Jahn-Teller, the use of a multiple vibronic model scheme becomes essential. Consistent results are obtained for

VIBRON and MCTDH for small molecules (Chapter 3), which gave us confidence to use the methodology for systems having more degrees of freedom (18-24, Chapter 5) where the use of time-independent methods is essentially not possible. In general, a reasonably good agreement is obtained in comparison with experiment. For C_4H_4, there is no experimental spectrum available and a predicted experimental spectrum is presented.

6.1 Future Directions

Convergence in MCTDH remains a major issue which needs more attention and a careful analysis, and so does a reliable method for finding the vibronically excited states. Challenges still remain in exploring the full potential and available methods of the MCTDH program and also the computational limitations thereof. If MCTDH hits the limits for systems at 24-30 degrees of freedom, there is a need for more efficient algorithms to do quantum dynamics on larger molecules, which is so vital to Chemistry, including transition metal complexes.

On the Electronic Structure front, there certainly are limitations to the DIP-STEOM methodology, and one needs to go beyond it towards the true multireference methods in order to find accurate excited states. The multireference version of EOMCC (MR-EOMCC) is in active development in our group which might be able to give much more

accurate vibronic models and thus will allow to do more accurate theoretical spectroscopy.

Spin orbit coupling also remains to be included in the model Hamiltonian, which is important for transition metal complexes as well as other heavy elements. This work is also being pursued currently in our group and in the near future the vibronic models will be able to incorporate the spin orbit effect.

With the theoretical methodology and computational tools available to us, a wide variety of challenging systems can be explored and interesting studies can be performed to gain more insight into the structure and reactivity of these systems. We also look forward to doing the Time-Resolved Photoelectron Spectra in near future.

A website on vibronic theory is also being put together in our group by Julia Endicott, from where the vibronic models of radicals/biradicals can be downloaded, and also the normal modes and potential energy surfaces can be visualized .

APPENDICES

Python program for merging two MCTDH operator files

```
#! /usr/bin/python


# Merge.py -- Merge two MCTDH operator files

# ----------------------------------------


# Prateek Goel - June 9th, 2012

# University of Waterloo

# Comments/Questions: p2goel@uwaterloo.ca

# ---------------------------------------
```

```
# If you find a bug, please contact your nearest

# Pest control agency!



import fileinput

import sys, os

from shutil import copyfile


# User Inputs and Usage of the Program


if __name__ == '__main__':

    usage = '''\


usage: python merge.py GSname GSstates IPname IPstates Mergedname Model


example: python merge.py GS.op 1 IP.op 3 COM.op quartic


Notes:
```

```
    1. Model can be -- linear, quadratic, cubic, quartic, full (grid=10)!

    2. Please remove artificial ground state from IP, if it is there to begin with.

    3. GS will have one artificial state, and no transition moments.
'''
try:
    oipfile = sys.argv[1]    # GS file name
    n1 = sys.argv[2]       # No of electronic states in GS (include artifical ground state)
    dipfile = sys.argv[3]   # IP file name
    n2 = sys.argv[4]       # No of electronic states in IP (exclude artifical ground state)
    newfile = sys.argv[5]   # Merged file name
    model = sys.argv[6]    # which model do you have -- linear, quadratic, cubic, quartic?
except IndexError:
    sys.exit(usage)

ipfile = 'start.op'    # dummyfile to make changes in GS
copyfile(oipfile,ipfile)

n1 = int(n1)
```

```
n2 = int(n2)



# Helper Function -- Replace a string with a new one in a file
# ------------------------------------------------------------
def replace(filename, oldstring, newstring, backupext=None):
    '''
    replace oldstring with newstring in file filename.
    if backupext is a string, create a backupfile that has
    backupext appended to the original file name.
    '''
    old = open(filename).read()             # load old file content
    new = old.replace(oldstring, newstring) # create new file content

    if old == new: # replacement had no effect - don't need to save
        print 'file %s unchanged' % filename
        return     # leave function, don't return any value

    # if we get here, the filecontent has changed. Save it
    if type(backupext) is str: # backup file requested by user
```

```
        if not backupext.startswith('.'): # make sure the extension starts with a dot
            backupext = '.' + backupext
        backupfilename = filename + backupext
        try:
            open(backupfilename, 'w').write(old)
            print 'back up file written successfully'
        except (IOError, OSError): # couldn't write backup file - leave
            print 'backup failed -- original file %s unchanged' % filename
            return

    # if we get here, backup file was either successfully created or not requested
    try:
        open(filename, 'w').write(new)
    except:
        print 'writing changed file %s failed'
    else:
        print 'file %s modified' % filename


# Helper Function to insert particular lines at a particular place
```

```
# ------------------------------------------------------------


def insertAll(startsip, endsip, startsdip, endsdip):


    '''
        How This Works:
    '''
    tempip = []
    tempdip = []


    for line in fread:
        if (line.startswith(startsdip) and line.endswith(endsdip)):
            tempdip.append(fread.index(line))


    nindex = tempdip[len(tempdip)-1]


    for line in gread:
        if (line.startswith(startsip) and line.endswith(endsip)):
            tempip.append(line)
```

```
    fread.insert(nindex+1, '\n')


    for line in tempip:
        fread.insert(nindex+2, line)



# Helper Function -- Diagonal and Off-diagonal coupling constants
# ----------------------------------------------------------------
def diag_coup():


    tindex = []
    findex = []


    for line in gread:
        if 'Diagonal Quadratic' in line:
            tindex.append(gread.index(line))
        if 'Cubic Coupling' in line:
            tindex.append(gread.index(line))


    tall = gread[tindex[0]:tindex[1]]
```

```
for line in tall:
    if 'Off_diagonal' in line:
        offindex = tall.index(line)

tdiag = tall[2:offindex]
toffdiag = tall[offindex+2:len(tall)]

for line in fread:
    if 'Off_diagonal' in line:
        findex.append(fread.index(line))

for line in tdiag:
    fread.insert(findex[0]-1, line)

findex2 = []

for line in fread:
    if 'Cubic Coupling' in line:
        findex2.append(fread.index(line))
```

```
    for line in toffdiag:
        fread.insert(findex2[0]-1, line)

    return


# ------------------------------------------------------------------
# Get, Set, Go
# ------------------------------------------------------------------
#
# Replace all electronic labels in GS

for i in range(n1-1,-1,-1):
    if i+1+n2 <= 9:
        replace(ipfile, 's0'+str(i+1), 's0'+str(n2+i+1))
    elif i+1+n2 > 9:
        replace(ipfile, 's0'+str(i+1), 's'+str(n2+i+1))

for i in range(n1-1,-1,-1):
```

```
    for j in range(n1-1,-1,-1):
        replace(ipfile, 'S'+str(i+1)+'&'+str(j+1), 'S'+str(n2+i+1)+'&'+str(n2+j+1))



# Open files to read and write (GS, IP, Combined!)


fread = open(dipfile, 'r').readlines()

fwrite = open(newfile, 'w')


gread = open(ipfile, 'r').readlines()


# Separate code for Merging Electronic Labels in Hamiltonian Section

# ------------------------------------------------------------------


temp = []

temp2 = []


for i in range(n1):

    for line in gread:
```

```
        if (line.startswith('EH') and line.endswith('S'+str(n2+i+1)+'&'+str(n2+i+1)+'
\n')):
            temp.append(line)

for line in fread:
        if (line.startswith('EH') and line.endswith('S'+str(n2)+'&'+str(n2)+' \n')):
            temp2.append(fread.index(line))

for line in temp:
    fread.insert(temp2[0],line)

# Writing Field Operators
# -----------------------

# Relaxation operator and Tmoms - copy from IP to ALL

etmom = []
mtmom = []

for line in gread:
```

```
    if 'Electronic transition moments' in line:
        etmom.append(gread.index(line))
    if (line.startswith('Mx') and line.endswith('ev \n')):
        mtmom.append(gread.index(line))

tmoms = gread[etmom[0]:mtmom.pop()+1]

lcons = []

for line in fread:
    if (line.startswith('EH') and line.endswith('ev \n')):
        lcons.append(fread.index(line))

needed = lcons.pop()

for i in range(len(tmoms)):
    fread.insert(needed+i+1, tmoms[i])

# Same code for tmom operator hamiltonian function (may be make a function)
```

```
etmomop = []

mtmomop = []


for line in gread:

    if 'HAMILTONIAN-SECTION_Ex' in line:

        etmomop.append(gread.index(line))


for line in gread:

    if line.startswith('end-operator'):

        mtmomop.append(gread.index(line))


tmomsop = gread[etmomop[0]:mtmomop.pop()+1]


put = []


for line in fread:

    if 'end-hamiltonian-section' in line:

        put.append(fread.index(line))


for i in range(len(tmomsop)):
```

```
    fread.insert(put[0]+i+1, tmomsop[i])


# Start Merging other things -- Call insertAll with proper keywords !!!


if model == 'linear':


    insertAll('EH', 'ev \n', 'EH_s0'+str(n2), 'ev \n')

    insertAll('C1', 'ev \n', 'C1', 'ev \n')

    insertAll('C1', 'q \n', 'C1', 'q \n')


elif model == 'quadratic':


    insertAll('EH', 'ev \n', 'EH_s0'+str(n2), 'ev \n')

    insertAll('C1', 'ev \n', 'C1', 'ev \n')

    insertAll('C1', 'q \n', 'C1', 'q \n')

    diag_coup()

    insertAll('C2', 'q \n', 'C2', 'q \n')

    insertAll('C2', 'q^2\n', 'C2', 'q^2\n')


elif model == 'cubic':
```

```
    insertAll('EH', 'ev \n', 'EH_s0'+str(n2), 'ev \n')
    insertAll('C1', 'ev \n', 'C1', 'ev \n')
    insertAll('C1', 'q \n', 'C1', 'q \n')
    diag_coup()
    insertAll('C2', 'q \n', 'C2', 'q \n')
    insertAll('C2', 'q^2\n', 'C2', 'q^2\n')
    insertAll('C3', 'ev \n', 'C3', 'ev \n')
    insertAll('C3', 'q^3\n', 'C3', 'q^3\n')

elif model == 'quartic':

    insertAll('EH', 'ev \n', 'EH_s0'+str(n2), 'ev \n')
    insertAll('C1', 'ev \n', 'C1', 'ev \n')
    insertAll('C1', 'q \n', 'C1', 'q \n')
    diag_coup()
    insertAll('C2', 'q \n', 'C2', 'q \n')
    insertAll('C2', 'q^2\n', 'C2', 'q^2\n')
    insertAll('C3', 'ev \n', 'C3', 'ev \n')
    insertAll('C3', 'q^3\n', 'C3', 'q^3\n')
```

```
    insertAll('C4', 'ev \n', 'C4', 'ev \n')

    insertAll('C4', 'q^4\n', 'C4', 'q^4\n')


elif model == 'full':


    insertAll('EH', 'ev \n', 'EH_s0'+str(n2), 'ev \n')

    insertAll('C1', 'ev \n', 'C1', 'ev \n')

    insertAll('C1', 'q \n', 'C1', 'q \n')

    diag_coup()

    insertAll('C2', 'q \n', 'C2', 'q \n')

    insertAll('C2', 'q^2\n', 'C2', 'q^2\n')

    insertAll('C3', 'ev \n', 'C3', 'ev \n')

    insertAll('C3', 'q^3\n', 'C3', 'q^3\n')

    insertAll('C4', 'ev \n', 'C4', 'ev \n')

    insertAll('C4', 'q^4\n', 'C4', 'q^4\n')

    insertAll('B3', 'ev \n', 'B3', 'ev \n')

    insertAll('B3', 'q \n', 'B3', 'q \n')

    insertAll('B3', 'q^2\n', 'B3', 'q^2\n')

    insertAll('B4', 'ev \n', 'B4', 'ev \n')

    insertAll('A4', 'ev \n', 'A4', 'ev \n')
```

```
    insertAll('B4', 'q \n', 'B4', 'q \n')

    insertAll('B4', 'q^3\n', 'B4', 'q^3\n')

    insertAll('A4', 'q^2\n', 'A4', 'q^2\n')


fwrite.writelines(fread)

os.remove(ipfile)
```

References

[1] H. Koppel, W. Domcke, and L. Cederbaum, Advances in Chemical Physics **57**, 59 (1984).

[2] L. Salem and C. Rowland, Angewandte Chemie International Edition in English **11**, 92 (1972).

[3] W. Borden, *Diradicals* (Wiley, 1982).

[4] J. Stanton and J. Gauss, Advances in Chemical Physics **125**, 101 (2003).

[5] L. Slipchenko and A. Krylov, The Journal of Chemical Physics **117**, 4694 (2002).

[6] A. Krylov, Annual Reviews of Physical Chemistry **59**, 433 (2008).

[7] J. Stanton and R. Bartlett, The Journal of Chemical Physics **98**, 7029 (1993).

[8] M. Nooijen and R. Bartlett, The Journal of Chemical Physics **106**, 6441 (1997).

[9] M. Nooijen and R. Bartlett, Journal of Chemical Physics **107**, 6812 (1997).

[10] M. Nooijen, Spectrochimica Acta Part A: Molecular and Biomolecular Spectroscopy **55**, 539 (1999).

[11] A. Krylov, Accounts of Chemical Research **39**, 83 (2006).

[12] A. Krylov, Center for computational studies of electronic structure and spectroscopy of open-shell and electronically excited species, http://iopenshell.usc.edu/.

[13] E. Wilson, J. Decius, and P. Cross, *Molecular vibrations: the theory of infrared and Raman vibrational spectra* (Dover Pubns, 1955).

[14] M. Nooijen, International journal of quantum chemistry **95**, 768 (2003).

[15] M. Baer and R. Englman, Molecular Physics **75**, 293 (1992).

[16] M. Beck, A. Jäckle, G. Worth, and H. Meyer, Physics reports **324**, 1 (2000).

[17] J. Stanton, J. Gauss, J. Watts, W. Lauderdale, and R. Bartlett, International Journal of Quantum Chemistry **44**, 879 (1992).

[18] M. Nooijen and A. Hazra, With contributions from JF Stanton and K. Sattelmeyer (2003).

[19] M. Beck, A. Jäckle, G. Worth, and H. Meyer, Multiconfiguration time-dependent, http://www.pci.uni-heidelberg.de/cms/mctdh.html.

[20] F. Ribeiro, C. Iung, and C. Leforestier, The Journal of chemical physics **123**, 054106 (2005).

[21] H. Longuet-Higgins, U. Opik, M. Pryce, and R. Sack, Proceedings of the Royal Society of London. Series A. Mathematical and Physical Sciences **244**, 1 (1958).

[22] W. Eisfeld and K. Morokuma, The Journal of Chemical Physics **113**, 5587 (2000).

[23] P. Monks et al., The Journal of Physical Chemistry **98**, 10017 (1994).

[24] D. Wang, P. Jiang, X. Qian, and G. Hong, The Journal of chemical physics **106**, 3003 (1997).

[25] W. Eisfeld and K. Morokuma, The Journal of chemical physics **117**, 4361 (2002).

[26] M. Wladyslawski and M. Nooijen, Coupled cluster approaches for the photoelectron spectrum of the no_3 radical revisited: A theoretical investigation of potential energy surfaces and conical intersections, in *ACS Symposium Series*, volume 828, pages 65–92, Washington, DC: American Chemical Society,[1974]- (Washington, DC: American Chemical Society,[1974]-, 2002).

[27] W. Borden and E. Davidson, Accounts of Chemical Research **14**, 69 (1981).

[28] S. Saddique and G. Worth, Chemical physics **329**, 99 (2006).

[29] K. Nakamura, Y. Osamura, and S. Iwata, Chemical physics **136**, 67 (1989).

[30] I. Bersuker and I. Bersuker, *The Jahn-Teller Effect* (Cambridge Univ Pr, 2006).

[31] P. Wenthold, J. Hu, R. Squires, and W. Lineberger, Journal of the American Chemical Society **118**, 475 (1996).

[32] L. Slipchenko and A. Krylov, The Journal of chemical physics **118**, 6874 (2003).

[33] X. Li and J. Paldus, The Journal of chemical physics **129**, 174101 (2008).

[34] N. Daniel et al., The neumark group, http://www.cchem.berkeley.edu/dmngrp/.

[35] T. Bally, CHIMIA International Journal for Chemistry, 59 **7**, 522 (2005).

[36] T. Bally and W. Borden, Reviews in Computational Chemistry **13**, 1 (1999).

[37] H. H. Chang, From electronic structure theory to molecular spectroscopy, 2003.

[38] A. Hazra, *Electronic Absorption Spectra From First Principles*, PhD thesis, Princeton University, 2005.

[39] A. Hazra and M. Nooijen, The Journal of Chemical Physics **122**, 204327 (2005).

[40] H. Jahn and E. Teller, Proceedings of the Royal Society of London. Series A, Mathematical and Physical Sciences **161**, 220 (1937).

[41] H. Koppel, L. Cederbaum, W. Domcke, and S. Shaik, Angewandte Chemie International Edition in English **22**, 210 (1983).

[42] D. M. Neumark, The Journal of Physical Chemistry A **112**, 13287 (2008).

[43] C. D. Sherrill, The Journal of Chemical Physics **132**, 110902 (2010).

[44] J. Stanton, The Journal of Chemical Physics **126**, 134309 (2007).

[45] I. Ufimtsev and T. Martinez, Journal of Chemical Theory and Computation **5**, 1004 (2009).

[46] I. Ufimtsev and T. Martínez, Computing in Science & Engineering **10**, 26 (2008).

[47] P. Wenthold and W. Lineberger, Accounts of Chemical Research **32**, 597 (1999).

[48] P. Wenthold, J. Hu, R. Squires, and W. Lineberger, Journal of the American Society for Mass Spectrometry **10**, 800 (1999).

[49] H. Köppel, L. Cederbaum, and S. Mahapatra, Handbook of High-resolution Spectroscopy (2011).